

**Some pages of this thesis may have been removed for copyright restrictions.**

If you have discovered material in Aston Research Explorer which is unlawful e.g. breaches copyright, (either yours or that of a third party) or any other law, including but not limited to those relating to patent, trademark, confidentiality, data protection, obscenity, defamation, libel, then please read our [Takedown policy](#) and contact the service immediately ([openaccess@aston.ac.uk](mailto:openaccess@aston.ac.uk))

THE DEOXIDATION OF STEEL WITH SIMPLE AND  
COMPLEX DEOXIDISERS.

A thesis submitted in application for the

degree of

Doctor of Philosophy

in

THE UNIVERSITY OF ASTON IN BIRMINGHAM

by

Paul Horace Lindon, M.Sc., B.Sc., A.I.M.

August 1967

Department of Metallurgy,

The University of Aston in Birmingham,

Gosta Green,

Birmingham, 4.

Summary: The deoxidation of steel with complex deoxidisers was studied at 1550°C and compared with silicon, aluminium and silicon/aluminium alloys as standards. The deoxidation alloy systems, Ca/Si/Al, Mg/Si/Al and Mn/Si/Al, were chosen for the low liquidus temperatures of many of their oxide mixtures and the potential deoxidising power of their constituent elements. Product separation rates and compositional relationships following deoxidation were examined.

Silicon/aluminium alloy deoxidation resulted in the product compositions and residual oxygen contents expected from equilibrium and stoichiometric considerations, but with the Ca/Si/Al and Mg/Si/Al alloys the volatility of calcium and magnesium prevented them participating in the final solute equilibrium, despite their reported solubility in liquid iron.

Electron-probe microanalysis of the products showed various concentrations of lime and magnesia, possibly resulting from reaction between the metal vapours and dissolved oxygen. The consequent reduction of silica activity in the products due to the presence of CaO and MgO produced an indirect effect on calcium and magnesium on the residual oxygen content.

Product separation rates, indicated by vacuum fusion analyses, were not significantly influenced by calcium and magnesium but the rapid separation of products having a high  $\text{Al}_2\text{O}_3/\text{SiO}_2$  ratio was confirmed.

Manganese participated in deoxidation, when present either as an alloying element in the steel or as a deoxidation alloy constituent. The compositions of initial oxide products were related to deoxidation alloy compositions.

Separated products which were not alumina saturated, dissolved crucible material to achieve saturation. The melt equilibrated with this slag and crucible by diffusion to determine the residual oxygen content. MnO and SiO<sub>2</sub> activities were calculated, and the approximate values of  $\gamma$  MnO deduced for the compositions obtained.

Separation rates were greater for products of high interfacial tension. The rates calculated from a model based on Stoke's Law, showed qualitative agreement with experimental data when corrected for coalescence effects.



# CONTENTS

PAGE

## SUMMARY:

### SECTION 1. INTRODUCTION:

1.1. Oxygen in Steel	.....	1
1.2. Deoxidation processes.	.....	4
1.3. Non-metallic inclusions in Steel	.....	5
1.4. The present work.	.....	6

### SECTION 2. REVIEW OF RELEVANT LITERATURE

2.1. Thermodynamic aspects of deoxidation.		
2.1.1. The iron-oxygen system.	.....	8
2.1.2. Oxygen deoxidiser equilibria in iron melts.		
2.1.2.1. Oxygen-carbon equilibria	.....	12
2.1.2.2. Oxygen-manganese equilibria	.....	15
2.1.2.3. Oxygen-silicon equilibria	.....	18
2.1.2.4. Oxygen-aluminium equilibria	.....	19
2.1.3. Calcium and magnesium as deoxidisers	.....	22
2.1.4. Slag equilibria and complex deoxidisers	.....	27
2.2. Kinetics of deoxidation processes:		
2.2.1. Nucleation and growth of products.	.....	32
2.2.2. Separation of products	.....	40
2.3. Technical applications of complex deoxidisers:		
2.3.1. Deoxidisers containing volatile metals.	.....	49
2.3.2. Deoxidisers based on the Mn-Si-Al system.....		53
2.4. Purpose of present work.	.....	55

## SECTION 3. EXPERIMENTAL PROCEDURE

PAGE

3.1. Selection of experimental conditions:	
3.1.1. Melt material .....	57
3.1.2. Crucible material .....	58
3.2. Experimental equipment	
3.2.1. Furnace .....	59
3.2.2. Furnace atmosphere .....	61
3.2.3. Turbulence in the melt .....	61
3.3. Selection of deoxidiser composition .....	62
3.4. Preparation of materials:	
3.4.1. Deoxidation alloys .....	63
3.4.2. Iron-oxygen alloys .....	65
3.5. Experimental melts:	
3.5.1. Melting procedure .....	66
3.5.2. Sampling and deoxidation procedure .....	68
3.6. Analysis and Metallography:	
3.6.1. Steel analysis .....	69
3.6.2. Deoxidiser analysis .....	71
3.6.3. Inclusion analysis .....	72
3.6.4. Metallography .....	73
3.7. Development of programme:	
3.7.1. Series 3 experiments. ....	74
3.7.2. Series 4 experiments. ....	75
3.7.3. Series 5 experiments. ....	76

## SECTION 4. EXPERIMENTAL RESULTS:

PAGE

4.1. Evaluation of experimental technique:	
4.1.1. Melt/crucible reaction. ....	77
4.1.2. Solidification of samples .....	77
4.2. Experimental data:	
4.2.1. Preparation of melts. ....	80
4.2.2. Deoxidation of melts. ....	81
4.3. Melt and inclusion analyses. ....	84
4.4. Metallographic examination:	
4.4.1. Inclusion types. ....	113
4.4.2. Inclusion content and size distribution.....	113

## SECTION 5. DISCUSSION OF RESULTS:

5.1. Introduction: .....	122
5.2. Control deoxidisers and effects of calcium and magnesium:	
5.2.1. Residual oxygen in the melts and equilibrium with products:	
5.2.1.1. Silicon and aluminium controls .....	123
5.2.1.2. Silicon-aluminium alloy controls and lime additions. ....	125
5.2.1.3. Silicon-aluminium deoxidisers containing calcium or magnesium. ....	128
5.2.2. Formation and separation of deoxidation products.	
5.2.2.1. Product compositions. ....	133
5.2.2.2. Product distribution. ....	136
5.2.2.3. Product separation rates. ....	140
5.3. Deoxidation with manganese - silicon - aluminium alloys:	
5.3.1. Product compositions:	

	PAGE
5.3.1.1. Effect of deoxidiser alloy composition .....	148
5.3.1.2. Effect of crucible material .....	153
5.3.2. Equilibrium relationships:	
5.3.2.1. Equilibrium with alumina saturated slags .....	156
5.3.2.2. Equilibrium with initial deoxidation products..	160
5.3.3. Formation and separation of products:	
5.3.3.1. Nucleation and growth .....	165
5.3.3.2. Separation rates .....	178
5.4. Practical implications: .....	190
5.5. Suggestions for further work .....	192
SECTION 6. CONCLUSIONS .....	194
APPENDIX A .....	198
APPENDIX B .....	201
APPENDIX C .....	201
APPENDIX D .....	205
ACKNOWLEDGMENTS .....	208
REFERENCES .....	209

## SECTION 1. INTRODUCTION.

1.1. Oxygen in steel. Steelmaking processes involve removing large amounts of dissolved impurity elements from molten iron. Most of the impurities are removed by oxidation reactions, and these are promoted by introducing oxygen into the melt from highly oxidising slags or gases.

As the concentration of oxidisable elements is reduced the activity of oxygen increases, until at the end of the refining period, a low carbon melt can contain up to 0.05% dissolved oxygen. The relationship between carbon and oxygen in a melt was determined by Marsh (1) for electric furnaces and Feters & Chipman (2) for open hearth furnaces. Their results are shown in fig. 1.1. The oxygen concentration always exceeds the equilibrium value because a state of supersaturation is required to keep the oxidation process active, and proceeding at an economic rate.

If a melt containing a high concentration of oxygen were cast without deoxidation treatment, the carbon - oxygen reaction would take place during cooling and solidification. The resulting carbon monoxide bubbles would cause the remaining liquid to effervesce in the mould and produce a steel with a high degree of porosity. This problem occurred in the early development of the Bessemer process and was solved by the addition of manganese which combined with part of the oxygen and reduced the intensity of carbon - oxygen reaction to acceptable levels.

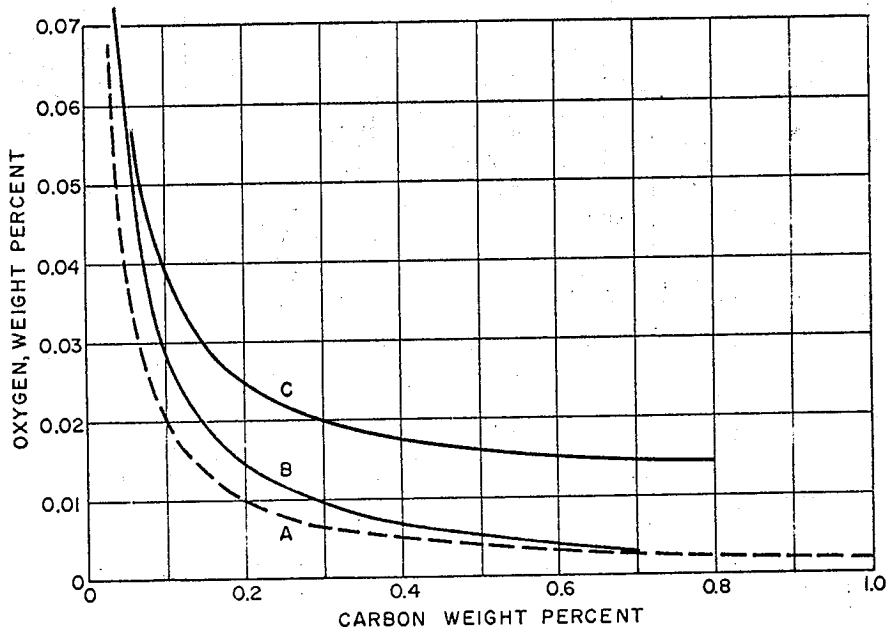


Fig. 1.1. Carbon - oxygen relationships in molten steel.

(After Marshall and Fetter & Chipman).

- A. Equilibrium at 1600°C
- B. Electric furnace.
- C. Open hearth furnace

Control of the carbon - oxygen reaction in the manufacture of rimming steels enables low carbon ingots to be produced, in which the carbon monoxide evolution is delayed until a solid skin is formed adjacent to the mould wall, and in which shrinkage cavities and pipe are eliminated by entrapping sufficient carbon monoxide to compensate for volume contraction on solidification.

The oxygen required for a controlled rimming intensity is quite high, and that residual oxygen which is not combined with carbon reacts with residual manganese and silicon to form non-metallic inclusions. Most of these inclusions become entrapped in the ingot. Iron oxide is usually present in the manganese silicate particles to an extent which raises the oxygen potential of the particle to approach equilibrium with the oxygen in the liquid steel.

Balanced, capped and semi killed steels are all grades of steel which are produced by controlling the rimming intensity and duration, mechanically or by deoxidiser additions. These steels contain less porosity than rimming steels, but do contain sufficient to compensate for some of the volume contraction on solidification.

The extensive segregation of impurities in rimming steels, together with the high concentration of inclusions and limited range of compositions, prevents their use in many engineering applications. High quality steels which require maximum

uniformity of composition and properties, a minimum concentration of non - metallic inclusions and the presence of oxidisable alloy elements, must be fully deoxidised. This reduces the oxygen activity to a level less than that required for carbon monoxide evolution and also minimizes the amount of oxide inclusions formed and entrapped during solidification.

1.2. Deoxidation processes. The reduction in oxygen activity is commonly achieved by the controlled addition of elements having a high affinity for oxygen and which are soluble in steel.

Deoxidation practice in the steel making industry is very varied but is usually divided into stages. Weak deoxidisers such as ferromanganese are added to the bath before tapping and the stronger ones, such as ferrosilicon, are added to the ladle. Aluminium, when used, is most often added to the ingot mould, or trumpet in the case of bottom poured ingots. Variations on this sequence include the use of alloy deoxidisers such as calcium silicide and silico manganese, and the division of some deoxidiser additions between stages. Part of the aluminium addition, for example, can be made to the ladle or to the metal stream during teeming.

The products of deoxidation are composed of one or more oxides which are very often associated with sulphides in commercial steel making. Their density is usually between 2 - 4 gm.cm<sup>-3</sup> which gives



them buoyancy, enabling most of them to separate from the melt. Some however, may remain entrapped in the steel and, together with the inclusions formed during solidification, act as harmful discontinuities in the structure.

1.3. Non - metallic inclusions in steel. Sources of exogenous inclusions in steel, and their contribution to the total inclusion content, have been the subjects of many investigations. The most significant sources considered have been slags, refractories and atmospheric environment during teeming.

Slags have been shown to contribute only indirectly. Slag/refractory reaction in the ladle produces an initially adherent glaze which contaminates subsequent heats using the ladle.(3) Chemical and mechanical erosion of the ladle, nozzle and hollow-ware refractories have received attention, (4-7) but Sims & Forgem (8) report the work of Malinovskii & Morozov (9) which concludes that reoxidation during teeming is the chief source of exogenous oxides. Teeming in non - oxidising atmospheres has been shown by Hultgren(10) and Narita (11) to give a significant reduction in exogenous inclusions, thus supporting the view of Malinovskii & Morozov.

Investigations by Richardson (12) show that approximately 90% of the inclusions in steel do not arise from slags or refractories. The work of Sicha (13), referred to by Plockinger(14), attributes 80 - 90% of the oxides in steel to the deoxidation process. There seems considerable scope therefore in attempts to produce cleaner steel by improved deoxidation processes.

The presence of inclusions in steel can cause deterioration of fatigue, impact and ductility properties; increased anisotropy and ductile/brittle transition temperatures; increased incidence of hot short or seams in working and a deterioration of the surface appearance.

Rees and Hopkins (15) showed a drastic reduction in strength of pure iron - oxygen alloys when the oxygen was increased in stages from 0.003% to 0.2%. Severe intergranular embrittlement and increasing ductile/brittle transition temperatures were noted. Iron oxide rich inclusions are not normally encountered in steels however, and Cummins(15a) and Frith (16) have shown that brittle and non - deformable inclusion such as alumina and aluminosilicates are the most detrimental to fatigue properties. Murray & Johnson (17) also agree that these properties are greatly reduced by alumina and rank silica as a less harmful inclusion. Relationships between fatigue properties and inclusion content or inclusion size have been demonstrated by Atkinson (18) and Duckworth & Ineson (19) respectively.

Seams and cracks on steel rope wire were shown by Rabinowitz (20) to be due to alumina and aluminosilicates resulting from aluminium deoxidation.

1.4. The present work. It is clear from the foregoing considerations that beneficial effects may be obtained by reducing

the concentration of oxide inclusions in steel, or by controlling their composition and size.

The following account reviews the literature relevant to deoxidation and describes experimental work with three complex deoxidiser systems. An attempt is made to understand complex deoxidation and the behaviour of deoxidation products.

## SECTION 2. REVIEW OF RELEVANT LITERATURE.

### 2.1. Thermodynamic aspects of deoxidation.

2.1.1. The iron-oxygen system: The solubility of oxygen in liquid iron, and its variation with temperature was first studied quantitatively by Herty and Gaines (21). Schenck (22) combined their results with the determinations at the monotectic point made by Rosenhain et.al. (23) and proposed the temperature function in eq.2.1.

$$\log [\%O]_{Fe \text{ max.}} = - \frac{6,800}{T} + 3.12 \quad \dots \quad \text{eq. 2.1.}$$

$[\%O]_{Fe \text{ max.}}$  is the oxygen solubility limit in iron and  $T$  is the temperature in  $^{\circ}K$ .

The results of subsequent work by Körber & Oelsen (24) using a direct method similar to that of Herty & Gaines, however was accepted as authoritative until the determinations of Chipman & Feters (25) and Taylor & Chipman (26).

The determinations by Chipman and his co-workers were also made by direct equilibrium between iron melts and iron oxide slags. Taylor & Chipman used a rotating crucible to reduce the influence of refractory, and also showed that furnace atmosphere and sampling methods had little effect on the results. Chipman (27) summarises the results of both investigations by equ. 2.2. in which  $[\%O]_{Fe}$

$$\log [\%O]_{Fe} = - \frac{6,320}{T} + 2.734 \quad \dots \quad \text{eq.2.2.}$$

is the solubility limit of oxygen in liquid iron. These solubilities are considerably lower than the earlier determinations and Bell (28) reasonably attributes the difference to low temperature readings in the early work in which optical pyrometers were used.

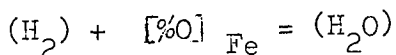
The oxygen solubility at the monotectic temperature (see fig. 2.1.) is calculated from eq. 2.2 as 0.167%, which compares favourably with the values of 0.15% determined by Sloman (29) and 0.16% determined by Fischer & vom Ende (30).

The most recent investigation is ~~of~~ Gokcen's (31) who equilibrated small melts in alumina crucibles with iron oxide slags. An oxidising atmosphere was maintained with  $H_2/H_2O$  gas mixtures. His results are described by equ. 2.3 for which he estimates an accuracy of 15% and claims less scatter than obtained

$$\log [\%O]_{Fe} = - \frac{5.752}{T} + 2.439 \quad \dots \quad \text{eq. 2.3}$$

by Chipman and his co workers. The differences between - equ. 2.2 & 2.3. however, are very small in the range 1550°C - 1650°C.

The work of Floridis & Chipman (32) on the reaction;



showed that oxygen dissolved in liquid iron did not obey Henry's Law, and variation of the activity coefficient  $f_o$  was described by equ. 2.4.

$$\log f_o = - 0.20 [\%O] \quad \dots \quad \text{eq. 2.4.}$$



in which the constant - 0.20 is the interaction coefficient  $e_o^o$ .

The solubility of oxygen in solid iron is very much less than in the liquid and attempts to measure solid solubility have produced many diverse results. Sloman (29) determined the solubility in slowly cooled samples by bracketing the compositions between which iron oxide could be detected and not detected. From this investigation the solubility limit was given as 0.003% - 0.006% O and a similar method used by Wever, Fischer & Englebrecht (34) gave the limit as 0.003 - 0.007%. These results may easily relate to the solubility in  $\alpha$  Fe because precipitation of iron oxide during cooling may have occurred.

Seybolt (35) measured the solubility of oxygen in zone refined  $\alpha$  Fe at 700°C - 900°C and obtained a value of 0.002% after equilibrating thin strips of iron with a surface layer of wüstite. The results from this were much lower than his previous work (36) which he rejected on the basis that impurities had caused internal oxidation.

The solubility of oxygen in  $\delta$  Fe was reported by Kitchener et-al (37) to be 0.003%  $\pm$  0.003%. Tankins & Gokcen (38) give eq.2.5 for the oxygen solubility.

$$\log [\%O]_{\delta Fe} = - \frac{1,2630}{T} + 5.51 \quad \dots \quad \text{eq. 2.5}$$

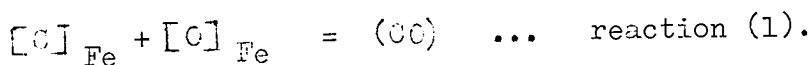
At 1450°C & 1528°C this indicates oxygen contents of 0.0145% & 0.031% respectively. Hepworth, Smith & Turkdogan (39) report solubilities of 0.0066% and 0.0088% for these temperatures

respectively. The techniques were very similar using zone refined iron and equilibrating in an oxidising atmosphere, but Tankins & Gokcen used thin foil which was electrolytically polished after the equilibration experiment. Surface contamination with such high area to volume ratio samples, could easily produce high results. Fig. 2.1a summarises the available data.

### 2.1.2. Oxygen - deoxidiser equilibria in iron

2.1.2.1 Oxygen - carbon equilibria. The literature concerning carbon - oxygen reactions in steel has been thoroughly reviewed in recent years by Elliott (40), Chipman (41) and Bodsworth (42).

The early work of Field and Vacher & Hamilton on reaction (1) assured that solutions of carbon



and oxygen in steel obeyed Henry's Law and these workers accordingly, simplified the equilibrium constant by writing 'm' as the product of the Wt % concentrations of carbon and oxygen at one atmosphere pressure of carbon monoxide. At 1600°C, values of 'm' are quoted between 0.002 and 0.0025. A value of 0.0020 is given by Fuwa & Chipman (43) as being applicable at 1600°C with an equilibrium gas of 1atm. pressure and a carbon content in the steel of 0.02-0.2%

Elliott (40) showed that the activity of carbon in pure iron - carbon alloys could be represented by the curve shown in fig. 2.2.,



which was calculated from a temperature dependent function proposed by Rist & Chipman (44). The activity is relative to an infinitely dilute solution in iron as standard state. The interaction coefficient  $e_C^C$  recommended by Bodsworth is + 0.23 and is taken from the data of Rist & Chipman (44) and Turkdogan et.al. (45)

The effect of carbon on the activity coefficient of oxygen and corresponding effect of oxygen on that of carbon, are given by Fuwa & Chipman as  $e_O^C = - 0.13$  and  $e_C^O = - 0.1$ .

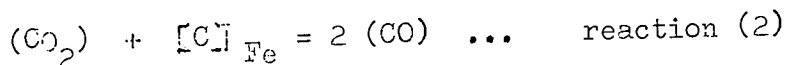
The equilibrium constant  $K_{c-o}$  for reaction (1) is given by equations 2.7 & 2.8

$$\log K_{c-o} = - \frac{7,541}{T} + 6.79 \quad \dots \quad \text{eq. 2.7}$$

$$\log K_{c-o} = - \frac{7,280}{T} + 6.65 \quad \dots \quad \text{eq. 2.8}$$

These agree very well at 1550°C and were determined by Richardson & Dennis (46) and Rist & Chipman (44) respectively. They seem to be the most reliable data available and will be used, where appropriate, in calculations involving carbon and oxygen.

At carbon contents less than 0.1%, the equilibrium partial pressure of carbon monoxide is reduced by reaction (2). Fig. 2.3 shows



the variation of equilibrium gas composition with change in carbon content.

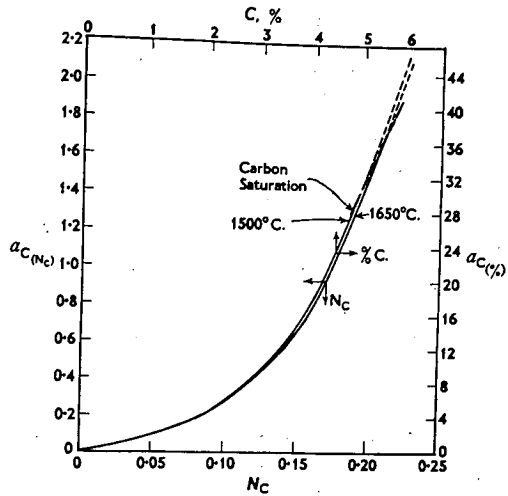


fig. 2.2. Activity of carbon in dilute iron - carbon alloys (40).

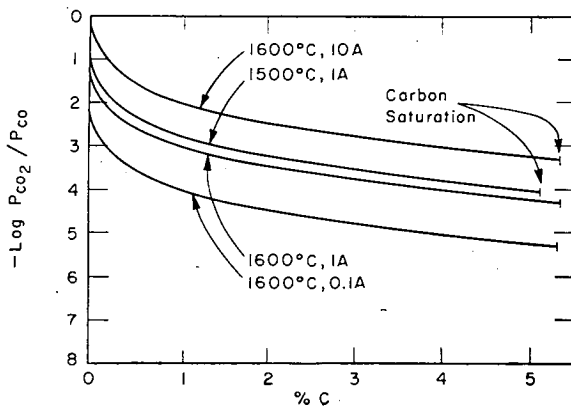
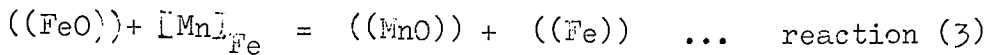


fig. 2.3.  $CO_2/CO$  ratios in equilibrium with iron - carbon alloys (40).

2.1.2.2. Oxygen - manganese equilibria. The influence of manganese on oxygen content of steel is best obtained from a consideration of reaction (3), where



double round brackets indicate a liquid state. The solution of manganese in iron is approximately ideal. Bell (28) concludes from a review of the available literature, that MnO and FeO are completely miscible in the liquid state and that complete miscibility in the solid state is probable. Fig. 2.4 is the diagram according to Hay, Howat & White which is reprinted by Levin & McMurdie. (47) The significant point made by Bell, was that only a limited range of FeO - MnO compositions are liquid at steel making temperatures. This was held to be a distinct disadvantage to manganese as a deoxidiser.

Mixtures of FeO and MnO behave approximately as ideal solutions in the liquid and solid states and because of this, the equilibrium constant  $K_{\text{MnO}}$  for reaction (3), can be expressed in terms of mole fractions of oxides and wt % concentrations of manganese. The values of  $K_{\text{MnO}}$  published in recent years, and reviewed by Bodsworth, are all very similar. Equation 2.9. is that determined by Chipman, Gero & Winkler. (48)

$$\log K_{\text{MnO}} - 0 = \frac{6,440}{T} - 2.95 \quad \dots \quad \text{eq. 2.9}$$

More recent investigations by Bell (49) & Fischer & Fleischer (50) give values of 3.5 and 3.4

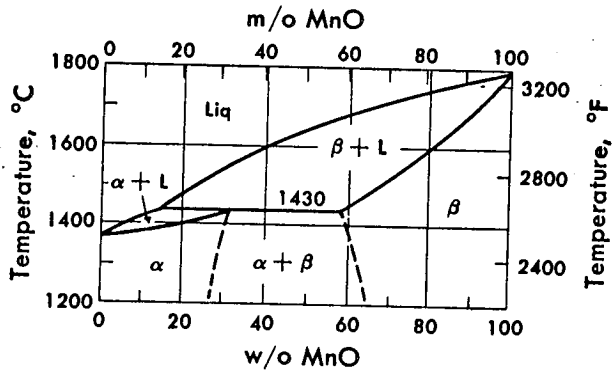


fig.2.4. FeO - MnO phase diagram.

respectively at 1550°C. Bell compares his results with those of previous determinations and obtains agreement with Chipman et. al. Slag compositions were similar in these investigations, but Fischer & Fleischer used MnO crucibles and their slags were not directly comparable. From this it appears that Chipman's value of  $K_{Mn-O}$  at 1550°C can be used over a wide range of compositions.

Caryll & Ward (51) introduced a new technique for the study of slag/metal equilibria with their use of levitation melting for determination of manganese - oxygen relations in steel. Higher temperatures and a greater variety of slag compositions were possible than could be employed by conventional techniques using refractory crucibles. The authors show that very rapid equilibration is achieved and that the high temperature compositions can be retained by quenching between a copper anvil and a copper faced piston. Analyses were made by using an electron-probe microanalyser.

The results from this complement those of Chipman et.al.(48) and the combined data are represented by equation 2.10

$$\log K_{Mn-O} = \frac{6,086}{T} - 2.76 \dots \text{equ. 2.10}$$

The oxygen content of the melt is obtained by combining  $K_{Mn-O}$  data with the oxygen solubility data from equ.2.2. Figs. 2.5 & 2.6 illustrate the manganese - oxygen relations of Chipman, Gero & Winkler.

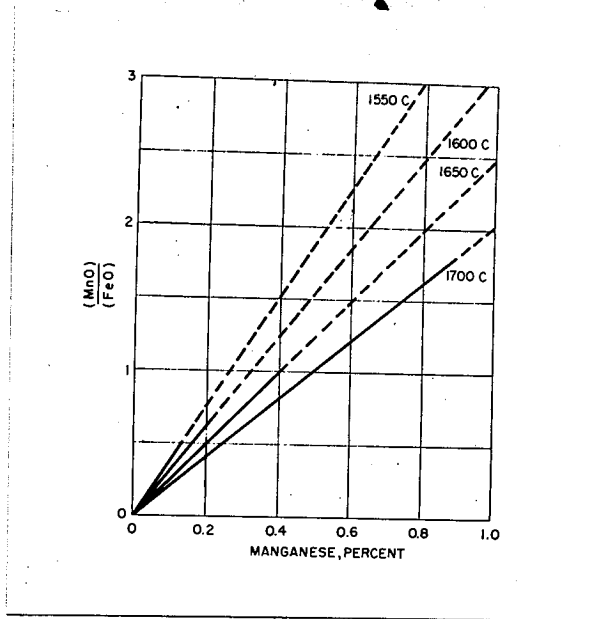


fig. 2.5

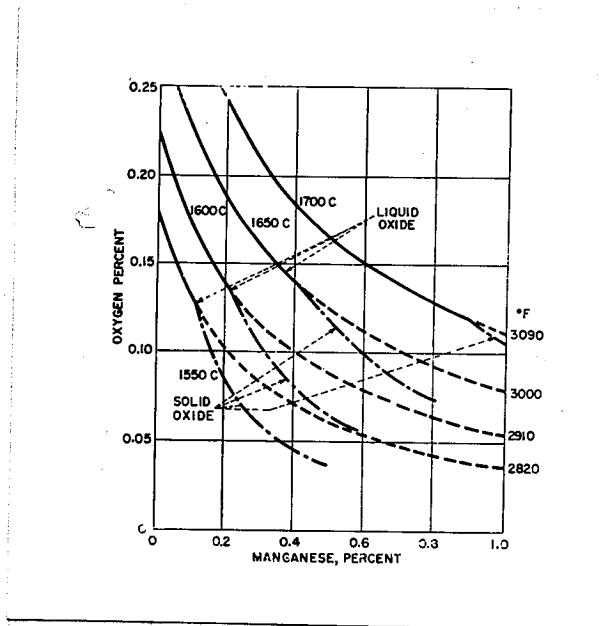
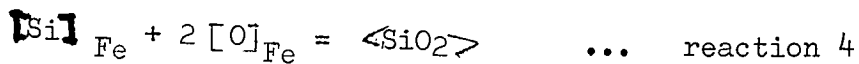


fig. 2.6

Manganese - oxygen equilibrium under FeO - MnO  
slags. (Chipman et.al. 48)

2.1.2.3 Oxygen - silicon equilibria. Early work on the equilibrium for reaction (4) has been included in



the literature review by Bell. (28) The  $\langle \rangle$  brackets denote solid state. Work by Hilty & Crafts (52) is critically examined and compared with that of Gokcen & Chipman (53) who used a gas/metal technique with  $\text{H}_2/\text{H}_2\text{O}$  mixtures. The data generally agree quite well but Gokcen & Chipman were able to make qualitative conclusions regarding the activities of oxygen and silicon. They proposed that the activity coefficient of oxygen was reduced by silicon; the activity coefficient of silicon increases with increasing concentration; and that these effects are compensating in pure iron - silicon - oxygen alloys containing 0.02-0.15% silicon. The result of this is that over a range of compositions, the solubility product  $[\% \text{Si}][\% \text{O}]^2$  remains constant.

Walsh, Ramachandran & Fulton (54) give a detailed appraisal of all determinations of reaction (4) equilibria from the time of Hilty & Crafts. Many determinations of the equilibrium constant  $K_{\text{Si} - \text{O}}$ , also included a quantitative assessment of the interaction coefficients  $e_{\text{Si}}^{\text{Si}}$  and  $e_{\text{O}}^{\text{Si}}$ . The value of  $e_{\text{Si}}^{\text{O}}$  is usually calculated from the reciprocal relationship  $e_{\text{Si}}^{\text{O}} = M_{\text{O}} \cdot e_{\text{O}}^{\text{Si}} / M_{\text{Si}}$ , where  $M_{\text{Si}}$  and  $M_{\text{O}}$  are the atomic weights of silicon and oxygen respectively.

The most recent and reliable work is due to Matoba Gunji & Kuwana (55) and Chipman & Pillay (56). Matoba et.al. conclude that the equilibrium is best represented by equ. 2.11 which Chipman & Pillay have confirmed.

$$\log K_{\text{Si} - \text{O}} = \frac{29,700}{T} - 11.24 \quad \dots \quad \text{equ. 2.11}$$

The interaction coefficients are linear functions of concentration up to 2% and are compatible with a constant solubility product. The coefficient  $e_{\text{Si}}^{\text{Si}}$  is given as a temperature dependent function in equ. 2.12, and in accordance with the

$$e_{\text{Si}}^{\text{Si}} = \frac{3,910}{T} + 1.77 \quad \dots \quad \text{equ. 2.12}$$

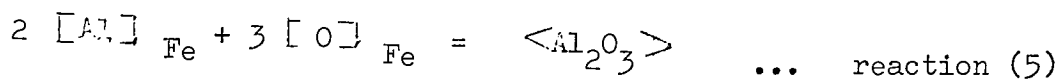
observation of a constant solubility product  $e_{\text{O}}^{\text{Si}}$  follows as  $0.5 e_{\text{Si}}^{\text{Si}}$ . These are the presently accepted values and were used with some success by Walsh et.al. in developing their thermodynamic model of deoxidation.

At low concentrations of silicon the equilibrium product is not solid silica, as indicated by reaction (4) but consists of liquid FeO-SiO<sub>2</sub> mixtures. The solubility of silica in FeO-SiO<sub>2</sub> mixtures, is approximately 50% at 1600°C and the oxygen content of iron in equilibrium with slag of this composition was found by Gokcen & Chipman to be 0.088%.

2.1.2.4. Oxygen - aluminium equilibria. Aluminium has the most stable oxide compared with oxides of other deoxidisers in common use, but measurement of the equilibrium constant  $K_{\text{Al} - \text{O}}$



for reaction (5) has been difficult due to problems in experimental technique and analyses



A theoretical constant was calculated by Chipman (57) using available thermodynamic data and showed that at 1600°C  $K_{\text{Al} - \text{O}}$  was  $2 \times 10^{-14}$ . A similar calculation by McLean & Ward (58), using more recent data and a value of  $\gamma_{\text{Al}}^{\circ} = 0.063$  for the Raoultian activity coefficient of aluminium in dilute solution with iron gives the equilibrium constant described by equation 2.13, from which  $K_{\text{Al} - \text{O}}$

$$\log K_{\text{Al} - \text{O}} = + \frac{64,090}{T} - 20.41 \quad \dots \quad \text{eq. 2.13}$$

is computed as  $1.5 \times 10^{-14}$  at 1600°C.

Early attempts to measure the equilibrium directly produced much higher values than the theoretical constant. Bell (49) and McLean & Bell (59) explain the high values of Wentrupp & Hieber (60) as being due to incomplete separation of alumina and those of Gelle & Dickze (61) by the interaction effects due to the presence of carbon in the melts. Hilty & Crafts' (62) constant is very high and they observed that at aluminium concentrations below 0.1% the inclusions consisted of  $\text{FeO} + \text{Al}_2\text{O}_3 \cdot \text{FeO}$  and at higher concentrations of aluminium they were  $\text{Al}_2\text{O}_3 \cdot \text{FeO} + \text{Al}_2\text{O}_3$ . The presence of hercynite ( $\text{Al}_2\text{O}_3 \cdot \text{FeO}$ ) was due to their method of equilibration and Chipman (63) shows that when the free energy

of hercynite formation is taken into account, the results of Hilty & Crafts approximate to those of other workers.

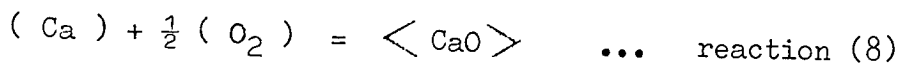
Determinations by Gokcen & Chipman (64) and the recent results of d' Entremont et.al., (65) and McLean & Bell (59) all give values of  $K_{Al - O}$  which are similar to the theoretical constant and also give values to the interaction coefficients. The value of  $e_{Al}^{Al}$  at 1600°C is widely accepted as approximately + 0.05 and the most recent value is that of McLean & Bell at + 0.048. There is a much greater discrepancy however, in the values quoted for  $e_{O}^{Al}$  and  $e_{Al}^{O}$  but their effects are much greater than  $e_{O}^{O}$  or  $e_{Al}^{Al}$  on the equilibrium constant  $K_{Al - O}$ . The effect of these interactions is agreed (59, 65 & 64) to produce a large negative deviation from Henry's Law,  $e_{O}^{Al}$  having a greater effect than  $e_{Al}^{O}$ .

Gokcen & Chipman quote the highest value for  $e_{O}^{Al}$  but the other values between these workers agree within a factor of three. This is not considered unreasonable in view of the experimental and analytical difficulties involved.

Sims (66) suggested, on the basis of Hilty & Crafts findings, that all steels deoxidised with aluminium would have hercynite in the equilibrium products instead of pure alumina. Subsequent work by Pillay et.al. (67) indicated, from observation of crucible attack, that a critical oxygen content in the iron was necessary for hercynite to be formed on contact with alumina. At 1600°C



the oxygen content of iron in equilibrium with solid magnesia and magnesium vapour at 1 atm. pressure would be  $1.5 \times 10^{-7}$  wt.% at  $1600^{\circ}\text{C}$ . A similar calculation can be made for calcium by combining the data for reactions 8 & 9 to give



$$\Delta G^{\circ} 8 = -187,900 + 45.7 T \quad \text{cals/mole.}$$



$$\Delta G^{\circ} 9 = 28,000 - 0.69 T \quad \text{cals/mole.}$$

the equilibrium constant of reaction (10a),  $K_{(\text{Ca}) - \text{O}}$ .

$$\frac{(\text{Ca}) + [\text{O}]_{\text{Fe}}}{\log K_{(\text{Ca}) - \text{O}}} = \frac{\langle \text{CaO} \rangle}{\dots \text{ reaction (10a)}} = - \frac{\Delta G^{\circ} 8 + \Delta G^{\circ} 9}{4.575 T} = + \frac{34,951}{T} - 9.84$$

From this it follows that the oxygen content of iron in equilibrium with solid lime and calcium vapour at 1 atm. pressure at  $1600^{\circ}\text{C}$  would be only  $1.48 \times 10^{-9}$  wt %.

The volatility of these metals is very high, and at  $1600^{\circ}\text{C}$  Chipman (68) gives the vapour pressure of calcium as 1.8 atm. and that of magnesium at 17.6 atm. This volatility and the apparent insolubility of calcium and magnesium caused little interest to be taken in their equilibrium with iron. Much of the work on solubility measurements however, failed because of experimental difficulties.

The most recent equilibrium study was that of Philbrook, Goldman & Helzel (70) who equilibrated liquid lime - alumina -

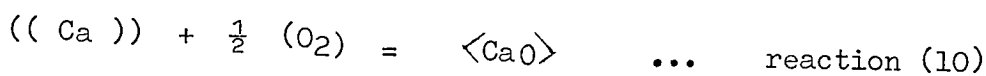
silica slags containing radioactive calcium with carbon saturated iron at 1600°C. They concluded that the calcium content of the iron was less than  $6 \times 10^{-5}$  wt %.(The lower limit of detection). This however, can be shown by the following treatment to be a reasonable result. Neglecting that the activity of lime in the slag is less than unity, and also neglecting the free energy of solution of calcium in iron, it follows that the calcium required for equilibrium with oxygen in a carbon saturated iron melt would be  $3 \times 10^{-6}$  wt % at 1600°C. In Philbrook's experiments therefore, it seems that residual oxygen in the iron prevented lime in the slag contributing a detectable amount of calcium to the melt.

It is only recently, with the work of Trojan & Flinn (71) and Sponseller & Flinn(72) , that solubilities of calcium and magnesium in iron base melts have been measured. The method used by these workers was to equilibrate calcium or magnesium with iron base melts in a pressurised furnace, such that a liquid layer of the volatile metal was maintained on the melt surface throughout the experiment.

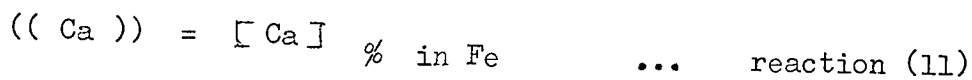
Trojan & Flinn, working with iron - carbon - silicon - magnesium melts at 1260 - 1420 °C, found magnesium solubilities up to 3% in carbon saturated iron containing silicon. They showed that the solubility increased with increasing temperature and increasing carbon and silicon contents. It would be difficult

to extrapolate their data to steel making conditions at 1600°C and much lower carbon and silicon contents, but it does seem likely that a significant solubility exists.

Sponseller & Flinn determined the solubility of calcium in iron at 1605°C as 0.032% and its activity coefficient  $\gamma_{Ca}$  as  $2.23 \times 10^{-3}$ . By using the regular solution concept and assuming that  $\gamma_{Ca}^{\circ}$  is approximately equal to the reported value of  $\gamma_{Ca}$ , a further step may be made to calculate the calcium - oxygen equilibrium in iron,  $K_{Ca-O}$ . Combining the free energy data for reactions (9), (10) and (11) provides an estimate for that of reaction (12).



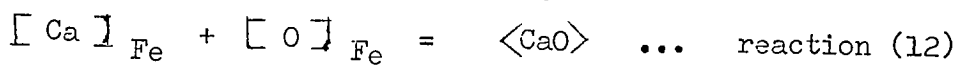
$$\Delta G_{10}^{\circ} = -152,850 + 25.78 T \quad \text{cals/mole.}$$



$$\Delta G_{11}^{\circ} = RT \ln \left[ \frac{\gamma_{Ca}^{\circ} \cdot 0.5585}{\text{At. wt. Ca}} \right] \dots \quad \text{equ. 17}$$

Substituting values in equ. 2. 17 gives:

$$\Delta G_{11}^{\circ} = 12,798 \quad \text{cals/gm. atom at } 1600^{\circ}\text{C}$$



$$\Delta G_{12}^{\circ} = \Delta G_{10}^{\circ} - \Delta G_{11}^{\circ} - \Delta G_{9}^{\circ} = -88,070 \text{ cal/mole at } 1600^{\circ}\text{C.}$$

$$\therefore K_{Ca-O} = 1.9 \times 10^{-10} \text{ at } 1600^{\circ}\text{C.}$$

It is evident, therefore, that if calcium went temporarily into solution during the deoxidation process and equilibrated with the oxygen before boiling out, a very low residual oxygen content would be obtained. Similar considerations would apply also for magnesium, but as its oxide stability is not as great as lime it would not be quite as effective a deoxidiser unless its solubility were greater.

2.1.4. Complex deoxidisers and oxide activities. The preceding section has considered the equilibria between individual deoxidiser elements and oxygen in liquid iron, but more than one deoxidiser is commonly added to steel. When two or more deoxidisers are present together in the steel, the product is likely to be a mixture of oxides and the equilibria established often differs from those of the individual deoxidisers.

A change in the degree of deoxidation accompanies the change in solute equilibria and, in general, enables a lower residual oxygen content to be achieved by lowering the activities of the component oxides in the product or by increasing the activity coefficients of the reacting solutes. The beneficial effects of solute interactions are small however, when compared with the possible reductions in oxide activities. Unfortunately there is very little quantitative data available for complex deoxidisers, as noted by Bell (28) & Chipman (41), except that relating to manganese - silicon deoxidation.

Bell (28) has reviewed much of the early work on manganese - silicon deoxidation and concluded that manganese increases the deoxidising power of silicon but not to the extent reported by Hilty & Crafts. It appears likely that the FeO - MnO - SiO<sub>2</sub> slags used by Hilty & Crafts picked up alumina from the crucible and their melts then equilibrated with FeO - MnO - SiO<sub>2</sub> - Al<sub>2</sub>O<sub>3</sub> slags. Samples of the slag were not obtained however, and no investigation of the inclusions was made. It is not possible therefore, to directly confirm this effect.

Healy (73) and Scimar (74) independently published calculated diagrams of the equilibrium between FeO - MnO - SiO<sub>2</sub> slags and molten iron. These diagrams showed agreement with the available data but, at the same time, Bell (49) reported an experimental study of the system at 1550°C and it is this latter work which is considered most applicable. Bell used crucibles of either silica or magnesia to obtain silica saturated or unsaturated slags respectively. The influence of manganese on silicon deoxidation is shown from his work in fig. 2.8. It was also concluded that ideal mixing of silicates occurred in the systems FeO - MnO - SiO<sub>2</sub> and FeO - MnO - SiO<sub>2</sub> - MgO and on this basis the isoactivity curves shown in fig. 2.9 were calculated. It is considered that these data are the most reliable for this system, even though the gas/metal equilibrium studies result in a higher equilibrium constant for silicon deoxidation than is indicated by Bell's work.



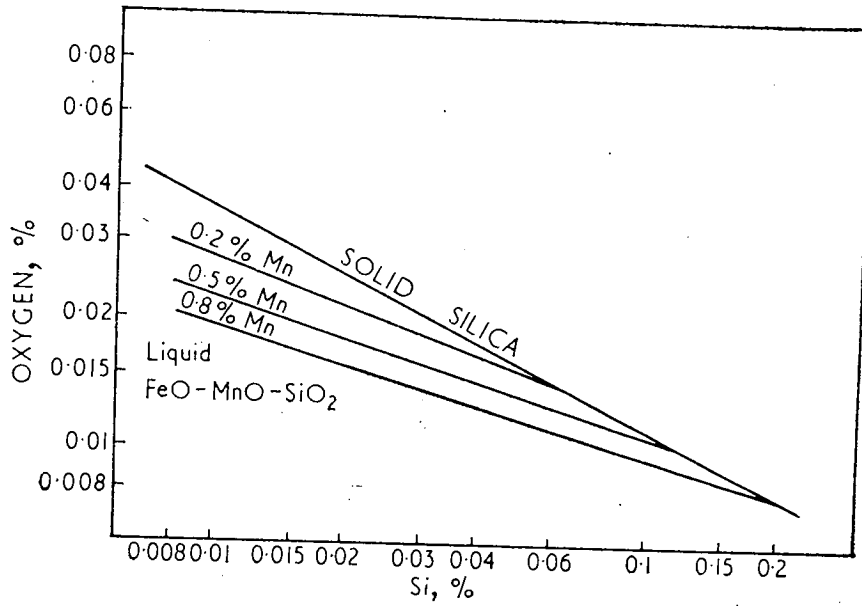


fig. 2.8. Effect of manganese on the silicon - oxygen equilibrium in liquid iron at 1550° C.

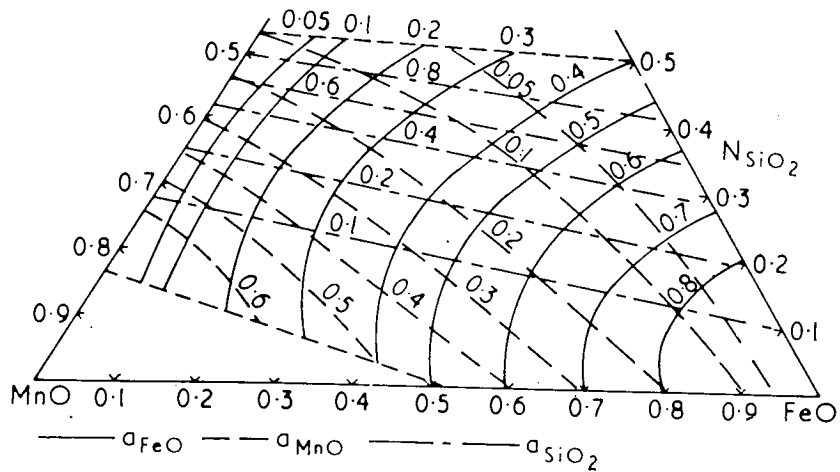


fig. 2.9. Isoactivity curves in FeO - MnO - SiO<sub>2</sub> slags at 1550° C.

Walsh & Ramachandran (75) relate the variation of silica activity in FeO - MnO - SiO<sub>2</sub> slags to the manganese : silicon activity ratio in the melt. In doing this, they combine the silicon - oxygen equilibrium constant of Chipman & Pillay with the manganese - silicon - oxygen data of Hilty & Crafts at various temperatures. On the basis of this data however, the activity of silica becomes unity at manganese : silicon activity ratios less than 1.7 whilst on the basis of Bell's data, the manganese:silicon ratio must be less than 4 to give silica of unit activity. The discrepancy is due to the effect of alumina in Hilty & Crafts experiments mentioned previously.

The effect of adding aluminium to the manganese - silicon deoxidiser has not been examined, but it is expected that alumina formed in the products would cause a decrease in the activity of silica and manganese oxide. If the criticism of Hilty & Crafts results is valid, then a slag containing alumina, silica, manganese oxide and iron oxide should equilibrate with a lower oxygen content melt for a given manganese : silicon ratio. The only activity data available on the manganese oxide - silica - alumina system is that of Sharma & Richardson (76). Manganese oxide activity is shown in fig. 2.10. This shows that at MnO concentrations of less than 0.4 mole fraction, the activity coefficient of MnO approaches a similar value to that of 0.2

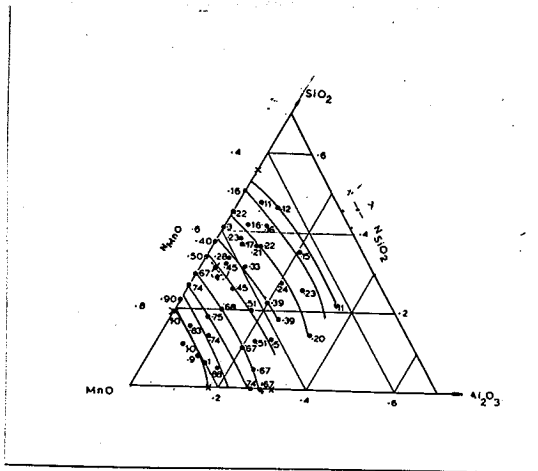


fig. 2.10. Activity of MnO in MnO - SiO<sub>2</sub> - Al<sub>2</sub>O<sub>3</sub> melts, relative to pure solid.

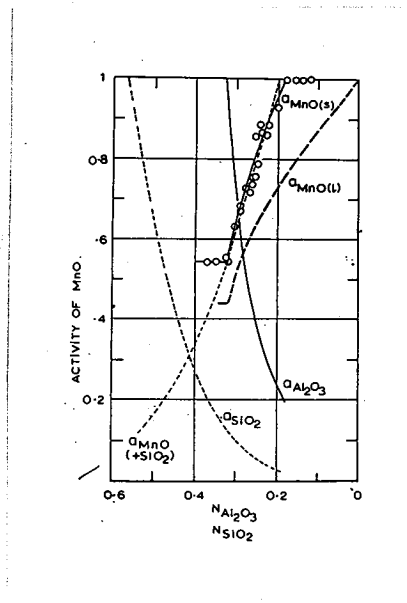


fig. 2.11 Activities in binary oxide melts.

obtained by Bell in the  $\text{MnO} - \text{SiO}_2 - \text{FeO}$  system. The activities of components in the  $\text{MnO} - \text{SiO}_2$  and  $\text{MnO} - \text{Al}_2\text{O}_3$  binary systems are shown in fig. 2.11 which is taken from Abraham, Davies & Richardson (77).

Deoxidation with calcium - silicon - aluminium or magnesium - silicon - aluminium alloys may result in products containing lime or magnesia in addition to silica and alumina. The consequent reduction in silica activity which would occur can be seen from figs. 2. 12 and 2. 13. These isoactivity curves are due to Cameron, Gibbon & Taylor (78) and Henderson & Taylor (79) respectively.

## 2.2. Kinetics of deoxidation processes.

2.2.1. Nucleation and growth of products. The bulk of research concerning deoxidation has been directed to the study of chemical equilibrium relationships and, because of this, very little information has been available on the kinetic aspects of formation and growth of inclusions. Within the past few years however, some theoretical and quantitative experimental work has been published which clarifies the situation, with particular reference to homogeneous nucleation.

von Bogdandy, Meyer & Stranski (80 & 81) studied the formation of oxides in iron - oxygen melts by equilibrating a column of the melt with a quantity of deoxidiser added to the top surface.

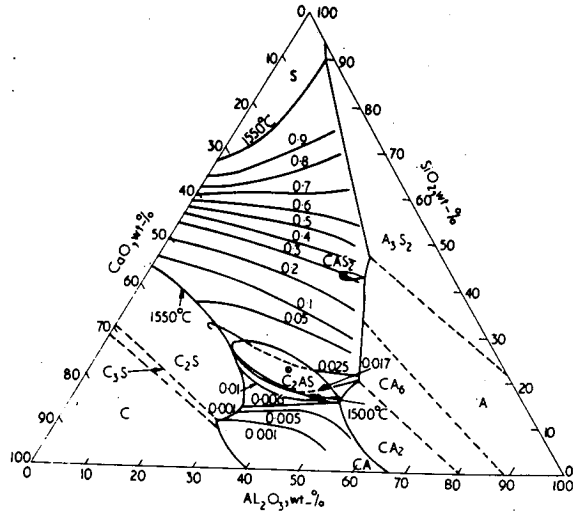


fig.2.12. Activity of silica in  $\text{CaO-Al}_2\text{O}_3\text{-SiO}_2$  system at  $1550^\circ\text{C}$

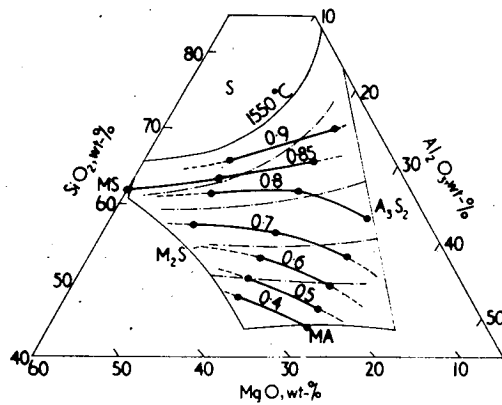


fig.2.13. Activity of silica in  $\text{MgO-Al}_2\text{O}_3\text{-SiO}_2$  system at  $1550^\circ\text{C}$ .  
(Full lines are those of Henderson & Taylor ).

Convection currents were virtually eliminated and penetration of the deoxidiser into the melt occurred only by diffusion. The column was quenched after predetermined diffusion periods and the diffusion zone was examined metallographically and analytically. Their results on aluminium deoxidation showed that the oxygen combined to form alumina in the aluminium rich zone and iron oxide in the aluminium deficient zone. Only a few traces of hercynite were observed throughout the experiments. The oxygen content was found to remain constant along the column and so it was concluded that the inclusions remained in their position of formation.

The supersaturation ratio ( $C_r / C_{cr}$ ), at which alumina is precipitated at  $1550^{\circ}\text{C}$ , was obtained from eq. 2.18 using the aluminium and oxygen concentrations measured at the boundary between unaffected melt and the zone rich in alumina particles.

$$\left(\frac{C_r}{C_{cr}}\right) = \frac{[\% \text{ Al}]^2 [\% \text{ O}]^3}{k_{\text{Al} - \text{O}}} \dots \text{ eq. 2.18}$$

$k_{\text{Al} - \text{O}}$  is the deoxidation constant of aluminium given as the reciprocal of the equilibrium constant  $K_{\text{Al} - \text{O}}$ . The saturation ratio was determined as  $3.6 \times 10^{14}$  and related to the average nucleus diameter,  $r_k$ , by the Gibbs - Thompson equation ( 2.19 )

$$\ln \left(\frac{C_r}{C_{cr}}\right) = \frac{2 \sigma \cdot M}{p \cdot R \cdot T \cdot r_k} \dots \text{ eq. 2.19}$$

$\sigma$  is the interfacial energy between alumina and iron,  $M$  is the

molar weight of alumina,  $\rho$  is its density and R is the gas constant in ergs / ° C mole.

From this Bogdandy et.al calculated the nucleus diameter was of the order of one molecule. The interpretation was that the rate controlling stage was the formation of a discrete alumina particle rather than the establishment of a large particle.

The work of Turpin and Elliot (82) starts with an application of the classical theory of Gibbs, Volmer & Becker, to homogeneous nucleation of oxide inclusions in steel. The critical supersaturation, expressed as a free energy term  $\Delta G_{crit}^{hom}$ , is calculated from eq. 2.20  $v$  is the molar

$$\Delta G_{crit}^{hom} = - 2.7 v (\sigma^3 / k T \log A)^{1/2} \dots \text{equ. 2.20}$$

volume of the nucleus species,  $\sigma$  is the interfacial tension between nucleus and matrix, k is Boltzmann's constant and A is a frequency factor characteristic of each oxide considered. Values of  $\Delta G_{crit}^{hom}$  were calculated using estimates of the interfacial tension, and the solute concentrations necessary for homogeneous nucleation were then calculated by the general expression shown in eq. 2.21,  $k_a$  is the activity product

$$\Delta G_{crit}^{hom} = - R T \ln \left( \frac{k_a}{k} \right) \dots \dots \text{equ. 2.21}$$

$a_{Si} \cdot a_{O}^2$  or  $a_{Al} \cdot a_{O}^3$  and k is the appropriate deoxidation constant. The results of these calculations are summarised in figs. 2.14 and 2.15 for the iron - oxygen - silicon and iron - oxygen - aluminium systems.

Useful experiments were made by equilibrating iron - oxygen melts with various residual silicon or aluminium contents and then quenching. The supersaturation for inclusion nucleation was obtained by the high degree of oxygen segregation to the liquid during solidification. On the basis of the results they conclude that the interfacial tensions between oxide and melt, in ergs.  $\text{cm}^{-2}$ , are approximately 250 for iron oxide, 1,250 for silica, 2,400 for alumina and 1,700 for hercynite.

The critical supersaturation calculated for alumina nucleation using equ. 2.20 and the above data at  $1550^{\circ}\text{C}$ , is - 66.6 k.cals/mole. Whilst that observed by von Bogdandy et.al is calculated from equ. 2.21 and their  $C_r/C_{cc}$  ratio, as - 121.5 k.cals/mole. The difference is due to uncertainty in the composition of von Bogdandy's melts at the point where supersaturation is reached.

The observations noted on figs. 2.14 & 2.15 concerning the conditions under which iron oxide is the nucleating phase, are supported by the results of other workers who produced similar inclusions to those of Turpin & Elliot at low silicon concentrations during deoxidation studies. Turpin & Elliot also concluded from the high supersaturation needed for homogeneous nucleation, that the liquid metal composition which determines the nucleus composition, restricts its growth to the addition of material having a similar composition.



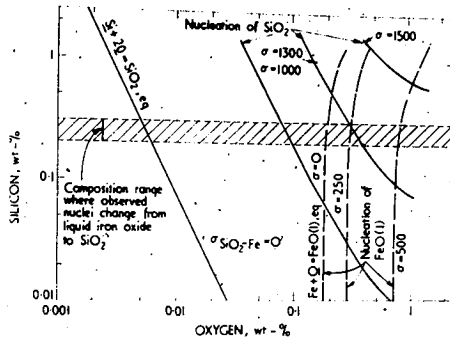


Fig. 2.15. Effects of interfacial tension and melt composition on nucleation of oxides in Fe-O-Si system, 1536°C (interfacial tension  $\sigma$  in ergs/cm<sup>2</sup> ).

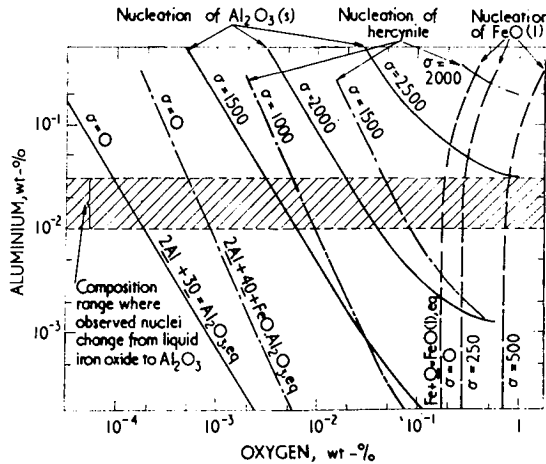


Fig.2.15. Effects of interfacial tension and melt composition on nucleation of oxides in Fe-O-Al system, 1536°C (interfacial tension  $\sigma$  in ergs/cm<sup>2</sup> ).

Applying the homogeneous nucleation theory to normal deoxidation practice led Turpin & Elliot to predict that a large number of small inclusions will be formed when a deoxidiser is added to the melt, because a very high degree of supersaturation will exist until the deoxidiser is completely dissolved and distributed throughout the melt. From this they suggest that less powerful deoxidisers will give the most rapid separation of products.

The very recent work of Woehlbier & Rengsdorff (83) used a technique similar to that of von Bogdandy et.al. with a very pure iron - oxygen melt and a 10% aluminium in iron alloy as deoxidiser. They reported exceptional nucleation difficulties at 1600°C and illustrated this by saying that no oxide nuclei were formed in the diffusion zone, although the aluminium concentration was 2.9% and, inclusions formed on quenching showed a high oxygen concentration to be present. The same experiment was repeated using a less pure iron, containing 0.07% oxygen instead of 0.16% and this was found to be partially deoxidised. It was concluded that a very high supersaturation is required for homogeneous nucleation of alumina but a much lower supersaturation is sufficient to enable growth of alumina on small heterogeneous nuclei without the appearance of hercynite.

It may be noted however, that at 1,600°C and aluminium concentrations in excess of 0.03%, the equilibrium % oxygen

increases with further increases in aluminium concentration because of the effect aluminium has on the oxygen activity coefficient. Assuming that the value of  $e_{O}^{Al} = -0.94$  applies up to an aluminium concentration of 2.9%, then the oxygen activity would be reduced by  $1.5 \times 10^{-3}$  and the system would be hardly supersaturated.

Further experiments by Woehlbier & Rengsdorff in which pure aluminium was stirred into the upper zone of the pure oxygen - iron melt, resulted in the formation of alumina inclusions from homogeneous nucleation at the point of addition. These inclusions were then carried down into the undeoxidised portion of the melt and reacted with residual oxygen to form hercynite. This technique provides the same result as would be expected from stirring alumina particles into a high oxygen content melt and allowing the equilibrium studied by McLean & Ward (58) to be approached. In the absence of any melt analyses or time dependent results, it serves only as a possible mechanism for the formation of hercynite.

The treatment of homogeneous nucleation made by Turkdogan (84) follows the same classical theory used by Turpin & Elliot and leads, by means of an example of silicon - manganese deoxidation, to the same conclusion regarding the formation of many small nuclei during the time taken for the deoxidiser to dissolve. He extends the theoretical approach by considering the growth of nuclei, using a

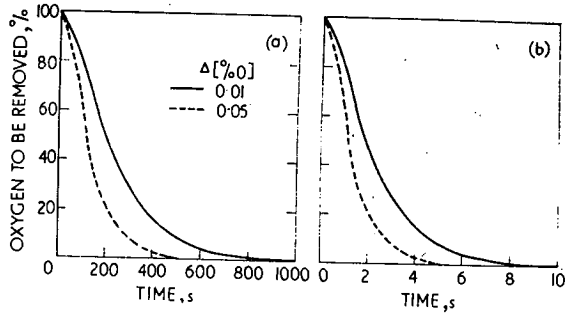
diffusion model developed for this purpose. The model results in the expression shown in equ. 2.22 for the

$$r_i = 0.379 r_o \left( \left[ \% O \right]_o - \left[ \% O \right]_m \right) \dots \text{equ.2.22}$$

radius of a growing inclusion  $r_i$  at any time,  $t > 0$ ,  $r_o$  is the radius of the spherical diffusion zone and is given as  $0.62 Z^{-\frac{1}{3}}$  where  $Z$  is the number of growing inclusions per  $\text{cm}^3$  and is assumed constant.  $\left[ \% O \right]_o$  is the initial oxygen content at time  $t = 0$  and  $\left[ \% O \right]_m$  is the oxygen content at any time  $t > 0$ .

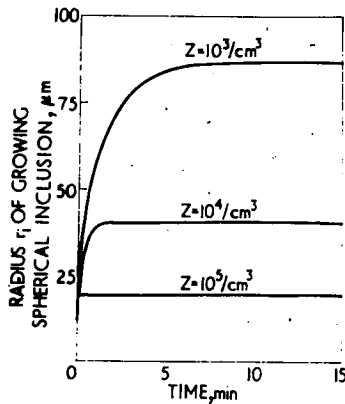
Fig. 2.16 shows the predictions made from this model which support the qualitative view that high supersaturations are likely to result in small inclusions which separate only slowly from the melt. Fig. 2.17 shows how the maximum size of inclusions and their rate of growth are dependent upon the concentration of nuclei. These figures summarise the important effects of nucleation and growth as applied to practical deoxidation procedures.

2.2.2. Separation of products. Two of the major objects in practical application of deoxidation during steel making, are to reduce the dissolved oxygen content to a low concentration, so that secondary products formed during cooling and solidification are minimized, and to eliminate as completely as possible, the primary products. The first of these objectives is largely determined by the thermodynamics of the process but the



Percentage of oxygen to be removed as a function of time for (a):  $Z=10^3/\text{cm}^3$  or  $r_0=6.2 \times 10^{-2} \text{ cm}$  (b):  $Z=10^6/\text{cm}^3$  or  $r_0=6.2 \times 10^{-3} \text{ cm}$  (particles are considered to be stationary in the melt).  $\Delta[\%O]$  is difference between initial and final equilibrium oxygen contents, e.g.  $\Delta[\%O]=[\%O]_0-[\%O]_1$

fig. 2.16. (from E.T. Turkdogan 84).



Effect of number of nuclei in melt on the rate of growth of oxide inclusions, as they rise in the melt, for  $[\%O]_0=0.05$  and  $[\%O]_1=0$

fig. 2.17. (from E.T. Turkdogan 84).

separation of primary deoxidation products is essentially controlled by physical factors.

Schenck (85) shows that flotation of oxide particles, which are less dense than liquid iron, has been the separation mechanism assumed since the earliest investigations and according to this model the rate of rise ( $v$ ) of a spherical particle is given by Stoke's Law, equ. 2.23

$$v = \frac{2}{9} \cdot g \cdot \frac{r^2}{\eta} \cdot (\rho_{Fe} - \rho_{ox.}) \dots \text{equ. 2.23}$$

where  $r$  is the radius of the particle,  $g$  is the gravitational constant,  $\eta$  is the viscosity of the steel and  $\rho_{Fe}$  &  $\rho_{ox.}$  are densities of the liquid steel and oxide respectively. The viscosity of liquid steel is approximately  $0.065 \text{ dynes cm.}^{-2}$ ,  $g$  is  $981 \text{ cm. sec}^{-2}$  and the density difference between the liquid steel and oxide can lie between 1 and  $4.7 \text{ gm.cm}^{-3}$  when the oxide is liquid ferrous oxide or solid silica respectively. This illustrates that the particle radius is the factor which can have the greatest influence on the separation rate and this is also the factor which is liable to the greatest variation.

The importance of particle radius was shown by C.H.Herty and his coworkers, (86) when they found that manganese - silicon deoxidation gave the cleanest steel if the manganese : silicon ratio was between 4 - 7 : 1. This range of manganese - silicon ratio corresponded to the ratio range which resulted in the

largest size of inclusions. Also, the product composition resulting from this addition practice was found to be in the very low liquidus temperature range of compositions at approximately 35 - 45% SiO<sub>2</sub>, 45 - 55% MnO, 10% FeO. (see shaded area in fig.2.18). This led to the conclusion that low melting point products were advantageous because their fluidity enabled them to coalesce, thus increasing their size and improving their rate of flotation. The application of Stoke's Law however, was largely qualitative and when steel viscosities & oxide densities were measured more accurately the quantitative use of the law was restricted to determination of the largest size of residual particle in melts of given depths after various times. It was not possible to calculate the total concentration of oxides unless the number and average size of particle were known.

More recently Fisher (87) described a kinetic study of deoxidation with silicon in high frequency induction furnaces, which showed that separation of primary deoxidation products was very much more rapid in turbulent conditions than in quiescent conditions. This effect of turbulence has also been observed by other workers including Plöckinger et.al. (88 & 14) and Duderstadt & Weller,(89) who used aluminium and other deoxidisers to confirm

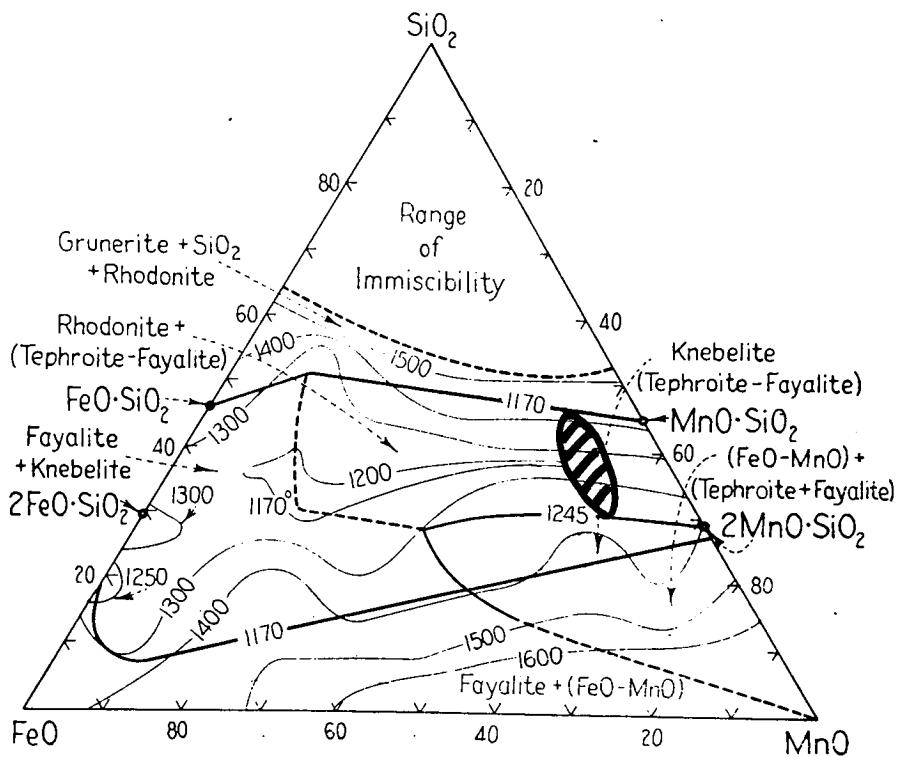


fig. 2.18  $\text{SiO}_2$  -  $\text{MnO}$  -  $\text{FeO}$  phase diagram (92).



the effect found with silicon. Fischer reported from the same work that primary silica products were separated very rapidly in basic lined furnaces ( CaO or CaO - CaF<sub>2</sub> ) but only slowly with acid lining. Further observations were that the time for total elimination of products decreased with increasing melt temperature, decreasing silicon addition and decreasing furnace size which increased the surface area to volume ratio.

Plöckinger & Wahlster (90) made a series of experiments in high frequency induction furnaces and found that deoxidation with silicon gave fluid, well coagulated products containing 98% silica, which confirmed the results of Fischer & Wahlster (91). Aluminium deoxidation resulted in solid alumina rich (97% Al<sub>2</sub>O<sub>3</sub>) particles which, although being smaller and less agglomerated, separated more rapidly than silica particles. Holding the melt quiescent in a ladle after deoxidation resulted in further separation of silica particles but very little further reduction in residual alumina was observed, all the separable particles having been removed in the initial period. They concluded from the difference in inclusion behaviour, that Stoke's Law was not entirely valid when comparing inclusion species and that the major reason for this was the difference in surface properties. They suggest that wetting of the silica, and silica rich particles, by the steel hinders their separation whereas alumina particles have a high surface tension and are not wetted and are,

therefore, unaffected by the melt/oxide interface properties. Repetylo et.al. (93) support this view by concluding from their work on aluminium deoxidation, that high interfacial tensions favour the rapid removal of particles. Crussard (94) has suggested that alumina particles in the form of clusters tend to separate as a single unit with a much larger radius than any of the individual particles. It should be noted, however, that the average density of such a unit would be approaching that of the melt and so some of the effect of increased size would be counteracted. The observation that residual alumina particles do not separate from a tranquil bath may be due to their small size or the mechanism of separation, or a combination of both.

Recent work by Ohkubo et.al. (95 & 96) has provided a model to explain the effects of turbulence and furnace lining material reported by Fischer & Wahlster, on the separation rate. The deoxidation experiments (95) were made in a high frequency induction furnace, using various temperatures, deoxidisers and furnace linings. They found that the oxide content of the steel could be expressed as a function of time by equ. 2.24

$$C = C_o e^{-kt} \quad \dots \quad \dots \quad \text{equ. 2.24}$$

where C is the oxide concentration at a time t following deoxidation at t = 0, C<sub>o</sub> is a constant and corresponds to the maximum oxide concentration i.e. concentration after addition of

deoxidiser but before any products have separated.  $k$  is the rate constant which depends upon, temperature, deoxidiser and crucible material. Ohkubo and Masui (96) include the surface area to volume ratio of the melt as a factor influencing  $k$ .

The work of Ohkubo et.al. (95) is at present, untranslated from the original Japanese but the model appears to assume that segregation of products by flotation, according to Stoke's Law, is completely eliminated and proposes that the mechanism of inclusion removal in an agitated bath is essentially one of reaction between the particle and crucible material. This model seems very reasonable provided that the turbulence is sufficient to present a melt surface in contact with the crucible which is continually changing and representing the oxide concentration in the bulk melt. Under these conditions, it is likely that an equation of the form shown in 2.25 would apply,

$$\frac{dc}{dt} = - k C \left( \frac{A}{V} \right) \quad \dots \quad \dots \quad \text{equ. 2.25}$$

where  $dc/dt$  is the rate of change of oxide concentration,  $C$  is the average oxide concentration of the bulk melt,  $k$  is the rate constant and  $A/V$  is the surface area to volume ratio of the melt. Upon integration between limits of  $t = 0$  at  $C = C_0$  and  $t = t$  when  $C = C$ , this would give equation 2.24.

The increase in separation rate of  $\text{SiO}_2$  in a basic lined furnace was confirmed and attributed to chemical reaction between

particle and furnace lining. Removal of silica by an acid lining would not involve chemical reaction and would depend only on surface action between particle and lining. The reduction of separation rate by increased silicon addition was also confirmed and can be explained because the residual dissolved oxygen after low silicon additions was approximately 0.09%. The deoxidation product therefore, would have been a liquid iron silicate (see section 2.1.2.3) which could react with, and adhere to, a siliceous lining to a greater extent than could solid silica products resulting from higher silicon additions. Rate constants determined after manganese - silicon deoxidation were greater than those determined for silicon acting alone and, similarly the rate constant for alumina separation was improved by the addition of manganese.

It is thought that this model can explain the rapid removal of oxides in the turbulent conditions during tapping where the reaction is likely to be between deoxidation products and ladle refractory &/or slag, and during teeming where reaction is likely to be with self-generated ingot scum.

Application of Stoke's Law to quiescent bath conditions to show a concentration - time relationship has also been attempted by Kawaw, Okubo & Sasajima (97). They show from experimental work that the size distribution of inclusions can be represented by equ. 2.26.

$$n = n_0 e^{-A\delta} \dots \dots \text{equ. 2.26}$$

where n is the number of inclusions per unit area having a radius greater than  $\delta$ .  $n_0$  and A are constants which may be determined experimentally.  $\delta$  was expressed in terms of Stoke's Law as  $(h / kt)^{1/2}$  where k is the product of collected constants and fixed values from equ. 2.23, h is the depth of the melt and t is the time.

From this basis equ. 2.27 was

$$\frac{c}{c_0} = \left( 1 - \frac{e^{-A\delta}}{6} \right) \left[ (A\delta)^3 + 3(A\delta)^2 + 6(A\delta) + 6 \right] \dots \text{equ.2.27}$$

derived, the symbols being as mentioned previously. Concentration - time curves calculated from this equation did not agree very well with their experimentally determined curves, and generally indicate a much slower separation rate than was observed. This equation however, will be discussed further in section 5, in the light of results from the present work.

From a consideration of the literature pertinent to product separation therefore, there seems to be fair agreement between experimental observations but it is only in recent years that the influences of some factors have been recognised and explained.

### 2.3. Technical applications of complex deoxidisers.

2.3.1. Deoxidisers containing volatile metals. Calcium has been used, in the form of calcium - silicon or calcium - aluminium alloys, for deoxidation over a period of years and various

opinions have been expressed concerning its effect.

Lillqvist (98) reports that none of the complex alloys available commercially were as effective as aluminium in preventing pinhole porosity in steel castings. Accordingly he recommends the use of aluminium, in quantities sufficient to produce type III sulphides, (66, 99 & 100) in preference to calcium containing deoxidisers. Ludwig (101) however, suggests that under certain optimum conditions of preliminary deoxidation the complex alloys can improve deoxidation efficiency and produce more favourable inclusion types.

Dunn (102) used various complex deoxidisers with type 302 stainless steel (18% Cr - 10% Ni) and claims that nickel - magnesium, calcium - magnesium - silicon, and calcium - manganese - silicon are more effective than calcium - silicon in producing cleaner steel of lower oxygen content. It may be noted from the work of Sponseller & Flinn (72) that 10% nickel increases the solubility of calcium in iron to 0.08% at 1600°C. Mandl & Skāla (103) concluded, from the results of iron - calcium - magnesium - silicon alloy deoxidation, that the optimum alloy composition for minimum inclusion content was approximately 28% calcium, 13% magnesium, 52% silicon with iron as balance. This is similar to the alloy used by Dunn (102), but has approximately 10% more magnesium. Ototani et.al. (104) used an alloy containing 23% calcium, 50% silicon, and 27% iron for deoxidation and found that

the cleanliness of the steel was improved. The optimum alloy composition found by Mandl & Skála, in the calcium - silicon - aluminium - iron system, was 30% calcium, 40% silicon, 20% aluminium and 10% iron which resulted in total oxide inclusion contents of approximately 0.012%. These figures agree well with the results of Tsekanski (105) who obtained a minimum oxide content of 0.016%, when using an alloy with 21% aluminium, 50% silicon, 22% calcium, 5% iron for ladle deoxidation. Much of the work on these systems supports the view referred to by Koch (106), that improved cleanliness is associated with, or due to, the turbulence caused by volatile metal vapour escaping from the steel.

Koch (106) made a detailed study of deoxidation with alloys containing calcium under an argon cover. He showed that ingot scum, composed of inclusions which had segregated to cavities near the surface, always contained more lime than the smaller and more evenly distributed residual inclusions. From this it was deduced that calcium combined with more of the total oxygen than had previously been thought. It was also noted that a greater proportion of the added calcium was lost by vaporization when the concentration of calcium in the deoxidation alloy was increased.

A patent taken out by Rossborough (107) describes calcium - silicon - aluminium alloys intended to produce low melting temperature oxides in the lime - silica - alumina system. (see phase diagram, fig. 2.19) The alloy compositions however, are based

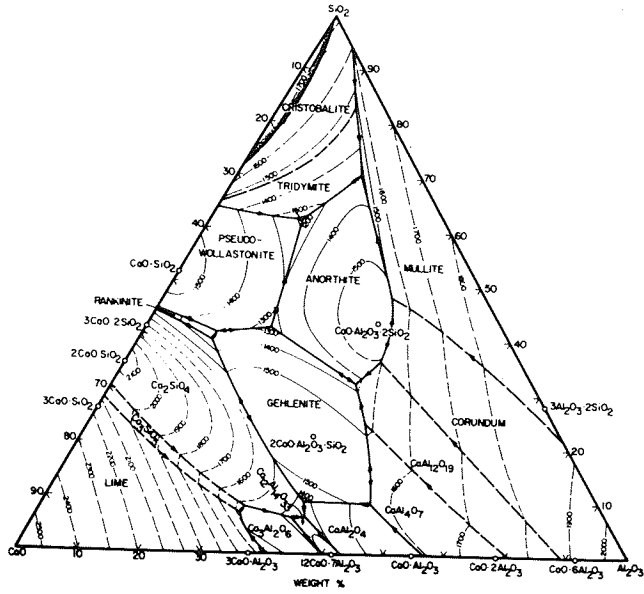


fig. 2.19.  $\text{CaO} - \text{SiO}_2 - \text{Al}_2\text{O}_3$  phase diagram

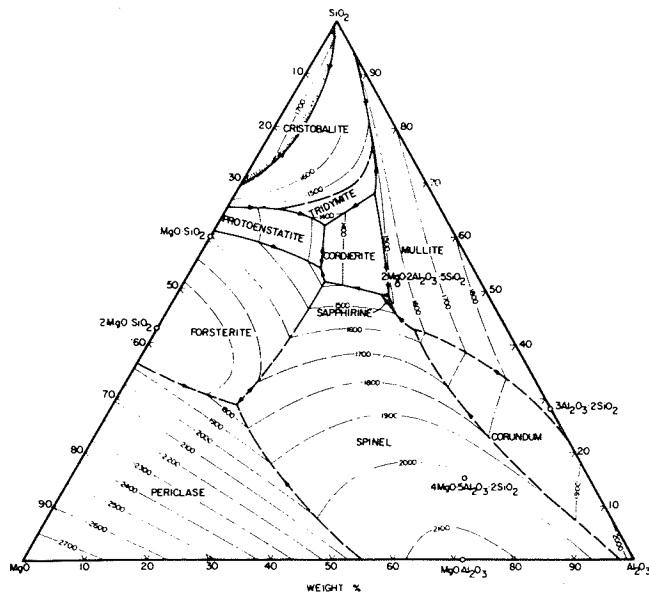


fig. 2.20.  $\text{MgO} - \text{SiO}_2 - \text{Al}_2\text{O}_3$  phase diagram



on stoichiometric calculations only, disregarding the appreciable effect of the necessary residual silicon and losses of aluminium and calcium.

Calcium - silicon - aluminium deoxidisers have also been studied by Wahlster & Feldhaus (108) who confirm much of Flöckinger & Rosegger's (88) work regarding the difference in separability between inclusion types and effects of turbulence. Flöckinger & Rosegger's view, that particle separation is dependent on the physical properties, is endorsed and it is added that these properties are dependent upon the particle composition. Wahlster & Feldhaus further conclude, in agreement with Koch, that calcium combines with part of the oxygen, but to a very variable extent. The efficiency of calcium is said to be less when added as calcium - aluminium alloy than when added as calcium - silicon alloy.

2.3.2. Deoxidisers based on the Mn-Si-Al system. Silico - manganese is probably the oldest of complex deoxidisers and many of its effects were determined from production plant trials as well as from laboratory experiments. Incorporation of aluminium into silico - manganese alloys however, has received much less attention, even though many low liquidus temperature compositions exist in the manganese oxide - silica - alumina system (see fig. 2.21.), and formation of liquid products was thought to be the beneficial result of using silico - manganese.

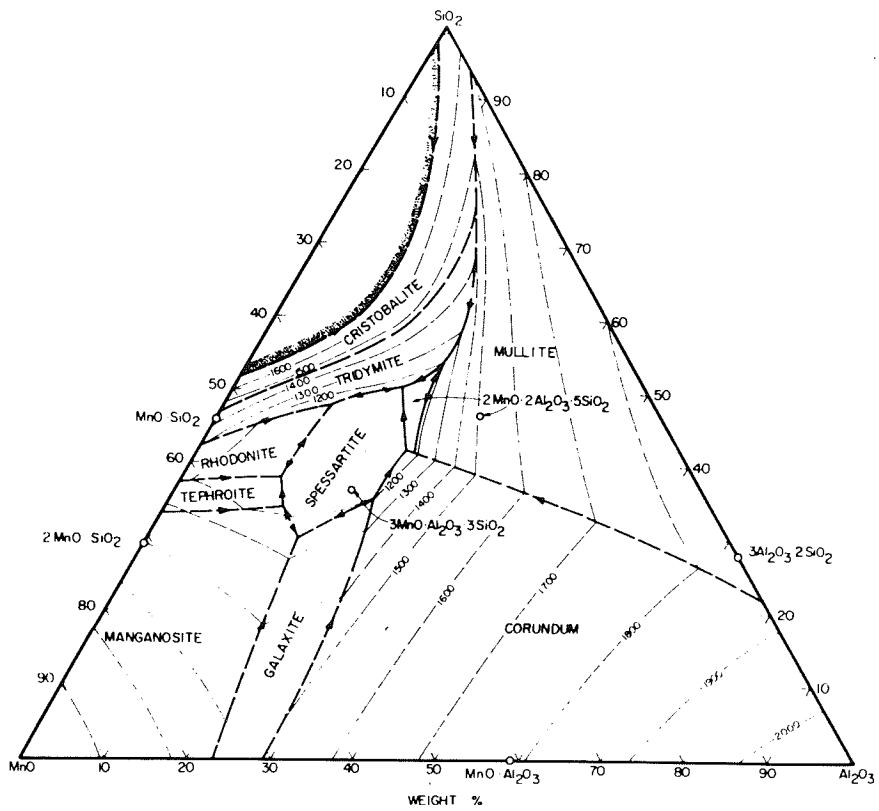


fig. 2-21. MnO - SiO<sub>2</sub> - Al<sub>2</sub>O<sub>3</sub> phase diagram

Mandl & Skála give the optimum composition of manganese - silicon - aluminium alloys for cleanest steel as approximately 58% manganese, 16% silicon, 10% aluminium and balance iron. They conclude, without theoretical interpretation, that complex alloys offer great possibilities for improving steel quality. The manganese oxide - silica - alumina system was examined by Göhler, (109) who determined temperatures at which various slag compositions became fluid and their surface tension at 1600°C. He subsequently tested various deoxidation alloys from the manganese - silicon - aluminium system and found that a ratio of 1 : 1 : 1 of these components gave similar residual inclusions to those found when using higher manganese and silicon contents. When the aluminium content of the alloy was increased however, there was an increase in inclusion content and also refractory attack with reduction of silica by aluminium. High aluminium contents were not therefore, recommended.

#### 2.4. Purpose of present work.

It may be seen from the preceding review that data concerning Ca-Si-Al and Mg-Si-Al deoxidisers, do not provide a clear or quantitative account of the function and effects of calcium and magnesium in complex deoxidisers. It is intended in the present work to examine the composition of products, and their separability from quiescent melts, in relation to the conditions of deoxidation.

Mn-Si-Al is to be studied because very little quantitative data is available and its oxide system provides a large range of compositions which are liquid at steel making temperatures. Comparison is then possible between silicon - aluminium deoxidisers containing volatile and non - volatile third elements.

## SECTION 3 EXPERIMENTAL PROCEDURE.

3.1. Selection of experimental conditions. The experimental programme was designed to investigate the deoxidation reaction and the behaviour of the resulting oxide products. The experimental conditions therefore, were carefully chosen to provide the clearest investigation of these objectives possible, with maximum freedom from external influences.

3.1.1. Melt material. The two criteria used for choosing a suitable melt material were that it should be free of sulphur and that it should contain a high concentration of oxygen.

The first of these conditions was imposed because the presence of sulphur is known to cause the formation of oxide/sulphide mixtures in the deoxidation product and the sulphide component of such inclusions greatly influences their character, behaviour and effects on the steel properties. (66,99 & 100)

The second condition is to enable a high concentration of inclusions to be formed on the addition of a deoxidiser, such that the composition and behaviour of the inclusions may be easily studied. In order to obtain a high oxygen concentration in the melt, it was necessary to choose a material which is free of elements having a high affinity for oxygen. The most readily available material which met these requirements of purity was carbonyl iron, the composition of which is shown in table 4.1.

An upper limit to the oxygen content was set by making it

comparable with that of steel at the end of refining. Typical values in basic open hearth steel making are 0.04 - 0.05% oxygen at this point if the carbon is less than 0.1% (109).

3.1.2. Crucible material. The most important consideration in the choice of crucible material, was that it should not take any part in the reactions occurring during the experiment.

Silica was not used because of its probable reduction by manganese or aluminium dissolved in the melt, at the 0.006 - 0.007% residual oxygen contents intended.

Recrystallised alumina was chosen because at 0.007% oxygen the residual aluminium is calculated as only 0.0001% (53). This equilibrium concentration of aluminium is sufficiently low to induce negligible melt/crucible reaction, even when aluminium is not present in the deoxidiser.

Magnesia crucibles were considered for use but, as the stability of magnesia at 1550°C is shown by fig. 2.7 to be almost the same as that of alumina, there appeared to be little advantage.

The oxygen content of the melt prior to deoxidation was limited by the use of alumina crucibles to 0.045%. Greater concentrations than 0.045% could involve the melt and crucible in reaction to produce hercynite, as shown by McLean & Ward (58) and described in section 2.1.2.4.

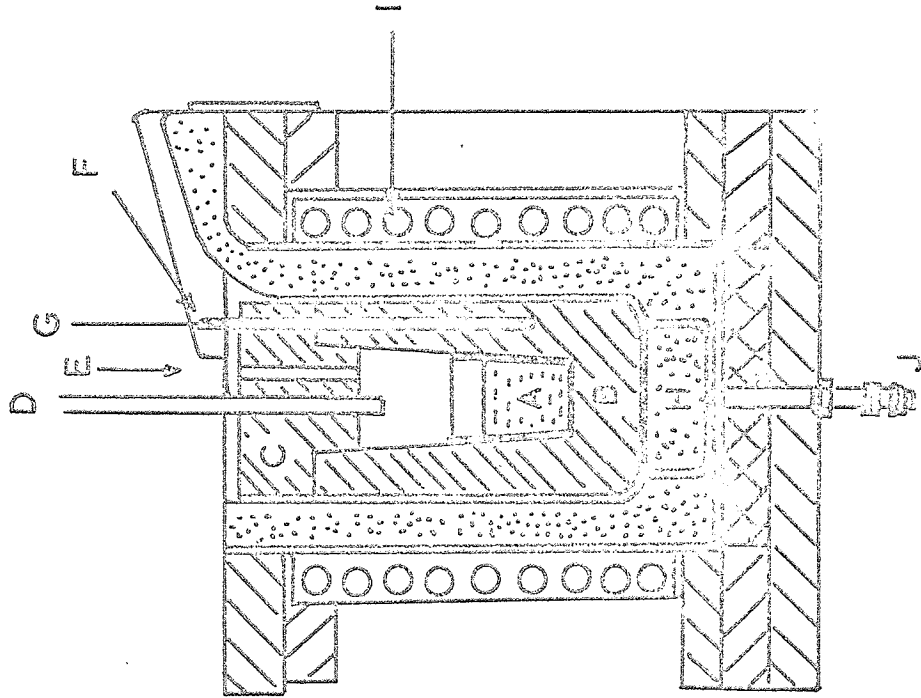
### 3.2. Experimental equipment.

3.2.1. Furnace. The furnace used was an H.F. melting unit, which used an A.E.I. - Birlec motor alternator set to supply high frequency current at 8.5 k Hz. The maximum rating was 20 kw. and adjustment of the power factor was made by switching in capacitance as required.

The furnace assembly is shown in fig. 3.1. by a vertical section diagram through the centre of the furnace. The graphite susceptor was made from electrode graphite and machined to fit closely into the furnace crucible. This prevented excessive wear by oxidation from circulating air.

Temperature measurement was by means of two platinum/platinum - 13% rhodium thermocouples connected to a multipoint recorder. One thermocouple was placed in the susceptor and this enabled the susceptor temperature to be monitored throughout the melting cycle. The second thermocouple was used for temporary immersion in the melt. When both thermocouples were in use, it was possible to determine directly the temperature difference between the melt and the susceptor by recording alternately from each of the thermocouples. The immersion thermocouple was protected by a silica sheath and access to the melt was obtained through the sampling hole provided in the lid.

- A IRON MELT CONTAINED  
IN ALUMINA CRUCIBLE
- B GRAPHITE SUSCEPTOR
- C SUSCEPTOR LID
- D ARGON INLET TUBE
- E SAMPLING HOLE
- F ALUMINA THERMOCOUPLE  
SHEATH
- G THERMOCOUPLE
- H FURNACE LINING
- I WATER COOLED INDUCTION  
COIL
- J EARTH LEAKAGE  
SPIDER



2003.1

FURNACE ASSEMBLY



3.2.2. Furnace atmosphere. It was considered necessary to prevent, as far as possible, any reoxidation of the melt during the holding period which followed the addition of the deoxidiser. Any such reoxidation would cause further oxides to be formed, and these would be expected to have a different composition and behaviour to the primary deoxidation products. The presence of any oxides other than the primary products of deoxidation would obscure the investigation of the deoxidation reaction and the products resulting from it.

The exposed surface of the melt was, therefore, protected by a non - oxidising atmosphere and argon was chosen for this purpose. A sealed furnace chamber was not used and so the argon flowed continuously at a controlled rate.

3.2.3. Turbulence in the melt. It was intended that the flotation rate of deoxidation products should be examined and compared with the rates indicated by Stoke's Law. This required the steel bath to be as free as possible from turbulence, in order that the mechanism of particle flotation should not be disrupted by agitation.

The heating system shown in fig. 3.1. supplied heat to the melt from a relatively large heated mass and so convection currents induced by thermal gradients should have been quite small.

Stirring of the melt by the induced current, was considered unlikely because the 'skin effect' concentrates the current at

the surface of a conductor. (110) In the experimental system, this current concentration would be at the periphery of the susceptor, the current density falling off exponentially from the surface. The penetration of the current also decreases as the frequency increases and so for the high frequency source used, it was considered that the current density in the melt was negligible.

Visual observation of the melt surface, and slag particles floating on it was used to verify that the melt was essentially quiescent.

3.3. Selection of deoxidiser compositions. The lime - alumina - silica phase diagram was examined for compositions having low liquidus temperatures and the ternary eutectic mixture at 14.7%  $Al_2O_3$ , 62%  $SiO_2$  and 23.3%  $CaO$ , having a melting point of  $1170^{\circ}C$ , was chosen as the composition to be aimed for as a suitable deoxidation product.

The deoxidation additions necessary to give this product composition were then calculated, assuming 100% utilization of the deoxidiser elements, the appropriate solute equilibria data described in section 2.1.2. and specific initial and final oxygen contents for the melt.

Specimen calculations are shown in appendix A. These illustrate the way in which the oxygen to be removed was apportioned between silicon, aluminium and calcium and the

stoichiometric deoxidiser additions derived. The additions required to satisfy the stoichiometric and equilibrium conditions were summated for each element and the deoxidiser composition and total addition computed from these data. In the cases where lime was to be included in the addition, the oxygen to be removed was apportioned only between silicon and aluminium in the appropriate ratio. The amount of lime to be added was determined from the amount of silica and alumina expected as a result of Si/Al deoxidation.

The initial assumptions were modified in the light of experience gained in the early experiments. Subsequent deoxidiser compositions were decided upon by varying the calcium and aluminium additions over a range as described in section 3.7.2. The magnesium containing and manganese containing alloys were chosen in a similar manner, using constant nominal silicon additions.

### 3.4. Preparation of materials

3.4.1. Deoxidation alloys. Deoxidation alloys were prepared in the same furnace that was used for experimental melts. The pure components, in the form of small granules or lumps, were well mixed after weighing and transferred to an alumina crucible. The mixture was then heated under an argon cover until completely molten. The melt was held at about 100°C superheat for 5 - 10 mins. and was briefly stirred at intervals.

Alloys containing calcium or magnesium lost a little of these elements whilst the melt was held above the liquidus temperature. The extent of the loss however, determined by comparison of nominal and actual compositions, was found to be very small. (see appendix B.) The alloys were allowed to cool and solidify in the furnace chamber after switching off the H.F. power. The argon atmosphere was maintained so that oxidation of the alloy surface during cooling was minimized.

Alloys containing manganese were found to attack alumina crucibles and so magnesia crucibles were used for series 5 alloys.

The buttons of alloys, weighing either 25 gm. or 50 gm. were freed from the crucibles and lightly ground to remove any adhering alumina or light oxides from the surface. They were then crushed to - 60 mesh and thoroughly mixed to ensure homogeneity and freedom from segregation consequent upon solidification.

The deoxidation alloy powders were pressure compacted, without binder, into square section bars for convenience in the subsequent experiments.

Some of the dilute calcium alloys were prepared by mixing commercial grade 30% Ca - calcium silicide with pure silicon and previously prepared Si/Al alloy powders. Similarly, the lime, silicon, aluminium deoxidisers were made up by mixing dried lime with Si/Al alloy powder. The mixed powders were compacted in the same way as the complex alloy deoxidisers. The lime

containing deoxidisers, however, were heated to  $650^{\circ}\text{C}$  in vacuo" prior to use in order to remove all moisture.

3.4.2. Iron - oxygen alloys. The carbonyl iron chosen as the raw material contained a much higher concentration of oxygen than was required in the experimental melts. The composition of the iron was therefore, adjusted by a preliminary treatment separate from the experimental melts. The preliminary treatment was made in two stages, one of which involved the addition of sufficient deoxidiser to reduce the oxygen content to approx. 0.05%.

The procedure in the first stage was to melt 325 gm. of carbonyl iron powder in an alumina crucible by the same technique as described in section 3.5.1. The melting part of the cycle however, differed from that of the experimental run because only 200 gm. of the powder could be charged to the crucible prior to melting. The balance of the charge (in a thin steel container 1" dia. x 1 -  $1\frac{1}{2}$ " high with 0.003" wall thickness) was added after the first 200 gm. had melted. When the whole of the charge was molten, the temperature was adjusted to  $1550^{\circ}\text{C}$  and a sample taken for analysis.

The premelt deoxidiser was added by the same method adopted in the experimental run (see section 3.5.1.) Aluminium additions of 0.06% were made to premelts used in series 4 and 5, and manganese additions of 0.65% were made to premelts for series 3.

The premelts were held at 1550°C for 15 mins. to allow flotation of the oxide products, and then allowed to cool after taking another sample for analysis.

Ingots surfaces were filed clean on the resulting premelts, so that any adhering alumina was removed. These ingots were then remelted in fresh crucibles. The remelting procedure was again similar to that of the experimental run but no deoxidation additions were made during this stage. The melt was held at 1550°C for 15 mins. in order to ensure that residual particles of alumina or hercynite from the premelt could separate. Samples were taken at melt out and just prior to cooling. All samples were analysed for oxygen content and the ingots set aside for the experimental work.

### 3.5. Experimental melts.

3.5.1. Melting procedure. The remelted ingot was pickled in hydrochloric acid to remove any traces of oxide formed during storage rinsed, and thoroughly dried. It was transferred to the furnace chamber in a new alumina crucible and the susceptor lid was set in place. The argon flow was started and melting commenced with the maximum possible power input of approx. 16 kw. The susceptor temperature was measured continually during melting by means of the thermocouple in the susceptor.

The charge was observed through the sampling hole in the lid and, when the metal became molten, the power input was reduced to

8 - 8.5 kw. at which, the susceptor temperature stabilized at approx. 1550°C. The immersion thermocouple was inserted and the recorder set to two point operation, so that both the melt temperature and the temperature difference between melt and susceptor could be measured. Adjustment of the power input was made to give a constant temperature of 1550°C in the melt. The immersion thermocouple was removed and subsequent temperature control was maintained by observation of the susceptor temperature with single point recorder operation.

The deoxidiser was taken from the compacted bar and a predetermined amount weighed out. This addition was enclosed in a thin steel cartridge and attached to the end of a silica plunging rod as shown in fig. 3.2.

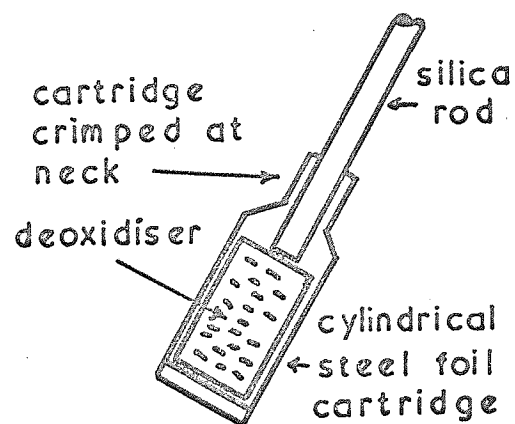


fig. 3.2

3.5.2. Sampling and deoxidation procedure. Sampling was performed by drawing off 8 - 10 gm. of the melt into a 4 mm. bore silica tube, using a safety pipette filler to provide the partial vacuum required in the tube.

The pipette was inserted into the melt through the sampling hole in the lid and withdrawn approx. 0.5 - 1 cm. from the bottom of the crucible before taking the sample. Samples were, by this method, always taken from a similar plane in the melt. A sample was always taken immediately before adding the deoxidiser and further samples were taken at intervals following deoxidation. The samples solidified very rapidly in the silica tube, and so the analyses and inclusion measurements made on them were assumed to be representative of the melt at the plane and time of sampling.

Additions of deoxidiser were made by removing the argon supply, lifting the susceptor lid and plunging the cartridge of deoxidiser below the melt surface. The melt was briefly stirred to ensure mixing of the deoxidisers and then the lid and argon supply were replaced. The furnace chamber was open at the top for 15 - 20 secs. during this operation.

Sampling times were reckoned from the completion of stirring of the bath. Deoxidation with alloys containing manganese took a little longer because the additions were larger and took a greater time to dissolve.

The deoxidised melts were held at 1550°C for 60 or 90 mins.



and approximately 10 samples were taken during this period. This allowed the progress of product separation to be examined and also allowed compositional changes to be studied. At the end of the holding period the melts were assumed to be free of suspended oxide particles. In some experiments, the melt temperature was checked during the holding period by means of an immersion thermocouple.

A few experiments were made in which the melt was held at 1550°C, after deoxidation for only short periods and then allowed to cool. Pipette samples were taken from these only prior to deoxidation. These ingots were examined for inclusions and compositions at various levels from the ingot bottom.

### 3.6. Analysis and metallography.

3.6.1. Steel analysis. Oxygen contents were determined by vacuum fusion analysis. The instrument used was the Balzer Exhalograph EA1, which is described by Ramsey, Winkler and Kraus. (111). Oxygen in the form of carbon monoxide is measured by an infra red absorption cell. Standardization and calibration of the instrument were made by metering quantities of pure carbon monoxide into the analytical system.

Silicon was determined by photometric analysis using the reduction of silico-molybdate by stannous chloride to produce the "molybdenum blue" complex. (112) The absorption was measured with a Hilger and Watts 'Spectrochem' in 2 cm. cells at a wavelength of

575 m $\mu$ . Regular checks were made by standard gravimetric analysis (113) of samples taken from the deoxidised ingots.

Aluminium analysis was also by direct photometric method using eriochrome cyanine R. The original method differed little from that proposed by Hill (114) but was modified in accordance with the recommendations of Picasso (115). The method finally used was that of Picasso but with the following modification.

The insoluble residue, left after decomposition of the sample in hydrochloric acid, was filtered onto a Whatman 541 paper, washed with hot water and ignited in a platinum crucible. The filtrate was reserved. The ignited residue was treated with 1 ml. conc. sulphuric acid and 3 mls. hydrofluoric acid to remove silica. The acids were evaporated and the resulting residue ignited for 5 mins. at 1,000°C and then fused with a few crystals of potassium bisulphate. The fused mixture was dissolved in hot water and added to the filtrate mentioned above. The analysis was then completed as described by Picasso.

Manganese was determined by the standard sodium bismuthate oxidation method (116) which employs a volumetric finish with ferrous ammonium sulphate and potassium permanganate.

Carbon was determined by combustion of the sample in oxygen and volumetric measurement of carbon monoxide by means of a Strohlein apparatus. (117)

3.6.2. Deoxidiser analysis. Constituents of the Ca/Si/Al and Mg/Si/Al deoxidisers were all determined gravimetrically. Samples were taken into solution by fusing with sodium carbonate/sodium peroxide mixture and leaching the fused residue with water and hydrochloric acid. The constituents were then separated and determined by the procedure adopted for slag analysis. (118)

Silicon was determined by dehydration of silicic acid followed by sulphuric acid/hydrofluoric acid treatment of the separated and ignited silica. Aluminium was precipitated as the hydroxide, filtered and ignited to alumina. Calcium was precipitated as calcium oxalate and ignited to calcium oxide, whilst magnesium was precipitated as phosphate and ignited to pyrophosphate.

Silicon in the Mn/Si/Al alloys was determined similarly to that indicated for the other deoxidisers, but silicic acid was precipitated by fuming with perchloric acid (113) instead of baking the salts from a hydrochloric solution.

Samples for manganese and aluminium analyses were dissolved in nitric acid with the aid of a little hydrofluoric acid. The solutions were fumed with sulphuric acid to remove the hydrofluoric acid, and the salts were dissolved in water. The samples for manganese determinations were then completed by sodium bismuthate oxidation and titration with ferrous ammonium sulphate and potassium permanganate. (119) The aluminium analyses were completed by taking appropriate aliquots and developing the aluminium eriochrome

complex by the same procedure used in steel analysis.

3.6.3. Inclusion analysis. Inclusion compositions were determined 'in situ' by the use of an electron probe X ray microanalyser. The instrument was a Cambridge Microscan Mk.2. It differed from the standard model only in that it had been equipped with two spectrometers and a light element kit.

One of the spectrometers was used for detection and measurement of iron and manganese radiations and lithium fluoride crystals were used for this purpose. The radiation from the lighter elements, calcium, magnesium, silicon and aluminium was detected and measured in the second spectrometer, which was open to the specimen chamber and employed gypsum crystals. Barium stearate crystals from the light element kit were used on occasions when the gypsum crystals were badly dehydrated. The gypsum crystals were preferred, when in good condition, because the 1st order  $K\alpha$  radiation could be used and this was found to be most convenient.

Specimen preparation and analytical conditions were the same as described by Ridal, Jones and Cummins (120 for an accelerating voltage of 19.6 kv. Absorption and atomic number corrections, proposed by the same authors, were applied to the apparent analyses. An example of the correction factor calculations is shown in appendix C.

Homogeneity of inclusions was checked by examination of the X ray images produced when the spectrometer was set, in turn, to the Bragg angle for detection of each element present. Line scans were also made under these conditions to reveal any concentration gradients not easily observed from the X ray image.

The minimum size of inclusion which could be analysed with confidence was approximately 5  $\mu$ . diameter and so inclusions in samples up to 12 - 20 mins only could usually be analysed. Wherever possible, 5 or more inclusions per sample were analysed.

3.6.4. Metallography. All the samples were examined metallographically to determine the shape of the particles and presence of any second phase. Quantitative metallography was not undertaken in the early part of the work because the inclusion concentration was followed during the course of separation by measurement of the oxygen content. The inclusion concentration was assumed to be proportional to the function,  $[\%O_t - \%O_e]$ , where  $\% O_t$  is the total oxygen content at any time and  $\%O_e$  is the equilibrium oxygen content of the oxide free melt. Manual counting techniques were time consuming and of limited accuracy and so it was thought that the extra information obtainable did not justify their use.

In the latter stages of the project however, a Metals Research Quantimet, image analysing computer, became available

and so a number of samples could be examined in detail. The instrument and its applications are described by C. Fisher (121) and also by H. Martensson. (122) Measurement of inclusion concentration was made in terms of % conc. by area and the size distribution was measured by counting the number of particles exceeding given diameters. The quantitative measurements were made at x 100 and between 25 and 75 fields were examined in each sample.

### 3.7. Development of programme.

3.7.1. Series 3 experiments. A short experimental series was made in which the premelt deoxidation was performed with manganese. Final deoxidation in these tests was made with; silicon, aluminium, silicon/aluminium alloy and silicon/aluminium alloy mixed with lime. An excess of 0.005% aluminium was added to the amount calculated from true aluminium - oxygen equilibrium, because the experiments were not true equilibrium studies. It was felt that Wentrupp & Hieber's apparent equilibrium constant might apply better to the conditions used.

Results from these experiments showed that manganese present in the premelt became involved with the deoxidation products. It was also found that the residual aluminium existing in ingots with 0.007% oxygen was on the lower limit of detection.

Subsequent experimental series did not use manganese deoxidised premelts and did not include the 0.005% excess aluminium addition to the experimental melt.

3.7.2. Series 4 experiments. This series contained tests using silicon, aluminium and silicon/aluminium alloy as control deoxidisers and silicon/aluminium/~~lime~~, calcium/silicon/aluminium and magnesium/silicon/aluminium as experimental complex deoxidisers.

The results indicated that lime was not taking part in the formation of the products to any significant extent and so lime inoculation was not pursued further. Deoxidation products resulting from the use of the other complex deoxidisers showed that the deoxidiser calculated in appendix A, did not produce the intended oxide composition. The lime content of inclusions was inconsistent and lower than that required. Deoxidiser compositions were then used which gave various increased calcium additions to the melt at constant nominal silicon and aluminium additions. Some of the deoxidisers were made up however, as mentioned in section 3.4.1, with commercial calcium silicide as the source of calcium. The aluminium content of this was reported to be 3% but was later found to be nearer 6% and so the aluminium additions covered a range and were greater than intended.

Calcium was found to contribute little to the deoxidation process and experiments with two magnesium/silicon/aluminium alloys indicated a similarity with the calcium/silicon/aluminium system. Work on these two deoxidiser systems was then discontinued.

3.7.3. Series 5 experiments. The manganese/silicon/aluminium system was chosen for complex deoxidation alloys because all of the components are commonly used for steel deoxidation, all are soluble in molten steel, none are very volatile and the oxide system  $MnO/SiO_2 / Al_2O_3$  contains many low liquidus temperature mixtures.

Deoxidiser compositions were chosen to provide manganese additions to the steel of 0.25 - 1.0% and aluminium additions of 0.003 - 0.03% with a constant nominal silicon addition, as used in the previous series.

This series was chosen for the quantitative metallographic examination because it was considered more representative of deoxidation processes than the previous series which employed deoxidisers containing calcium or magnesium.



## SECTION 4. EXPERIMENTAL RESULTS.

### 4.1. Evaluation of experimental technique.

4.1.1. Melt/crucible reaction. The alumina crucibles used both for melt preparation and the experimental melts, suffered various degrees of attack. The extent of this attack, and the type of product resulting from it, depended upon the stage of processing reached and the deoxidiser used for predeoxidation treatment.

The crucible attack which occurred in those premelts deoxidised with aluminium was quite severe and is illustrated by fig. 4.1. Deoxidation of the premelt with manganese in series 3 however, resulted in very little crucible attack and this is shown by fig. 4.2. Fig. 4.3 shows the light green product resulting from remelting a predeoxidized ingot. Aluminium had been used as the deoxidiser but no residual aluminium was detectable.

Crucible attack was not observed after an experimental run. Fig. 4.4 shows that a few particles of the melt adhere to the crucible walls, together with a little ingot scum.

4.1.2. Solidification of samples. The pipette samples were taken in silica tubes 5.5 mm. O.D. x 4 mm. bore, and measured 4 mm. dia. x 8 - 12 cm. long. These samples solidified and cooled very rapidly, reaching a temperature less than 700°C within 10 seconds.



fig. 4.1



fig. 4.2



fig. 4.3



fig. 4.4

Cooling curve measurements on furnace cooled ingots showed that solidification started approximately 30 seconds after switching off the H.F. power and was completed within 3 mins. Extraction of the crucible from the furnace and chilling it in a shaped iron block, produced only a small decrease in solidification time and caused substantial scaling of the ingot surface.

The macrostructures of a chilled ingot and a furnace cooled ingot are shown in figs. 4.5 & 4.6 . The absence of directionality of solidification in the furnace cooled ingot as compared with the strong columnar growth in the chilled ingot, is readily seen.

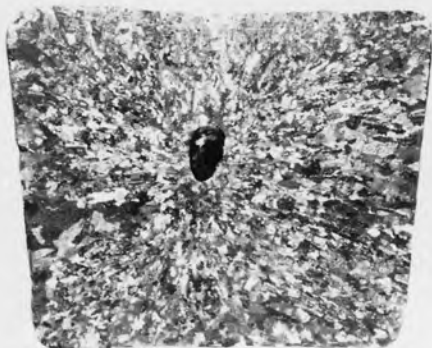


fig. 4.5 Chilled ingot.



fig. 4.6 Furnace cooled ingot.

Ingot macrostructures 1.5 x full size.

The difference in temperature between the melt and the susceptor was measured as 10-20°C. This temperature difference varied between experiments but varied little during the course of an experiment.

#### 4.2. Experimental data.

4.2.1. Preparation of melts. The carbonyl iron used as the starting material for all the experiments was of the composition shown in table 4.1.

O	N	C	Co	Ni	S
0.110	0.004	0.028	0.02	0.07	0.001

The premelts contained 0.09-0.1% dissolved oxygen at melt out. The premelt deoxidation treatment for series 4 and 5 was the addition of 0.06% aluminium and this produced a residual oxygen content of 0.05-0.06% after a 15 min. holding period.

A further reduction of 0.01-0.015% oxygen occurred as a result of the remelting stage.

Fig. 4.7 shows the changes in oxygen content during the preparation stages of the ingot used in experiment 4 C 1.

The premelt deoxidation treatment given in series 3 was the addition of 0.55% manganese which resulted in a residual oxygen content of 0.045-0.055% and a residual manganese content of 0.35-0.45%. Remelting of these ingots resulted in a loss of 0.01-0.02% oxygen and 0.03-0.05% manganese.

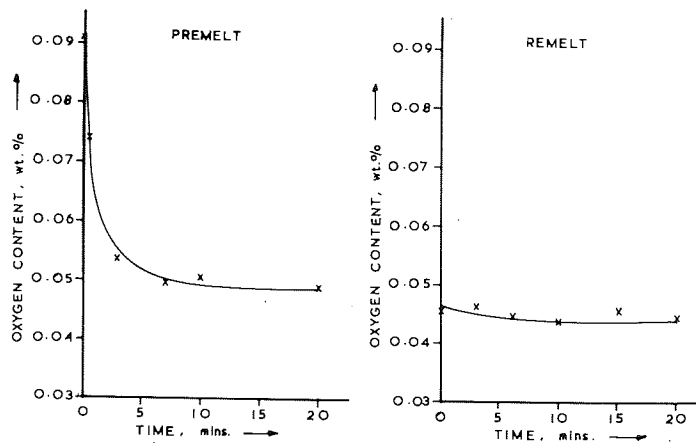


fig. 4.7 Change of oxygen content during melt preparation.

4.2.2. Deoxidation melts. The deoxidiser composition and addition for each experiment is given in table 4.2. The first digit identifies the series number 3,4 or 5. The letter C denotes deoxidation with one of the control deoxidisers i.e. Si, Al or Si/Al alloy, and E denotes the use of a Ca, CaO, Mg or Mn containing complex deoxidiser. The experiment number within a series is identified by the number following the letter C or E.

Experiments 4E5, 4E7, 4E10, 4E12 and 4E13 involved cooling the melts immediately after deoxidation as described in section 3.5.2. Experiment 4E11 was treated similarly but was cooled 5 mins. after deoxidation.

Table 4.2

EXP. No.	DEOXIDIZER COMPOSITION Wt %						ADDITION
	Mn	Si	Al	Ca	Mg	CaO	Wt %
3C2		100					0.289
3C4			100				0.062
3C5*		94.8	5.2				0.291
3E1		86.2	4.7			9.1	0.320
4C1		97	3				0.277
4C2			100				0.044
4E1		89	3.2			7.8	0.300
4E2		90.2	3.8	6			0.282
4E3		90.2	3.8	6			0.282
4C4			100				0.146
4C6			100				0.110
4E4		85.9	4.1	10			0.295
4E5		85.9	4.1	10			0.295
4E6		87.8	3.9	8.3			0.289
4E7		64	6	30			0.433
4E8		64	6	30			0.433
4E9 <sup>+</sup>		67	3	30			0.452
4E10		67	3	30			0.452
4E11		87	3	10			0.295
4E12		87	3		10		0.295

Table 4.2 continued

EXP. No.	DEOXIDISER COMPOSITION Wt %						ADDITION Wt %
	Mn	Si	Al	Ca	Mg	CaO	
4E13		92	3		5		0.279
4E14		92	3		5		0.279
5E1 <sup>‡</sup>	64.5	35.8	0.9				0.777
5E2	73.5	26.9	0.4				1.027
5E3	77.2	24.8	0.2				1.277
5E4	46.2	54.4	1.5				0.527
5E5	63.0	35.0	2.2				0.789
5E6	62.3	35.4	4.2				0.809
5C2		100					0.290

\* Calculated compositions of blended deoxidizers used in experiments 3C5-4E8. (see section 3.4.1 page 64 )

+ Nominal compositions of deoxidation alloys used in experiments 4E9-4E14. (see section 3.4.1 page 64 )

‡ Analysed compositions of deoxidation alloys used in experiments 5E1-5E6.

4.2.3. Location of ingot samples. The sectioning of the deoxidized ingots for examination is shown in fig. 4.8.

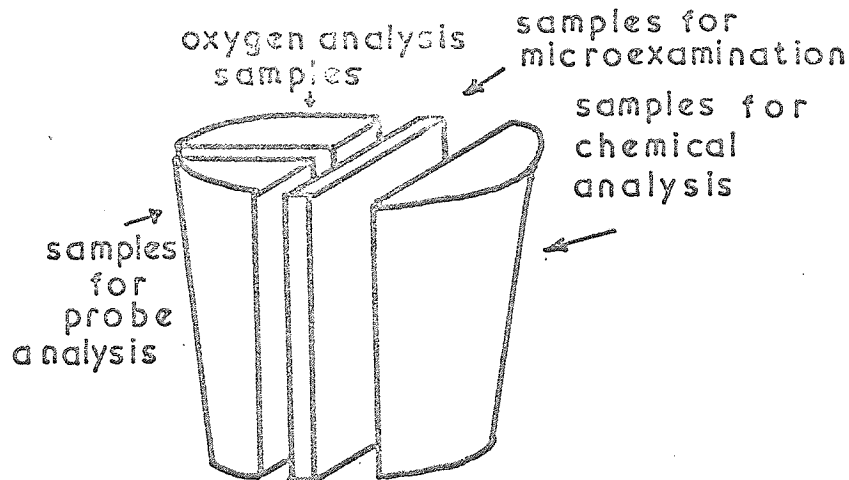


fig. 4.8 Ingot sample locations.

4.3 Melt and inclusion analysis.

The combined data from vacuum fusion analysis, chemical analysis and microprobe analysis are summarized and presented in tables 4.3 to 4.28

The inclusions resulting from deoxidation were, except in the case of experiment 5E6, particles either of pure oxide phases or of a homogeneous glassy nature. The deoxidation treatment used in experiment 5E6 resulted in the formation of inclusions having alumina particles in a glassy matrix. Figs. 4.9a - 4.9f illustrate this by means of the X ray image and the X ray line scan. The X ray image shows the distribution of elements in a



typical inclusion and the line scan shows the relative concentrations of the elements in the two phases. The reported inclusion analyses for experiment 5E6 were calculated from the estimated proportions of the two phases and their analysed compositions.

The value n, under the inclusion analysis heading, refers to the number of inclusions analysed to give the mean analysis quoted. Where more than one analysis is quoted, they are the mean values for composition groups which are distinctly different. The sampling time refers to the completion of deoxidiser addition as zero. Ing. denotes a sample taken from the deoxidised ingot and the descriptions Top and Bot. identify the position in the ingot as top or bottom respectively.



EXPERIMENT No. 3C4

TABLE 4.4		EXPERIMENT No. 3C4										
SAMPLE	HELT ANALYSIS					INCLUSION ANALYSIS					wt %	
	O	Si	Al	Mn	C	n	MnO	Al <sub>2</sub> O <sub>3</sub>	SiO <sub>2</sub>	CaO		FeO
Prein	0.0522			0.36	0.018							
- $\frac{1}{2}$ min	0.0470			0.35								
+ $\frac{1}{2}$ "	0.0187		0.019									
1 "	0.0105		0.013	0.35								
3 "	0.0051		0.004									
7 "	0.0134		0.003	0.36	0.018							
15 "	-		0.001	0.35	0.037							
30 "	0.0368		0.001	0.36	0.027							

TABLE 4.5 EXPERIMENT No. 3C5

SAMPLE TIME	NET ANALYSIS				INCLUSION ANALYSIS							wt % TOTAL
	O	Si	Al	Mn	C	n	MnO	AL <sub>2</sub> O <sub>3</sub>	SiO <sub>2</sub>	CaO	FeO	
Prem	0.0550											
-½ min	0.0395				0.017							
+½ "	0.0347	0.240	0.013	0.33		1	22.1	36.1	30.8		1.8	90.8
1 "	0.0339	0.237	0.012			3	19.3	42.6	34.5		2.6	99.0
2 "	0.0322	0.239	0.011									
5 "	0.0267	0.233	0.009			2	22.2	38.2	34.6		2.8	97.8
10 "	0.0168	0.222	0.005	0.4		2	22.9	41.9	32.4		2.7	99.9
15 "	0.0118	0.222	0.003		0.016							
30 "	0.0081	0.214	-		0.016							
45 "	0.0078	0.210	0.003		0.018							
60 "	0.0074	0.212	0.002									
Ing	0.0075	0.212	0.002	0.34	0.027							

T A B L E 4 . 6                      E X P E R I M E N T   N o .   3 E 1

SAMPLE TIME	M E L T   A N A L Y S I S   W t %					I N C L U S I O N   A N A L Y S I S   W t %						
	O	Si	Al	Mn	C	n	MnO	Al <sub>2</sub> O <sub>3</sub>	SiO <sub>2</sub>	CaO	FeO	TOTAL
Prem	0.0567											
1/2 min	0.0384				0.026							
1 1/2 "	0.0365	0.246	0.012	0.35								
1 "	0.0341	0.241	0.013									97
2 "	0.0338	0.236	0.011			1	20.1	38.3	32.9	2.4	4.0	97.7
5 "	0.0279	0.233	0.009			1	20.3	40.6	33.1	1.9	2.7	98.6
10 "	0.0164	0.226	0.003	0.35		2	21.0	42.6	31.3	2.3	2.4	99.6
15 "	0.0110	0.216	0.002		0.027	1	19.1	39.8	32.9	1.9	2.7	96.3
30 "	0.0069	0.218	-		0.027							
45 "	0.0066	0.210	0.002									
60 "	0.0060	0.212	-		0.035							
Ing	0.0061	0.209	0.002	0.33	0.031							

T A B L E 4. 7                      E X P E R I M E N T   N o .   4 C 1

S A M P L E	M E L T   A N A L Y S I S   W t %						I N C L U S I O N   A N A L Y S I S   W t %						
	O	Si	Al	Mn	C		n	MnO	Al <sub>2</sub> O <sub>3</sub>	SiO <sub>2</sub>	CaO	FeO	TOTAL
Prem	0.0440												
- $\frac{1}{2}$ min	0.0356												
+ $\frac{1}{2}$ "	0.0358	0.235	0.0091										
1 $\frac{1}{2}$ "	0.0320	0.224	0.0048				2	31.7	67.8			2.4	101.9
3 "	0.0260	0.230	0.0029				1	31.0	65.8			4.5	101.3
7 "	0.0160	0.233	0.0017										
15 "	0.0104	0.208	0.0017										
30 "	0.0083	0.198	0.0013										
60 "	0.0074	0.195	-										
Ing.	0.0072	0.195	0.0005										

TABLE 4.8		EXPERIMENT No. 4 C 2					EXPERIMENT No. 4 C 3						
SAMPLE	TIME	MELT ANALYSIS Wt %				C	SAMPLE	TIME	MELT ANALYSIS Wt %				
		O	Si	Al	Mn				O	Si	Al	Mn	C
Prem		0.0553					Prem		0.0531				
- $\frac{1}{2}$ min		0.0458					- $\frac{1}{2}$ min		0.0464				
+ $\frac{1}{2}$ "		0.0320		0.044			+ $\frac{1}{2}$ "		0.0244	0.378			
1 $\frac{1}{2}$ "		0.0278		0.022			1 $\frac{1}{2}$ "		0.0209	0.382			
2 $\frac{1}{2}$ "		0.0249		-			2 $\frac{1}{2}$ "		0.0185	0.375			
4 "		0.0215		0.011			4 "		0.0152	0.390			
7 "		0.0146		0.005			7 "		0.0120	0.395			
10 "		0.0137		0.0028			10 "		0.0091	0.395			
20 "		0.0137		0.0004			15 "		0.0068	0.395			
40 "		0.0112					25 "		0.0068	0.376			
Ing		-					40 "		0.0069	-			
							60 "		0.0068	0.398			
									0.0066	0.389			





T A B L E 4. 10                      E X P E R I M E N T   N o .   4 E 2

SAMPLE TIME	M E L T   A N A L Y S I S   Wt %				I N C L U S I O N   A N A L Y S I S					Wt % TOTAL		
	O	Si	Al	Mn	C	n	MnO	Al <sub>2</sub> O <sub>3</sub>	SiO <sub>2</sub>		CaO	FeO
Prem	0.0446											
-½ min	0.0402											
+½ "	0.0379	0.235	0.010			1		9.5	58.7	27.6	2.5	98.4
1 "	0.0362					1		27.6	53.9	15.4	2.8	99.7
2 "	0.0327	0.230	0.0044			3		35.7	47.2	11.8	5.2	99.9
5 "	0.0242					1		17.0	47.8	25.3	3.0	93.1
8 "	0.0171	0.231										
12 "	0.0112											
20 "	0.0068	0.228										
30 "	0.0050											
45 "	0.0039	0.232										
60 "	0.0036											
Ing	0.0034	0.235	0.0012									

T A B L E 4. 11      E X P E R I M E N T   N o . 4 E 3

S A M P L E	N E T   A N A L Y S I S   W t %				I N C L U S I O N   A N A L Y S I S   W t %							
	O	Si	Al	Mn	C	n	MnO	Al <sub>2</sub> O <sub>3</sub>	SiO <sub>2</sub>	CaO	FeO	TOTAL
Prem	0.0553											
- $\frac{1}{2}$ min	0.0508											
+ $\frac{1}{2}$ "	0.0455	0.200	0.0062			2	8.5	61.9	23.2	4.4		98.0
1 "	0.0431					1	8.5	59.5	29.3	3.6		100.9
2 "	0.0429	0.198	0.0028			1	17.1	57.1	14.1	7.8		96.3
5 "	0.0321					1	8.0	60.9	27.9	4.4		101.1
8 "	0.0223	0.204				1	29.8	54.8	7.0	4.9		96.5
12 "	0.0155					1	21.2	57.5	15.0	3.2		96.9
20 "	0.0122	0.196				1	15.0	60.3	21.4	3.0		99.7
30 "	0.0105					4	35.7	54.2	7.7	3.2		100.8
45 "	0.0083	0.196	0.0004			3	35.8	53.1	8.1	3.8		100.8
60 "	0.0073					3	41.2	49.0	8.2	3.2		101.6
Ing	0.0072	0.198	-		0.058							

TABLE 4. 12

EXPERIMENT No. 4 C 4

SAMPLE	M E L T A N A L Y S I S						I N C L U S I O N A N A L Y S I S						wt %
	O	Si	Al	Mn	C	n	FeO	CaO	SiO <sub>2</sub>	Al <sub>2</sub> O <sub>3</sub>	FeO	TOTAL	
Prem	0.0563												
- $\frac{1}{2}$ min	0.6289												
+ $\frac{1}{2}$ "	0.0064												
1 "	0.0040												
2 "	0.0025												
4 "	0.0016												
6 "	0.0015												
8 "	0.0011												
12 "	0.0013		0.084										
20 "	0.0006												
40 "	0.0007												
60 "	0.0008		0.083										
Ing "	0.0005		0.087										

TABLE 4. 13

EXPERIMENT No. 4 C 6

SAMPLE	MELT ANALYSIS Wt%					INCLUSION ANALYSIS Wt%						
	O	Si	Al	Mn	C	n	MnO	Al <sub>2</sub> O <sub>3</sub>	SiO <sub>2</sub>	CaO	FeO	TOTAL
Prem	0.0627											
- 1 min	0.0566											
+ 1/2 "	0.0266		0.093									
1 "	0.0142		0.075									
2 "	0.0058		0.061									
4 "	0.0022		0.058									
6 "	0.0018											
9 "	0.0011											
15 "	0.0009		0.053									
30 "	0.0009											
45 "	-		0.053									
Ing	0.0005		0.053									

TABLE 4. 14

EXPERIMENT No. 4 E 4

SAMPLE TIME	MELT ANALYSIS wt %				INC LUSION ANALYSIS						wt % TOTAL	
	O	Si	Al	Mn	C	n	MnO	Al <sub>2</sub> O <sub>3</sub>	SiO <sub>2</sub>	CaO		FeO
Prem	0.0479											
- 1 min	0.0423											
+ 1/2 "	0.0351		0.0138			1		26.6	48.8	16.2	8.2	99.8
						1		31.9	40.4	10.3	16.6	99.2
						1		20.2	54.5	23.1	3.3	101.1
1 "	0.0336	0.226	0.0128			2		37.0	42.9	13.4	3.6	96.9
2 "	0.0320					4		40.3	42.7	12.8	4.4	100.2
5 "	0.0252		0.0109			4		40.3	42.0	12.4	2.6	97.3
8 "	0.0181	0.224	0.0069			4		42.5	40.8	12.3	3.2	98.8
12 "	0.0131					4		48.7	36.8	12.9	3.1	101.5
20 "	0.0082	0.220										
30 "	0.0052											
45 "	0.0039	0.217										
60 "	0.0041											
Ing	0.0041	0.229	0.0004									

T A B L E 4. 15      E X P E R I M E N T      N o. ' s 4 E 5 & 4 E 7												
S A M P L E	M E L T   A N A L Y S I S    Wt %					I N C L U S I O N   A N A L Y S I S					Wt %	
	O	Si	Al	Mn	C	n	MnO	Al <sub>2</sub> O <sub>3</sub>	SiO <sub>2</sub>	CaO		FeO
4 E 5 Prem	0.0643											
- 1 min Ing. Top	0.0593					1	8.2	10.0		29.7	2.3	101.1
"						9	6.0	59.6		32.8	1.8	100.2
"						1	4.8	58.5		35.3	1.5	100.1
Ing. Bot.	0.0538	0.234	0.0083			2	22.9	64.4		8.0	3.2	98.5
"						5	16.1	62.6		16.8	2.9	98.4
"						1	12.3	59.9		25.1	2.2	99.8
4 E 7 Prem	0.0209											
- 1 min Ing. Top	0.0198					2	61.8	2.8		33.5	2.2	100.3
"	0.0187					1	53.4	4.1		37.8	2.5	97.8
Ing. Bot.	0.0167	0.245	0.025			1	66.1	5.2		27.2	2.7	101.2
"						1	78.8	2.4		11.6	4.	96.8

TABLE 4. 16

EXPERIMENT No. 4 E 6

SAMPLE TIME	MELT ANALYSIS				INCLUSION ANALYSIS				TOTAL			
	O	Si	Al	Mn	C	n	MnO	Al <sub>2</sub> O <sub>3</sub>		SiO <sub>2</sub>	CaO	FeO
Prem	0.0579											
- 1 min	0.0530											
+ 1/2 "	0.0469	0.212	0.0095			1		29.2	56.1	7.9	5.3	98.5
1 "	0.0458					1		15.8	59.8	20.3	4.5	100.4
2 "	0.0452	0.195	0.0105			1		23.0	59.2	10.7	6.0	98.9
5 "	0.0309	0.205	0.0065			1		17.5	56.6	17.8	5.3	97.2
8 "	0.0202					3		30.9	54.3	9.3	4.4	98.9
12 "	0.0129	0.198	0.0030			2		18.3	59.2	17.5	4.1	99.1
20 "	0.0087					4		30.7	52.1	10.1	4.2	97.1
30 "	0.0069					2		22.1	59.1	15.4	3.4	100.0
45 "	0.0063	0.208	0.0004			5		32.2	51.3	11.0	4.4	98.9
60 "	0.0055					4		34.6	48.6	11.9	4.1	99.2
90 "	0.0042					3		33.4	51.8	11.3	4.0	100.5
Ing		0.206	0.0027									

TABLE 4. 17

EXPERIMENT No. 4 E 8

SAMPLE	HELT ANALYSIS Wt %						INCLUSION ANALYSIS						TOTAL
	O	Si	Al	Mn	C		n	FeO	Al <sub>2</sub> O <sub>3</sub>	SiO <sub>2</sub>	CaO	FeO	
Prem	0.0423												
- 1 min	0.0349												
+ 1/2 "	0.0304	0.250	0.024				1		21.3	40.1	37.0	1.5	99.9
1 "	0.0283						1		17.5	40.0	41.1	1.4	100.0
							1		80.5	2.9	10.3	3.6	96.8
2 "	0.0206	0.247	0.015				1		64.2	14.3	22.3	1.6	102.4
							1		68.9	8.3	15.7	5.2	98.1
5 "	0.0166						1		83.7	5.6	6.6	2.0	97.9
							1		82.7	2.4	12.2	1.8	99.1
8 "	0.0069	0.242	0.0036										
12 "	0.0050												
20 "	0.0036	0.238	0.0025										
30 "	0.0020												
45 "	0.0021	0.242	-										
60 "	0.0017												
90 "	0.0019												
Ing	0.0017	0.239	0.012										

Many particles present approaching

100% Al<sub>2</sub>O<sub>3</sub>



TABLE 4. 18

EXPERIMENT No. 4 E 9

SAMPLE TIME	MELT ANALYSIS						INCLUSION ANALYSIS						TOTAL
	O	Si	Al	Mn	C	n	Mno	Al <sub>2</sub> O <sub>3</sub>	SiO <sub>2</sub>	CaO	FeO		
Prem	0.0641												
- 1 min	0.0603					2		30.9	36.7	27.2	3.6		98.4
+ 1/2 "	0.0512	0.340	0.035			1		41.7	38.3	20.0	3.1		103.1
						1		59.9	24.2	15.2	5.1		104.4
1 "	0.0537	0.330				1		67.8	19.1	9.0	3.3		99.2
						2		67.8	20.6	9.9	2.9		101.2
2 "	0.0464	0.326	0.027			3		59.2	25.8	12.0	3.0		100.0
5 "	0.0246					2		56.7	25.7	13.7	2.8		98.9
8 "	0.0119	0.317	0.009										
12 "	0.0064												
20 "	0.0036	0.322	0.0085										
30 "	0.0026												
45 "	0.0020	0.308											
60 "	0.0016												
90 "	0.0015												
Ing	0.0014	0.284	0.009		0.047								

T A B L E 4. 19      E X P E R I M E N T   N o. 4 2 1 0   & 4 E 1 1

S A M P L E	M E L T   A N A L Y S I S   W t %					I N C L U S I O N   A N A L Y S I S					W t %	
	C	Si	Al	Mn	C	n	MnO	Al <sub>2</sub> O <sub>3</sub>	SiO <sub>2</sub>	CaO		FeO
4 E 1 0 Prem	0.0558											
- 1 min	0.0587											
Ing	0.0440	0.264	0.013			1		10.0	56.1	29.4	2.4	97.9
						1		22.9	50.9	22.3	4.1	100.2
						4		14.0	53.2	28.5	3.1	98.8
						3		21.8	51.6	22.7	4.0	100.1
						1		49.8	36.7	8.3	5.4	100.2
						1		29.5	48.3	15.8	3.8	97.8
4 E 1 1 Prem	0.0489											
- 1 min	0.0477											
+ 5 "												
( $\frac{3}{2}$ ) h	0.0348	0.215	0.0088			1		29.3	55.4	14.0	2.3	101.0
						6		36.9	50.8	8.7	2.1	98.5
( $\frac{3}{4}$ ) h	0.0229					4		35.3	51.9	9.7	2.0	98.9
( $\frac{1}{2}$ ) h	-					4		36.8	51.8	9.1	2.9	100.6
( $\frac{1}{4}$ ) h	0.0216					4		35.5	52.9	9.1	1.9	99.4
0	0.0153	0.210	0.0063			4		36.9	52.3	8.9	2.5	100.6

T A B L E 4. 20      E X P E R I M E N T   N o. ' s   4 E 1 2   &   4 E 1 3

S A M P L E	R E F E A N A L Y S I S   W t %				I N C L U S I O N   A N A L Y S I S						W t %		
	O	Si	Al	Mn	C	n	MnO	Al <sub>2</sub> O <sub>3</sub>	SiO <sub>2</sub>	MgO		FeO	TOTAL
4 E 1 2													
Prem	0.0529												
- 1 min	0.0490												
Ing. Top.	0.0385					3		5.3	59.1	36.8	1.5	102.7	
"						2		12.3	61.8	26.3	2.0	102.4	
Ing. Bot.	0.0362	0.225	0.0071			2		9.5	63.8	22.8	2.2	98.3	
"						5		21.4	59.9	15.0	2.6	98.9	
4 E 1 3													
Prem	0.0262												
- 1 min	0.0237												
Ing.	0.0210	0.238	0.0088			1		9.1	47.9	39.3	3.3	99.6	
"						1		46.4	28.8	25.7	1.8	102.7	
"						3		57.8	5.4	26.0	1.9	101.1	
								Many particles approach 100% Al <sub>2</sub> O <sub>3</sub>					

TABLE 4.21

EXPERIMENT No. 4 E 14

SAMPLE	HELT ANALYSIS				C	INCLUSION ANALYSIS						TOTAL	
	O	Si	Al	Mn		n	PbO	Al <sub>2</sub> O <sub>3</sub>	SiO <sub>2</sub>	FeO	FeO		
Prep	0.0486												
- 1 min	0.0404												
4 1/2 "	0.0356	0.234	0.0075										
1 "	0.0329				1		29.1	48.7	12.9	4.8		95.5	
2 "	0.0298	0.232	0.0068		1		31.3	51.2	13.3	4.4		100.2	
5 "	0.0223				3		32.7	52.2	11.0	4.3		100.2	
8 "	0.0167	0.234	0.0036		3		32.5	50.6	13.4	3.5		100.0	
12 "	0.0114				3		35.9	48.4	13.8	3.2		101.3	
20 "	0.0080				2		38.5	46.5	14.7	2.0		101.7	
30 "	0.0066												
45 "	0.0062	0.228	0.0018										
60 "	0.0056												
90 "	0.0053	0.227											
Ing	0.0052	0.225	0.0005									0.028	

TABLE 4. 22

EXPERIMENT No. 5 E1

SAMPLE	NET ANALYSIS					INCLUSION ANALYSIS					TOTAL	
	Wt %	Wt %	Wt %	Wt %	Wt %	Wt %	Wt %	Wt %	Wt %	Wt %		
TIME	O	Si	Al	Mn	C	n	MnO	Al <sub>2</sub> O <sub>3</sub>	SiO <sub>2</sub>	CaO	FeO	TOTAL
Prem												
- 1 min	0.0526											
+ 3 "	0.0441	0.223	0.0063	0.498		5	30.3	12.0	53.0		3.4	98.7
1 "	0.0407	0.220	0.0050			5	30.7	13.2	53.5		3.2	100.4
2 "	0.0370	0.215	0.0038	0.462		5	31.4	9.0	56.1		3.3	99.8
5 "	0.0222					5	31.5	11.1	54.8		3.2	100.6
8 "	0.0137	0.211	0.0020	0.463		5	30.6	17.1	50.0		3.3	101.0
12 "	0.0092					3	27.1	30.4	40.5		2.5	100.5
20 "	0.0064	0.210	0.0018	0.461		2	26.7	35.6	35.6		3.3	101.2
30 "	0.0060					1	27.0	35.7	34.0		3.0	99.7
45 "	0.0054	0.220	0.0010	0.461								
60 "	0.0052											
90 "	0.0046											
Ing	0.0044	0.211	0.0005	0.460								

T A B L E 4. 23      E X P E R I M E N T   N o . 5 E 2

SAMPLE TIME	B E L T   A   N A L Y S I S   W t %					I N C L U S I O N   A N A L Y S I S   W t %						
	O	Si	Al	Mn	C	n	MnO	Al <sub>2</sub> O <sub>3</sub>	SiO <sub>2</sub>	CaO	FeO	TOTAL
Prem	0.0432											
- 1 min	0.0389											
+ 1/2 "	0.0248	0.235	0.0028	0.695		6	41.0	6.6	48.1		2.9	98.6
1 "	0.0218	0.237	0.0023	0.665		5	41.0	10.4	46.3		3.1	100.8
2 "	0.0187	0.236	0.0023	0.688		5	41.9	7.5	47.6		2.7	99.7
5 "	0.0107					4	38.7	13.1	45.1		2.6	99.5
8 "	0.0056	0.232	0.0020	0.670		3	33.9	22.4	40.6		2.5	99.4
12 "	0.0052					2	31.1	31.0	33.9		3.8	99.8
20 "	0.0047	0.228	0.0025	0.670								
30 "	0.0046											
45 "	0.0044	0.224	0.0025	0.678								
60 "	0.0046											
90 "	0.0044											
Ing		0.237	0.0020	0.655	0.029							

T A B L E 4. 24

E X P E R I M E N T N o. 5 E 3

S A M P L E T I M E	F E L T A N A L Y S I S W t %				I N C L U S I O N A N A L Y S I S							W t % T O T A L	
	O	Si	Al	Mn	C	n	MnO	Al <sub>2</sub> O <sub>3</sub>	SiO <sub>2</sub>	CaO	FeO		
Prem	0.0432												
- 1 min	0.0472												
+ 1/2 "	0.0214	0.256	0.0027	0.878		5	48.4	3.1	45.2		2.4	99.3	
1 "	0.0156	0.258	0.0030	0.862		5	49.4	3.0	45.5		2.4	100.3	
2 "	0.0143					5	49.4	3.3	45.1		2.3	100.1	
3 1/2 "	0.0098	0.250	0.0028	0.855		5	47.8	4.0	45.0		2.4	99.2	
6 "	0.0051					3	37.1	18.8	42.6		2.2	100.7	
9 "	0.0042	0.247	0.0022	0.860									
13 "	0.0035					1	29.5	37.5	30.3		2.4	99.7	
20 "	0.0033	0.252		0.860									
30 "	0.0032		0.0049										
45 "	0.0033	0.253		0.845									
60 "	0.0030												
90 "	0.0029												
Ing "	0.0030	0.248	0.0049	0.833									

TABLE 4. 25

EXPERIMENT No. 5 E 4

SAMPLE TIME	M E L T A N A L Y S I S Wt %						I N C L U S I O N A N A L Y S I S Wt %					
	O	Si	Al	Mn	C	n	MnO	Al <sub>2</sub> O <sub>3</sub>	SiO <sub>2</sub>	CaO	FeO	TOTAL
Prem	0.0507											
- 1 min	0.0493											
+ $\frac{3}{4}$ "	0.0354	0.238	0.0038	0.254		5	17.2	17.1	61.4		2.7	98.4
1 $\frac{1}{2}$ "	0.0324					5	17.3	15.2	63.6		2.8	98.9
3 "	0.0248	0.237	0.0025	0.225		5	16.8	15.1	65.3		2.6	99.8
5 "	0.0175					5	17.2	18.9	61.7		2.5	100.3
8 "	0.0107	0.235	0.0018	0.210		4	19.4	26.4	50.5		2.6	98.9
12 "	0.0076					3	18.5	32.7	44.9		2.8	98.9
20 "	0.0073	0.235	0.0018	0.205								
30 "	0.0066	0.235	0.0010	0.205								
45 "	0.0060											
60 "	0.0054	0.235	0.0006	0.208								
90 "	0.0051											
Ing	0.0058	0.235	0.0008	0.195	0.028							



TABLE 4. 26

EXPERIMENT No. 5 E 5

SAMPLE TIME	MELT ANALYSIS					INCLUSION ANALYSIS					TOTAL	
	O	Si	Al	Mn	C	n	MnO	Al <sub>2</sub> O <sub>3</sub>	SiO <sub>2</sub>	CaO		FeO
Frem	0.0529											
- 1 min	0.0473											
+ 1/2 "	0.0373	0.248	0.0090	0.464		5	27.7	31.1	39.3		2.4	100.5
1 "	0.0371					5	27.9	31.8	38.2		2.4	100.3
2 "	0.0324	0.251	0.0088	0.450		5	26.9	31.5	38.6		2.7	99.7
4 "	0.0230					4	26.4	34.5	37.3		2.5	98.9
7 "	0.0125	0.242	0.0044	0.444		4	25.0	37.7	35.4		2.3	100.4
10 "	0.0090					4	24.7	36.7	35.1		2.8	99.3
15 "	0.0071	0.237	0.0028	0.430		2	24.8	37.6	35.3		2.8	100.5
20 "	0.0054					3	24.7	36.1	35.6		2.8	99.2
30 "	0.0055	0.236	0.0022	0.420								
45 "	0.0051											
60 "	0.0042	0.236	0.0010	0.420								
90 "	0.0031											
Ing	0.0026	0.235	0.0016	0.415								

TABLE 4. 27

EXPERIMENT No. 5 E 6

SAMPLE	M E L T A N A L Y S I S W t %				I N C L U S I O N A N A L Y S I S W t %							
	O	Si	Al	Mn	C	n	MnO	Al <sub>2</sub> O <sub>3</sub>	SiO <sub>2</sub>	CaO	FeO	TOTAL
Prem	0.0547											
- 1 min	0.0545											
+ ½ "	0.0419	0.266	0.0244	0.515		2	23.1	45.5	29.3		2.8	100.7
1 "	0.384					1	17.9	52.2	28.4		2.0	100.5
2 "	0.0323	0.258	0.0176	0.504		1	17.0	60.0	21.3		2.3	100.6
4 "	0.0231					1	20.9	50.5	25.9		2.2	99.5
7 "	0.0137	0.254	0.0079	0.500		1	22.2	44.5	29.6		2.5	98.8
10 "	0.0090					1	20.7	51.7	25.0		2.4	99.8
15 "	0.0063	0.258	0.0025	0.500		1	18.6	58.5	20.7		2.4	99.8
20 "	0.0044											
30 "	0.0043	0.250	0.0020	0.488								
45 "	0.0042											
60 "	0.0038	0.250	0.0020	0.479								
90 "	0.0035											
Ing	0.0033	0.245	0.0015	0.475								

T A B L E 4. 28

E X P E R I M E N T No. 5 C 2

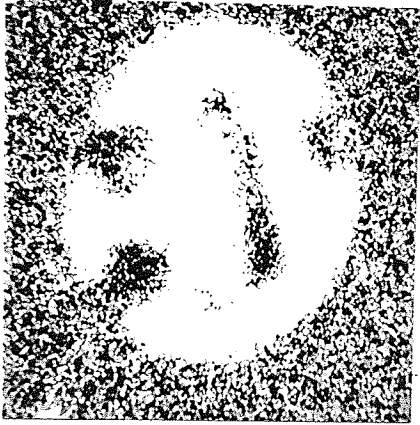
S A M P L E T I M E	M E L T A N A L Y S I S Wt %				I N C L U S I O N A N A L Y S I S Wt %							
	O	Si	Al	Mn	C	n	MnO	Al O	SiO <sub>2</sub>	CaO	FeO	TOTAL
Prem	0.0518											
- 1 min	0.0476											
+ 1/2 "	0.0271	0.243										
1 "	0.0238											
2 "	0.0222	0.259										
4 "	0.0165											
7 "	0.0123	0.259										
10 "	0.0102											
15 "	0.0083	0.250										
20 "	0.0074											
30 "	0.0073	0.253										
45 "	0.0071											
60 "	0.0073	0.251										
90 "	0.0067											
Ing	0.0067	0.248										0.028

X RAY IMAGE

X 1,000

LINE SCAN

X-



- X

fig 4.9a Mn  $K\alpha$  radiation

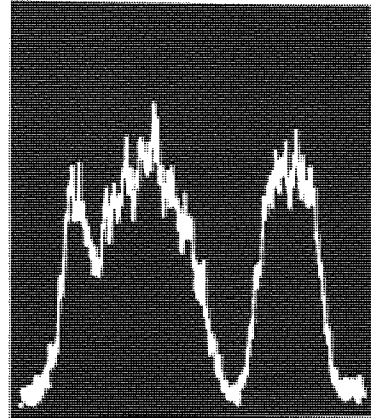


fig 4.9 b



fig 4.9c Si  $K\alpha$  radiation

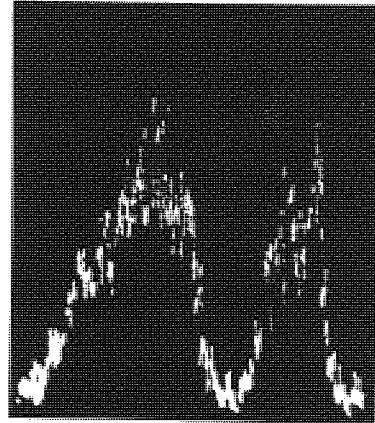


fig 4.9d

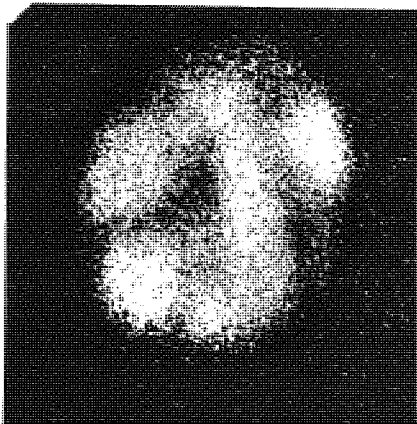


fig 4.9e Al  $K\alpha$  radiation

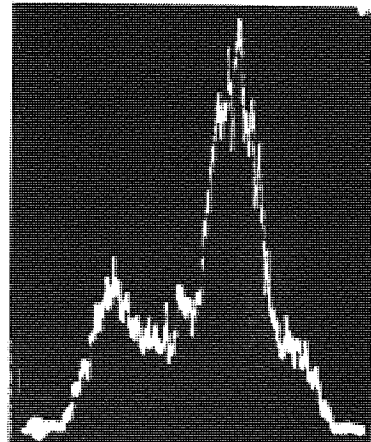


fig 4.9f

Line scan traverses made at x - x.

#### 4.4. Metallographic examination.

4.4.1 Inclusion types. Typical examples of the inclusions found as a result of different deoxidation treatments are shown in figs. 4.10 to 4.15. Figs. 4.10 and 4.11 show the products of silicon and aluminium deoxidation respectively. The glassy silicates shown in figs. 4.12 and 4.13 are representative of the inclusions found as a result of Si/Al, Ca/Si/Al, Mg/Si/Al and Mn/Si/Al deoxidation and also of the inclusions formed by silicon deoxidation of a manganese containing premelt in series 3. The distinctly heterogeneous inclusions shown in figs. 4.14 and 4.15 resulted only from the Mn/Si/Al deoxidation of experiment 5 E 6.

4.4.2 Inclusion content and size distribution. The results of a quantitative metallographic examination on series 5 experiments are set out in tables 4.29 to 4.31. The sample identification is the same as used previously.  $n$  is the number of fields examined,  $\bar{\%} A$  is the mean concentration of inclusion expressed as percentage of total area examined,  $\sigma$  is the standard deviation of the mean  $\bar{\%} A$ , and  $1.96 \sigma / \sqrt{n}$  defines the 95% confidence limits by the relation shown in equ. 4.1 assuming a normal distribution of results.

$$95\% \text{ C.L.} = \bar{\%} A \pm 1.96 \sigma / \sqrt{n} \quad \dots \quad \text{equ. 4.1.}$$

The diameter of the particles  $d$  is given in microns.  $A_t$  is the total field area examined for each sample.

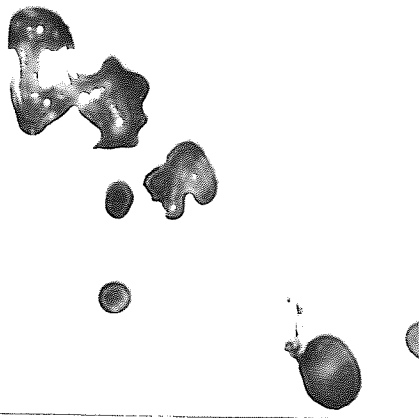


fig. 4.10 Silica particles  
x 800

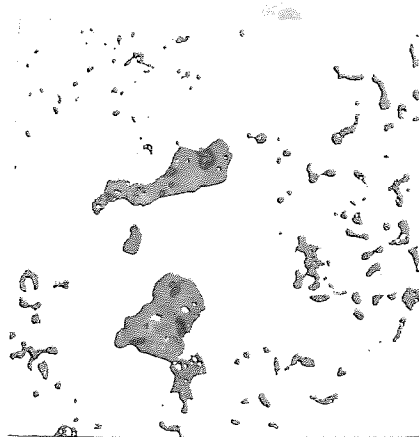


fig. 4.11 Alumina particles  
x 200



fig. 4.12  
x 800

Glassy silicate particles

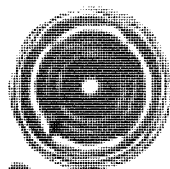


fig. 4.13  
x 800

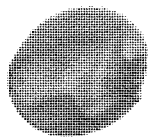


fig. 4.14  
x 500

Alumina plates precipitating  
within glassy silicates.



fig. 4.15  
x 800

Figs. 4.16 to 4.25 are photomicrographs of experiment 5 E 5, shown at a magnification of x 100. They serve to illustrate the change in particle size distribution and inclusion concentration during the holding period after deoxidation.

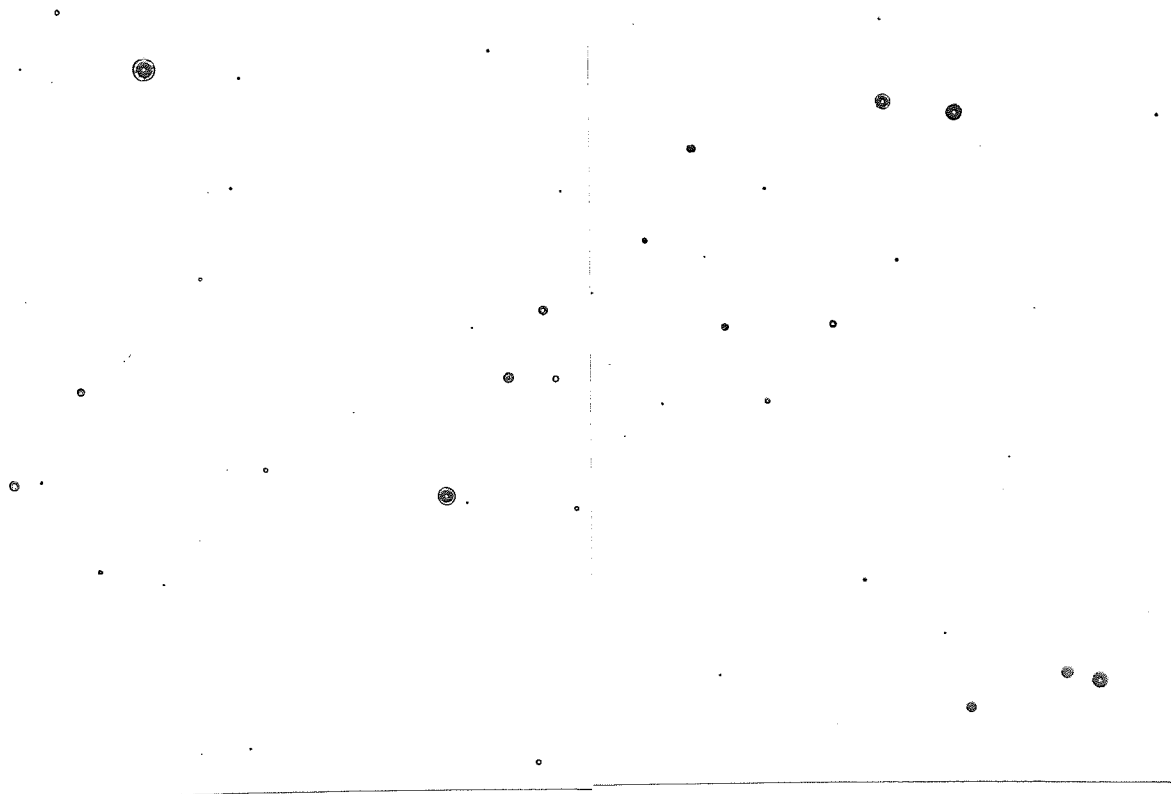


fig. 4.16

$\frac{1}{2}$  min.

fig. 4.17

1 min.

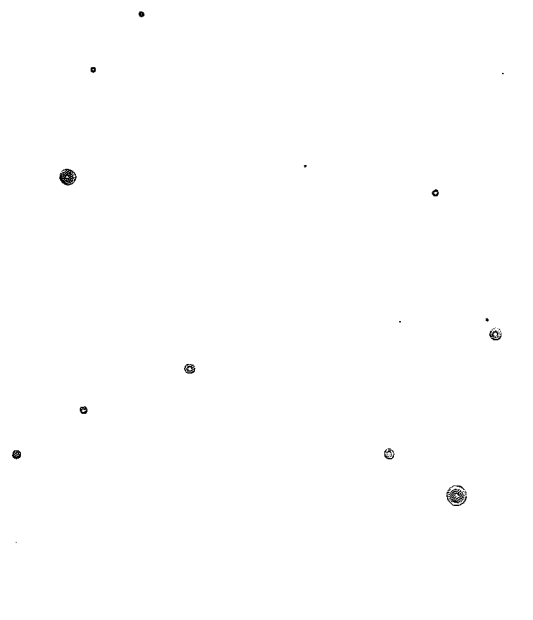


fig. 4.18

2 min




fig. 4.19

4 min.




fig. 4.20

7 min




fig. 4.21

10 min.



fig. 4.22

15 min. fig. 4.23

20 min.

fig. 4.24.

60 min. fig. 4.25

90 min.

EXP.	SAMPLE	AREA ANALYSIS				95% C.L. At $\lambda_d$	SIZE DISTRIBUTION NUMBER OF INCLUSIONS > d									
		n	% A	$\sigma$	0.030		0	5	10	15	20	25	30	35		
5E1	1/2 min	72	0.129	0.129	0.030	5.76	569	100	29	13	4	2	1			
"	1 "	67	0.104	0.125	0.030	7.06	534	119	24	10	8	2				
"	2 "	64	0.080	0.079	0.019	8.65	634	97	23	4	2					
"	5 "	53	0.049	0.040	0.011	6.20	421	61	7	3						
"	8 "	40	0.034	0.023	0.007	3.89	237	27	3							
"	12 "	25	0.021	0.015	0.006											
"	20 "					5.76	286	13								
"	45 "	50	0.017	0.008	0.002											
"	90 "	41	0.010	0.007	0.002	3.89	200									
5E2	1/2 "	61	0.141	0.084	0.021	8.94	1,071	165	25	6	2					
"	1 "	72	0.149	0.098	0.023	7.78	982	158	35	9						
"	2 "	53	0.117	0.089	0.024	8.21	696	91	18	8	5	1				
"	5 "	38	0.087	0.037	0.012	7.92	667	83	6							
"	8 "	47	0.045	0.031	0.009	6.76	303	33	3							
"	12 "	35	0.017	0.014	0.005	2.45	94	5	1							
"	90 "					3.17	99	1								

TABLE 4.30		AREA ANALYSIS				d	SIZE DISTRIBUTION									
EXP.	SAMPLE	n	% A	$\sigma$	95% C.L.		0	5	10	15	20	25	30	35		
5E3	1/2 min	74	0.142	0.136	0.031	10.60	1,478	156	37	16	2	2	1			
"	1 "	54	0.115	0.110	0.029	7.83	731	98	23	9	4	1				
"	2 "	60	0.117	0.167	0.042	8.70	703	104	21	8	4	3	2	1		
"	3 1/2 "	63	0.043	0.047	0.012	9.14	441	59	6	1						
"	6 "	45	0.021	0.016	0.005	6.52	231	20								
"	90 "	23	0.005	0.003	0.001	3.34	106									
5E4	1/2 "	65	0.260	0.115	0.028	9.80	2,062	394	46	6	1	1				
"	3/4 "	69	0.250	0.118	0.028	10.40	2,260	382	49	4						
"	1 1/2 "	69	0.233	0.082	0.019	10.40	2,484	336	44	4						
"	3 "	63	0.210	0.156	0.039	9.70	1,669	231	43	13	4					
"	5 "	61	0.154	0.073	0.018	9.40	1,494	192	30	7						
"	8 "	51	0.111	0.072	0.020	7.85	1,090	113	13	4						
"	12 "	54	0.041	0.022	0.006	8.31	604	46	2							
"	60 "	29	0.022	0.010	0.004	4.46	214	2								



The distribution of inclusions in ingots cooled immediately after deoxidation showed only a little concentration towards the top surface. The distribution of inclusions in the vertical plane after a period of holding at  $1550^{\circ}\text{C}$  however, is shown in fig. 4.26. This refers to the ingot of experiment 4E11.

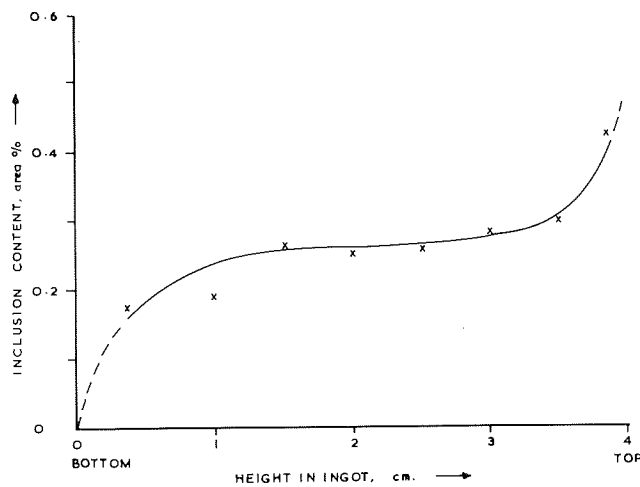


fig.4.26 Inclusion distribution in the vertical plane of deoxidized ingot, 5 mins. after completion of addition.

## SECTION 5. DISCUSSION OF RESULTS

5.1. Introduction      The experiments can be divided into three groups according to the composition of deoxidiser used.

(a) Silicon, aluminium or silicon-aluminium alloy deoxidisers.

(b) Deoxidisers containing calcium, magnesium or lime.

(c) Deoxidisers containing manganese.

Comparison will be made firstly between deoxidisers of group (a) and those of group (b). Finally the manganese containing alloys (group c) will be discussed in relation to group (a) and (b) individually and collectively.

It is hoped in the discussion, especially of manganese-silicon-aluminium alloys to show that product nucleation occurred in solute rich zones surrounding the deoxidiser during its dissolution and that the product compositions were related to the deoxidation alloy composition. Oxygen desaturation of the melt by solute diffusion and growth of product nuclei took place very rapidly because of a high concentration of nuclei, but the initial products changed in composition to approach equilibrium with the melt as homogeneity of solute distribution was achieved.

Reaction between separated products and the crucible material resulted in alumina saturated slags which determined the residual oxygen content by controlling solute equilibria in the melts.

Under the quiescent conditions of the present experiments, product separation occurred at a rate which could not be quantitatively accounted for by Stoke's Law. Coalescence of low liquidus temperature products was indicated and these products separated more rapidly than higher liquidus temperature products. Interfacial tension between product and melt is also an important property and it has been shown that a high interfacial tension favours rapid product separation.

Calcium or magnesium in the deoxidiser participate only to a limited extent in deoxidation by vapour/melt reaction and the distribution of initial products having appreciable lime or magnesia contents, supports the conclusion of low melting point products coalescing and rapidly floating out of the melt.

## 5.2. Control deoxidisers and effects of calcium and magnesium

### 5.2.1. Residual oxygen in the melts and equilibria with products

5.2.1.1. Silicon and aluminium controls It was expected that equilibrium between residual solutes and the deoxidation products would be approached rapidly because the small product particles provided a large surface area: volume ratio, and with a large number of particles the diffusion distances were small. Turkdogan (84) showed that for a diffusion controlled reaction nucleation and growth were complete within 30 secs, if the concentration of particles was  $10^5 \text{ cm}^{-3}$ . For the present, this is assumed to represent equilibrium.

The measured oxygen and deoxidiser concentrations at any time following deoxidation represented the total contents however, i.e. they included the proportions combined in residual oxide particles. The equilibrium relationships therefore, were indicated only when all products had separated from the melt.

Completeness of oxide separation and approach to equilibrium can be examined by the silicon and aluminium control deoxidations, for which the data appertaining to equilibrium are shown in table 5.1.

TABLE 5.1. Control experiment data.

EXP	TIME MINS	$f_O$	$f_{Si}$	$f_{Al}$	$h_O$	$h_{Si}$	$h_{Al}$	$k'Si-O$	$k'Al-O$
4C3	60	0.81	1.5	-	0.0054	0.585	-	$1.7 \times 10^{-5}$	-
5C2	90	0.87	1.3	-	0.0053	0.322	-	$1.1 \times 10^{-5}$	-
4C2	60	0.99	-	1.0	0.0111	-	0.0004	-	$2.2 \times 10^{-13}$
4C4	60	0.83	-	1.0	0.0004	-	0.085	-	$4.6 \times 10^{-13}$
4C6	60	0.89	-	1.0	0.0005	-	0.053	-	$2.6 \times 10^{-13}$

( $h$  represents Henrian activity,  $k'Si-O$  and  $k'Al-O$  are the apparent deoxidation constants of silicon and aluminium respectively).

The deoxidation constants measured at 60 mins. are considerably greater than the values indicated by the equilibrium data reviewed in sections 2.1.2.3. and 2.1.2.4., thus indicating



that some oxide particles persist in the melt. After 90 mins however  $k'_{\text{Si-O}}$  becomes similar to the value determined by Bell (49) and so it was assumed that separation of products was almost complete after holding the melt for 90 mins.

The apparent deoxidation constant of aluminium can be explained by assuming a residual alumina content of approximately 0.0005% and it was likely that very lengthy holding periods would have been required for more complete separation than this. Another contributing factor was the analytical accuracy when the oxygen content was as low as 4 p.p.m., and aluminium contents of this magnitude were on the lower limit of detection for the method employed. In both cases the errors would be expected to increase the value of  $k'_{\text{Al-O}}$ .

The value of  $k'_{\text{Si-O}} = 1.1 \times 10^{-5}$  will therefore be used in subsequent calculations of silica activity, assuming complete product separation after 90 mins, but the errors involved in  $k'_{\text{Al-O}}$  prevent similar activity calculations being made for alumina.

#### 5.2.1.2. Silicon - aluminium alloy control and lime additions

The residual silicon and oxygen contents of experiment 4C1, indicate an activity product of  $h_{\text{O}}^2 \cdot h_{\text{Si}} = 1.0 \times 10^{-5} = k'_{\text{Si-O}}$   $a_{\text{SiO}_2}$ , from which the silica activity is calculated as 0.91 if  $k'_{\text{Si-O}}$  is  $1.1 \times 10^{-5}$ . The product composition, shown in table 4.7 for this experiment can be seen from Fig. 5.1.



to lie in the mullite + liquid phase field at  $1550^{\circ}\text{C}$  but no evidence of phase separation was observed in the product particles. An approximate silica activity of 0.75 is obtained by extending the silica isoactivity lines in Fig. 2.12 to the silica-alumina binary system. The estimated activity of 0.91, compared with this approximate value of 0.75, suggests that product separation was not complete and, as the melt was only held for 60 mins, and the oxygen content decreased by 0.001% in the 30 mins to 60 mins period, it seems likely that the lower value is the more accurate.

Addition of lime powder to a deoxidiser which was essentially the same as that used for experiment 4C1, resulted in products having a similar silica: alumina ratio but containing a small proportion of lime, as shown in table 4.9. The calculated silica activity of 0.73 compares well with the value of approximately 0.75 found from Fig. 2.12 and the oxygen analyses indicate that very little residual oxide is present in the melt. Sufficient lime was added to this melt to give a slag containing approximately 23% lime and 18% alumina, if no aluminium or lime were lost, and from Fig. 2.12 the silica activity for this composition is found to be 0.65. This slag composition is in the liquid range at  $1550^{\circ}\text{C}$  and the liquidus temperature of the inclusion composition is close to  $1550^{\circ}\text{C}$ . The final oxygen content of the melt would not have been greatly affected therefore if equilibrium were established.

with a slag formed by separated lime and deoxidation products instead of with the deoxidation products only. If the slag became saturated with alumina from the crucible the silica activity would only decrease to 0.6 and this would decrease the residual equilibrium oxygen content by only 3 P.P.M.

Comparison of the silica activities in products from experiments 4E1 and 4E11, shows that the addition of lime to the silicon - aluminium deoxidiser had very little effect on the equilibrium residual oxygen content of the melt.

5.2.1.3. Silicon aluminium deoxidisers containing calcium or magnesium. Data for the equilibria in series 4 melts, to which volatile metal additions had been made are summarised in table 5.2.

TABLE 5.2 Silicon-Oxygen Equilibria						
EXP.	$f_O$	$f_{Si}$	$h_C$	$h_{Si}$	$k_{Si-O}^{SiO_2}$	$a_{SiO_2}$
4E2	0.86	1.20	0.0030	0.301	$0.271 \times 10^{-5}$	0.25
4E4	0.88	1.27	0.0035	0.283	0.347 " "	0.32
4E6	0.88	1.25	0.0037	0.260	0.356 " "	0.32
4E8	0.86	1.31	0.0015	0.313	0.070 " "	0.064
4E9	0.84	1.35	0.0012	0.383	0.055 " "	0.050
4E14	0.88	1.27	0.0046	0.286	0.605 " "	0.55

The activity of silica in the deoxidation products of experiment 4E2 lies in the range 0.3 - 0.7 according

to the inclusion compositions shown in table 4.10 and the activity curves shown in fig 2.12, but these compositions relate to inclusions found up to 2 mins. after deoxidation and it is likely that the compositions become more consistent at longer holding times and result in a more consistent silica activity. Experiment 423 used a similar deoxidiser and the activity of silica at the composition shown in Table 4.11 for the 12 min. sample is found from fig. 2.12 to be 0.55. Equilibrium must have been established with a slag of low silica activity and only a slag on the melt surface could provide the silica activity of 0.25 indicated by the melt analysis.

A possible mechanism for the formation of a surface slag having a low silica activity was for the separated deoxidation products to coalesce at the melt surface/crucible wall interface and to become saturated with alumina from the crucible. The initial products, containing a high proportion of lime, were liquid at 1,550°C and so when they separated and gathered at the melt surface/crucible interface, as they were observed to do, solution of alumina from the crucible to saturate the slag at 1550°C was likely to occur. A slag containing 20% lime, 40% silica and 40% alumina could be produced in this way. This composition lies on the alumina saturation boundary and has a silica activity of 0.25.

Experiment 4E2 therefore suggests that final equilibrium is established between the melt and an alumina saturated slag at the surface. Experiment 4E3 is not included in table 5.2 because table 4.11 shows a decrease of 0.01% oxygen between the 45 & 60 min samples, thus indicating that the equilibrium concentration had not been achieved at 12 mins. in 4E3.

Product compositions shown in table 4.14 for experiment 4E4 are more consistent than those for 4E2 and 4E3, showing only a 10% increase in alumina content between the 1 and 12 min. samples with a corresponding decrease in silica content. These compositions lie inside the alumina + liquid phase field at 1570°C but no evidence of alumina precipitation within the products was observed. Extending the silica isoactivity lines into this region on fig. 2.12 indicates a silica activity of 0.3 for the product composition. This agrees well with the value of 0.32 calculated from the melt analysis and as the products are saturated in alumina at the observed composition, it is unlikely that more alumina could be picked up from the crucible.

Experiment 4E6 gave products similar in composition to those of experiment 4E3 but with 10 - 15% more silica and correspondingly less alumina. The silica activity of products in the 12 and 20 min. samples (Table 4.16) is found

from fig. 2.12 as 0.5 but these products are liquid at 1550°C and may dissolve 5 - 10% alumina from the crucible when separated from the melt. This increase in alumina content to achieve alumina saturation at 1550°C would lower the silica activity to approximately 0.35 which agrees with the value calculated from the melt analysis. This is taken as a further indication that the equilibrium residual oxygen content is controlled by the slag on the melt surface as well as by the residual concentration of deoxidisers.

Deoxidation products in melts 438 and 439 may be seen from tables 4.17 and 4.18 to consist of alumina or particles very rich in alumina. The silica activity is so low that the residual oxygen appears to equilibrate with dissolved aluminium and alumina at unit activity, giving  $k^{Al-O}$  as  $4.8 \times 10^{-13}$  and  $1.4 \times 10^{-13}$  in experiments 438 and 439 respectively. The comments concerning analytical accuracy and incomplete separation of oxides made in connection with the aluminium control experiments probably apply to these experiments also.

In neither experiment however, was the aluminium added in stoichiometric excess of the oxygen but the calcium additions were very high 0.15%. Table 4.17 shows that lime contents of up to 41% were found in the products of melt 438 and so it is proposed that the initial products

separated to produce a slag rich in lime and alumina in which the silica activity was very low and the melt equilibrated with this slag. The composition 50% alumina, 30% lime and 20% silica lies on the 1550°C liquidus boundary and has a silica activity of approximately 0.05.

Experiment 4B) shows similar effects to those found in 4A) but the lime content of the products does not reach such a high concentration and the composition of products found in the 2 and 5 min. samples indicate a silica activity of 0.05 if the line in fig. 2.12 extended into the solid + liquid phase field. The inclusions residual in the melt at 5 min. must have had a similar silica activity to the surface slag but the latter probably contained more lime.

The deoxidiser for experiment 4B14 contained 5% magnesium in place of calcium and it resulted in products having a fairly consistent magnesia content but which increased in alumina content during the holding period. This increase in alumina caused the product composition to approach the 1550°C liquidus boundary with the liquid + mullite phase field. The product compositions shown in table 4.21, all indicate a silica activity of 0.6 which is close to the value of 0.55 calculated from the melt composition. This experiment shows that the effects of magnesium on the residual oxygen content are similar to those of calcium.



The residual oxygen did not, in any of the experiments fall below a level which could be reasonably accounted for by equilibration of the oxygen with silicon or aluminium and the products. It was concluded therefore, that calcium and magnesium were not residual in the melt in sufficient quantities to contribute directly to a lower equilibrium oxygen content.

It is clear however, that calcium and magnesium do contribute in achieving a low equilibrium oxygen content by formation of some lime or magnesia which reduces the activity of silica in the products and thus increases the deoxidising power of silicon.

#### 5.2.2. Formation and separation of deoxidation products

5.2.2.1. Product composition. The composition of particles containing lime or magnesia can be seen from labels 4.10 - 4.21 to lie within a very wide range, various compositions often being found in a particular sample. The greatest fluctuation in composition occurred in the lime and alumina contents whilst, in products of acid slag composition, the silica content varied only within a narrow range. (See especially tables 4.11 and 4.16). Alumina acted as a base in the acid slag composition range and so  $Al^{+++}$  ions could replace  $Ca^{++}$  ions in the deoxidation products. Very little change in silica activity accompanied such a substitution of aluminium ions for calcium ions and it is possible

therefore, for particles of different compositions to be formed which equilibrated with the same silicon and oxygen contents of the melt. Deoxidation products from most of the experiments contained silica in excess of the orthosilicate composition and behaved as acid slags.

Despite the large fluctuations in lime content of products in the individual samples, it can be seen that the particles having maximum lime contents were observed only in samples taken within approximately 2 mins. of deoxidation. It can further be seen from the tabulated data in section 4, that the lime or magnesia content of inclusions found near the top surface of the ingot was greater than the maximum observed for inclusions in the pipette samples. These differences cannot be explained only in terms of the deoxidise compositions and are considered to result from the particular conditions of product formation and separation. This is discussed further in the following section 5.2.2.2.

The effects of increasing aluminium additions to the melt by using higher aluminium concentrations in the deoxidiser were obscured to some extent by the variable proportions of lime and alumina in the products but the general trend is shown in fig. 5.2. This is as expected, in that the alumina content of the product increases as the ratio ( $\Delta\%$  O: % Al added) becomes smaller  $\Delta\%$  O is the total oxygen removed from solution. Pure alumina products result when ( $\Delta\%$  O: % Al added) becomes less than the stoichiometric ratio of

0.889 for alumina formation. The alumina contents in fig 5.2 are

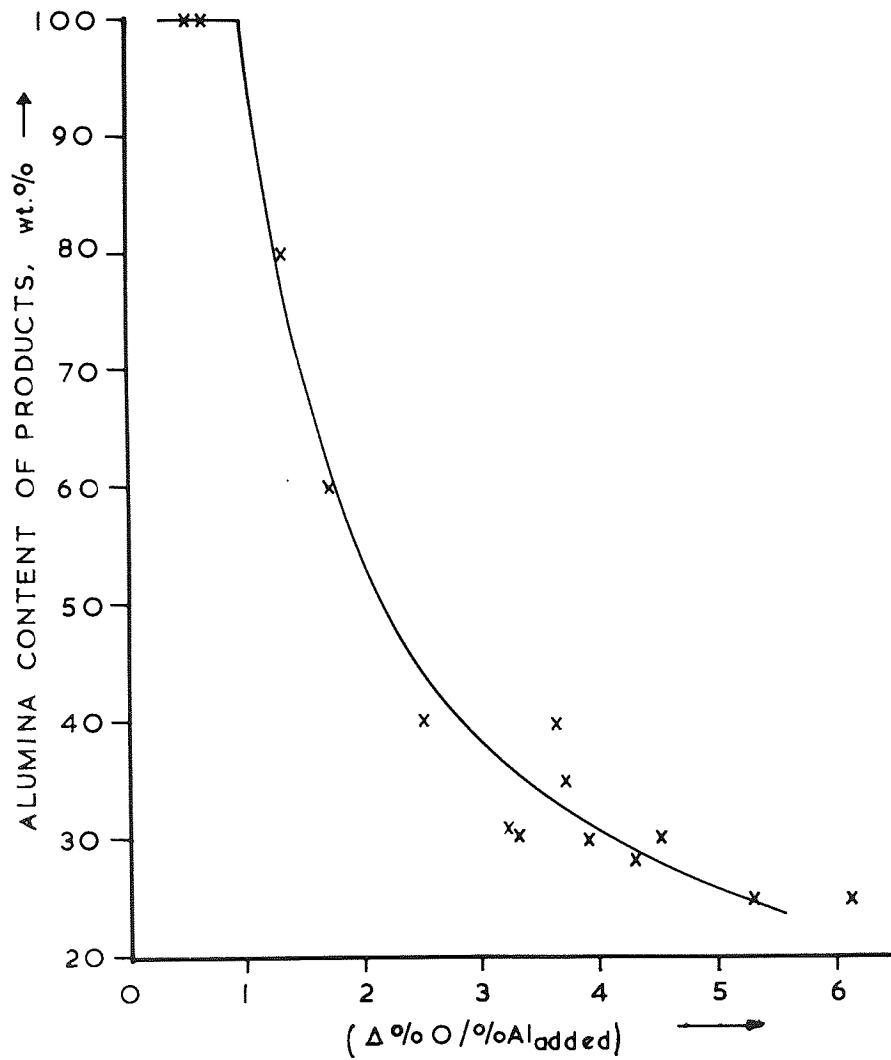


Fig. 5.2. Variation in alumina content of deoxidation products with the ratio of ( $\Delta\% \text{O} : \% \text{Al added}$ ).

mostly those from inclusions with approximately 10%  
lime, so that the data are more comparable between melts.  
 $\Delta\% O$ : is the measured value or, in the cases of ingots  
quenched without a holding period,  $\Delta\% O$  was calculated  
from the initial oxygen content and the residual found from  
experiments using a similar deoxidiser and a holding period.

$\% Al$  added was calculated from the deoxidiser composition  
and total addition except in cases where the  $1/2$  min melt  
analysis indicated that this was in error. In such cases  
the initial aluminium content was estimated by calculating  
the aluminium lost as oxide in the first  $1/2$  min from the  
known oxygen removed and average alumina content of the  
products.

4.2.2.2. Product Distribution. The variation of  
inclusion concentration along the vertical plane of an ingot  
is shown in fig 4.26, and this curve is confirmed by plotting  
the oxygen contents from table 4.19 as shown in fig. 5.3.  
These results refer to an ingot which had been held for 5  
mins. to allow segregation of the particles by flotation  
but a similar curve has been obtained by other workers  
(123) using the same technique with an immediate quench  
after deoxidation. These latter results were obtained by  
determining inclusion concentrations with a lineal traverse  
technique (124)

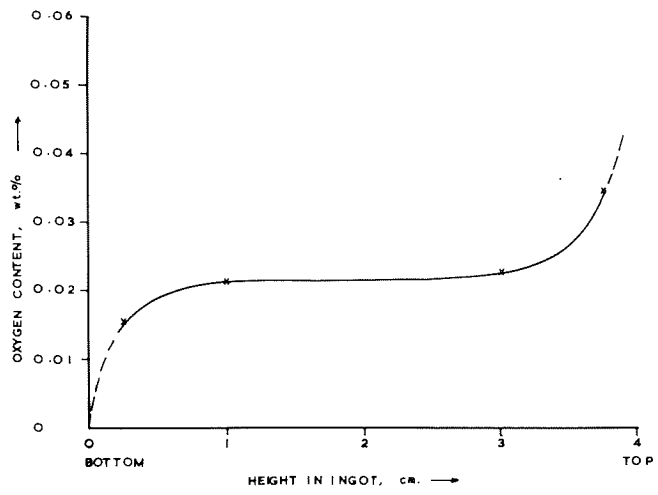


Fig. 5.3. Variation of oxygen content in the vertical plane of an ingot. (Re-experiment ~~1~~ 4 E11).

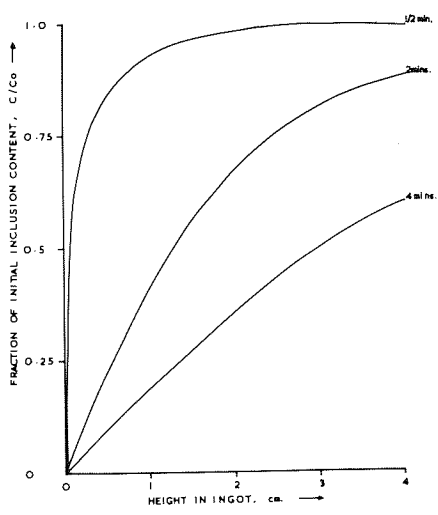


Fig. 5.4. Variation of oxygen content in the vertical plane of an ingot, according to the model of Ohkubo

The flat portion of the curve and the increase in inclusion concentration near to the ingot surface, are not consistent with the curves shown in fig. 5.4. The curves in fig. 5.4. were calculated from equation 2.27 assuming the Stoke's Law model of Ohkubo et. al (95). Turbulence associated with boiling off the calcium and mixing in the deoxidiser would cause a small departure from the quiescent conditions assumed for equation 2.27 but only stirring on addition of the deoxidiser applies to the experiments of Peace et.al (123) because they used no volatile constituents in their deoxidisers. It is further expected that strong turbulence would exist for only a short time and that it would not be likely to promote a high concentration of inclusions near the melt surface. It seems more likely therefore, that the differences are due to coalescence of particles altering the inclusion size distribution which is considered constant in equation 2.27.

Calcium and magnesium boiled off very rapidly when added to melts and so the presence of particles containing high lime or magnesia contents near the ingot surface indicated that they were formed very quickly and segregated towards the surface. Many of the lime or magnesia rich inclusions were larger than the size predicted by Turkdogan (84) on a basis of growth by diffusion and  $10^5$  growing

particles per  $\text{cm}^3$ . The lime rich inclusions have low liquidus temperatures, and this feature, in addition to the size, further indicates a coalescence of initial products.

Inconsistency of lime and magnesia contents suggests that the particles were not formed by homogeneous reaction between solutes in liquid iron. It may be noted here that manganese - silicon - aluminium deoxidation were of uniform composition within a particular sample. It is proposed therefore, that reaction of dissolved oxygen with calcium occurred essentially with calcium vapour according to reaction 8.

The conclusions of Koch (106) that calcium takes part in the initial stages of deoxidation, and that the large lime rich particles separate rapidly, were confirmed by these results. Coalescence of the liquid lime - silica - alumina products is thought to be involved to a large extent in producing the observed particle distribution.

Low concentrations of lime in residual inclusions, found after a 10 min. holding period, were probably due to silica and alumina growing on small lime rich inclusions. A similar mechanism is likely when lime is added to the deoxidiser, as in experiments 3 El, and 4 El, which produced only small amounts of lime in the products. In these

latter experiments a large proportion of the added lime escaped rapidly as no inclusions of high lime content were observed, although the size of lime particles was approximately  $10 \mu\text{m}$  and according to Stoke's Law they should have taken 3 mins to float out from the bottom of the bath.

5.2.2.3. Product Separation Rate It has already been mentioned that turbulence by boiling off volatile metals or by mixing the deoxidiser would have existed for only a short time and this leaves only the possibility of induction stirring to disturb product flotation. Forsten and Miek-Oja (125) have calculated the depth of penetration of H.F. current in graphite as 1.6 mm when the frequency was 400 Kc/sec. The H.F. supply in the present work was only 8.5 Kc/sec and this gives a depth of penetration of 1.1 cm, but as the wall thickness of the graphite susceptor was 3 cm at the level of the crucible it is believed that negligible induction stirring occurred in the melt.

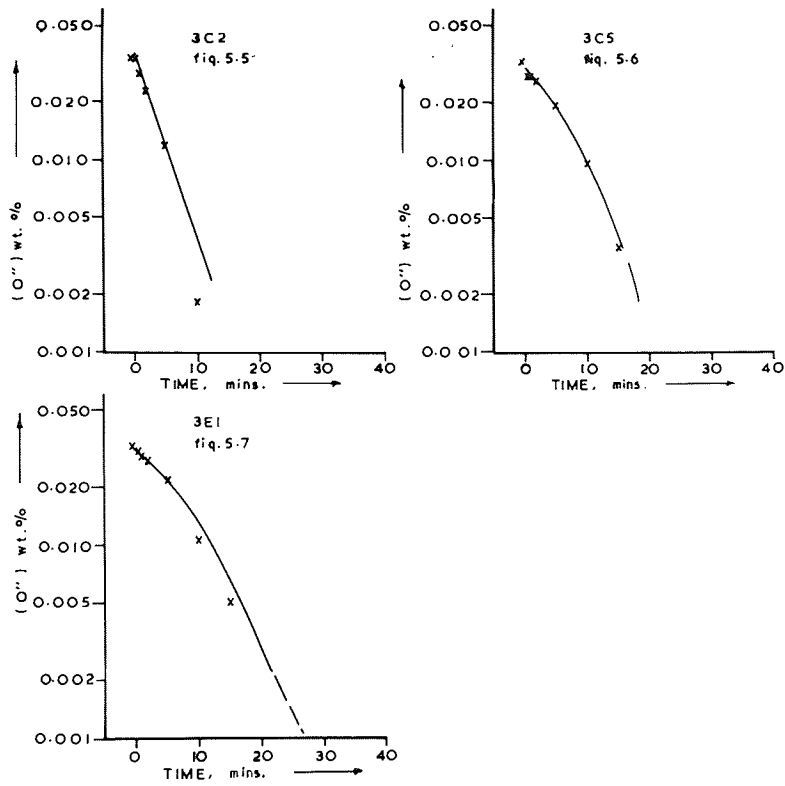
The mode of product separation may therefore be considered as undisturbed flotation of particles from a quiescent melt. The difference in separation rates shown by figs. 5.5 - 5.21, can then be attributed to the compositional differences and consequent differences in particle properties.

It is assumed that the oxide content of a melt at any time following deoxidation, is proportional to the



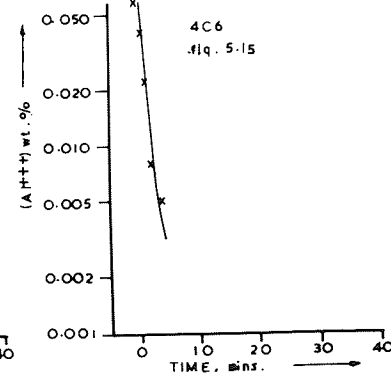
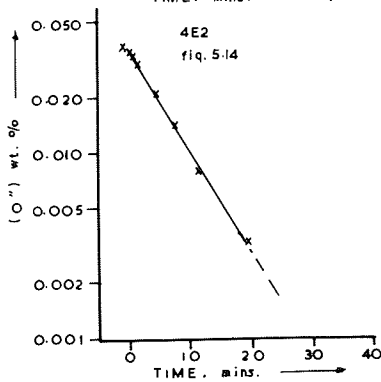
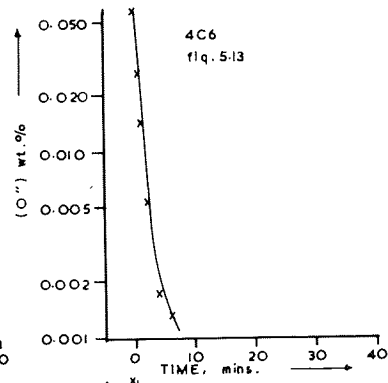
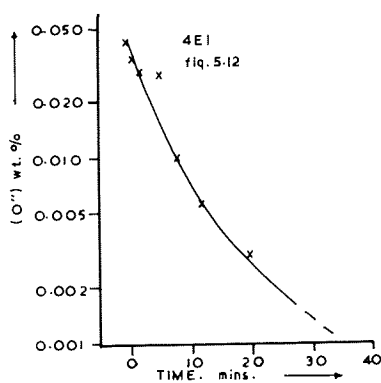
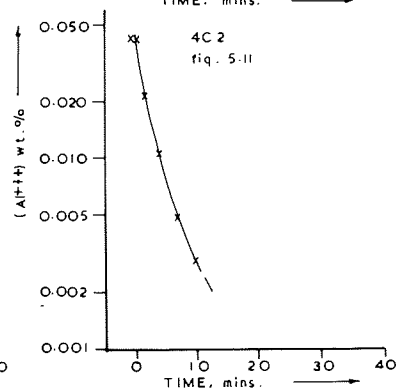
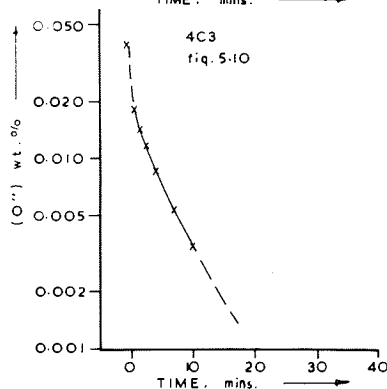
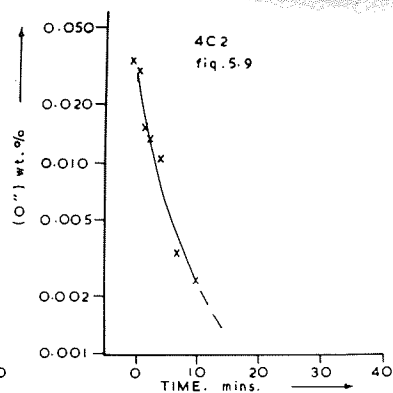
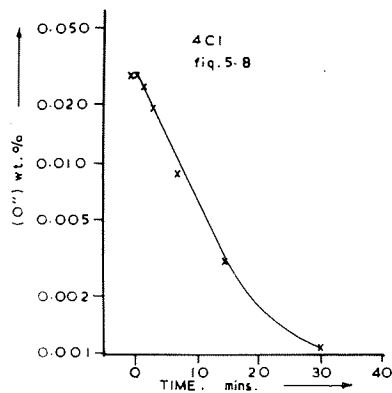
the difference between the total observed oxygen content (  $\% O_t$  ) and the residual oxygen content at the end of the experiment (  $\% O_r$  ). On this basis the curves shown in figs 5.5 - 5.21 were constructed to compare the separation rates of products from series 3 and 4 experiments. Use of a log scale on the ordinate gives, in most cases, an approach to linear relationships during the early stages of separation. The rates may then be compared by the time taken for 90% separation of products or the reciprocal of this time which defines the slope of the initial part of the curve (  $d \log \% O'' / dt$  ).  $\% O''$  represents the function of oxide content (  $\% O_t - \% O_r$  ). The derived parameters are shown in Table 5.3.

No distinct relationships are apparent from these results, but a number of effects can be seen by comparison of rates within and between groups of each product type. Comparison of the silicon and aluminium control groups shows that fastest separation rates were achieved when the products were pure alumina. It can further be seen for aluminium deoxidation that separation rates increase as the added aluminium is increased and the maximum separation rate was found when the added aluminium was in stoichiometric excess of the oxygen content. (cf. melts 4C2 and 4C6)



figs. 5.5 - 5.22 Progress of product separation

after deoxidation.



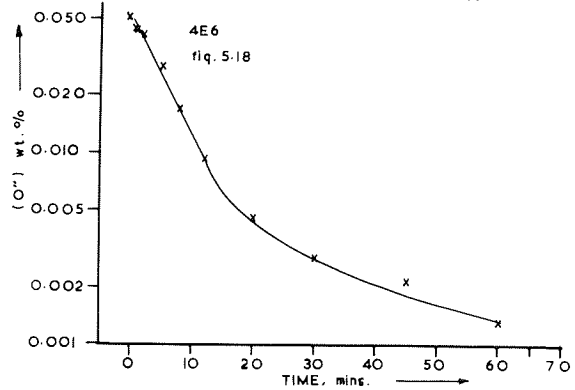
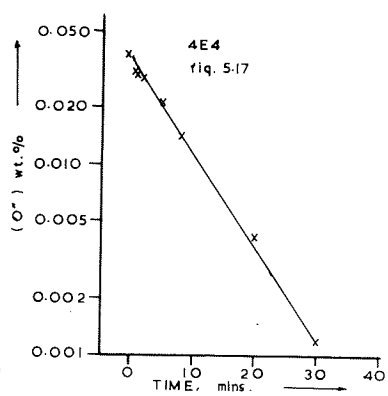
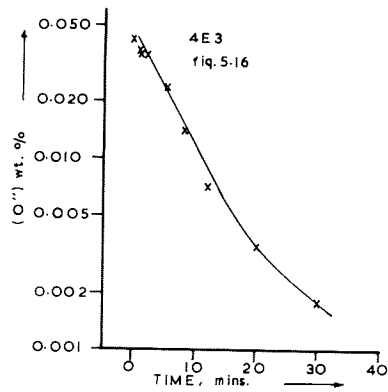
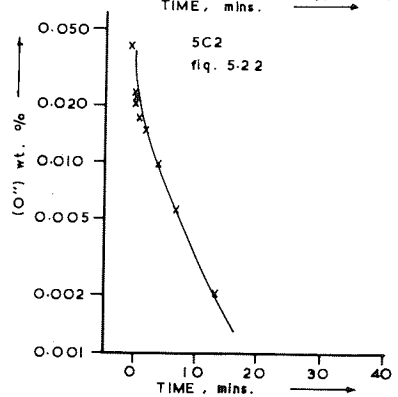
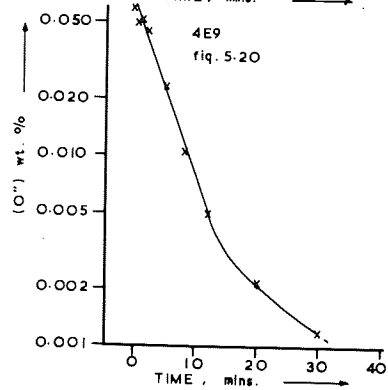
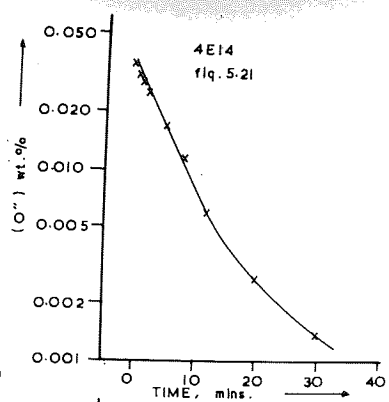
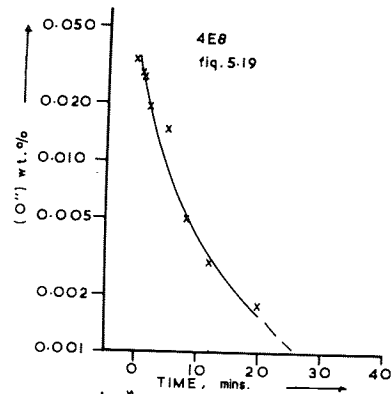


TABLE 5.3 PRODUCT SEPARATION RATES

EXP No.	TYPL OF PRODUCT	FIG NO.	TIME FOR 90% Separation	$\frac{d \log \frac{X}{1-X}}{dt}$
4C2	Alumina	5.10	8.0 mins.	- 0.125
4C2	" $\frac{2}{3}$	5.11	8.0 "	- 0.125
4C6	" $\frac{2}{3}$	5.15	2.3 "	- 0.44
4C6	"	5.16	2.5 "	- 0.4
4C3	Silica	5.9	12.5 "	- 0.080
5C2	"	5.22	12.8 "	- 0.078
3C2	"	5.5.	10.5 "	- 0.095
3C5	MnO- SiO <sub>2</sub>	5.7	16.5 "	- 0.061
4C1	SiO <sub>2</sub> - Al <sub>2</sub> O <sub>3</sub>	5.8	15.0 "	- 0.067
3E1	CaOMnO-SiO <sub>2</sub> -Al <sub>2</sub> O <sub>3</sub>	5.6	19.0 "	- 0.053
4E1	CaO-SiO <sub>2</sub> -Al <sub>2</sub> O <sub>3</sub>	5.12	16.0 "	- 0.063
4E2	"	5.13	18.0 "	- 0.056
4E3	"	5.14	18.0 "	- 0.056
4E4	"	5.17	20.5 "	- 0.049
4E6	"	5.18	17.5 "	- 0.057
4E8	"	5.19	11.8 "	- 0.085
4E9	"	5.20	11.0 "	- 0.091
4E14	MgO-SiO <sub>2</sub> -Al <sub>2</sub> O <sub>3</sub>	5.21	17.0 "	- 0.059

$\frac{2}{3}$  These values were obtained from plotting combined aluminium instead of combined oxygen.

A decrease in the residual equilibrium oxygen content accompanied the increase in aluminium addition and fig. 5.22 shows that the surface tension of iron containing 0.011% oxygen is 1,400 ergs. cm<sup>-2</sup> whilst at .0005% oxygen a value of approximately 1,800 ergs. cm<sup>-2</sup> is found by extrapolation. These oxygen and surface tension values correspond to separation rate constants ( d log % O"/dt) of - 0.125 and - 0.4 respectively.

Solid silica products separated more rapidly than the liquid products of complex deoxidation and it is probable that the surface tension of liquid silicates is less than that of solid silica. It is also noted that the separation rate of solid silica is less than that of solid alumina, even when the residual oxygen content is less than in the alumina experiment. The interfacial tension between oxide and iron  $\sigma_{\text{oxide/Fe}}$  however, is greater for alumina/iron than for silica/iron according to estimates based on Antonov's rule, shown in equation 5.1, and the

$$\sigma_{\text{Oxide/Fe}} = \sigma_{\text{Fe}} - \sigma_{\text{Oxide}} \dots \dots \dots \text{Equ 5.1.}$$

the data recommended by Turpin & Elliot (82)

Approximate values for the interfacial tensions are:  
 $\sigma_{\text{SiO}_2/\text{Fe}}$  1,500 ergs cm<sup>-2</sup>,  $\sigma_{\text{Al}_2\text{O}_3/\text{Fe}}$  1,900 ergs. cm<sup>-2</sup> at 0.01% residual oxygen and  $\sigma_{\text{Al}_2\text{O}_3/\text{Fe}}$  2,300 ergs. cm<sup>-2</sup> at 0.0005% residual oxygen.

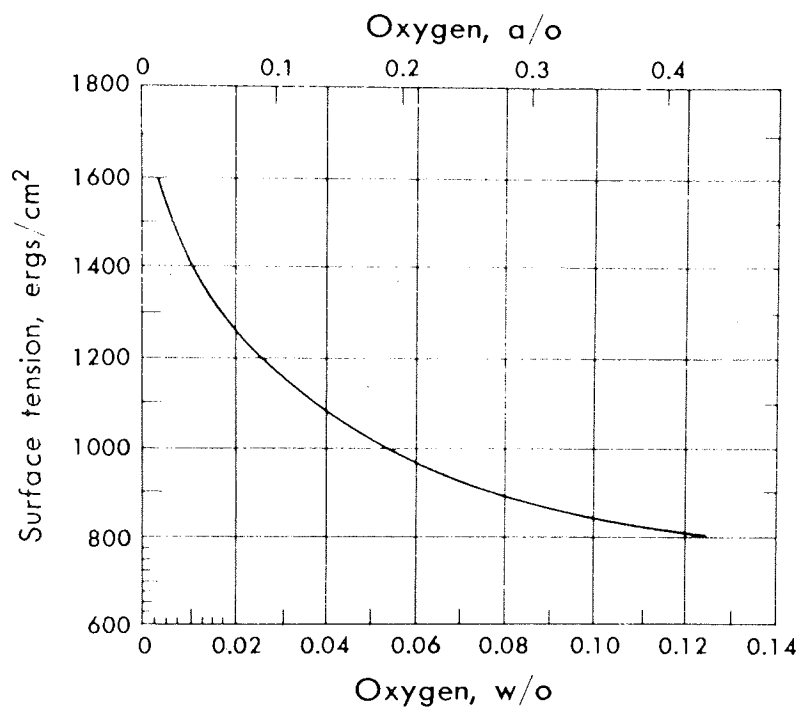


Fig. 5.22 Effect of oxygen content on the surface tension of pure iron. ( 129 )

These results clearly indicate that the interfacial tension between oxide and melt is an important factor influencing the rate of product separation. Products of complex deoxidation indicated that high alumina products separated more rapidly than silica rich ones, but inconsistency in the product compositions containing lime, and lack of surface tension data for the CaO/MgO - SiO<sub>2</sub> - Al<sub>2</sub>O<sub>3</sub> system, prevented direct correlation between separation rate and interfacial tension. It seems reasonable however, to assume that increased alumina content of the products will increase the interfacial tension and further support the deductions made from the control experiments. Plockinger's (90) view that wetting of particles hinders their separation is confirmed.

Calcium or magnesium in the deoxidiser have negligible effect on the separation rate of most of the deoxidation products, although a small proportion of lime or magnesia rich products, formed in the early stages of deoxidation do separate rapidly because of their large size.

### 5.3 Deoxidation with manganese - silicon - aluminium Alloys

#### 5.3.1. Product composition

5.3.1.1. Effect of deoxidation alloy composition Initial oxygen contents and silicon additions were nominally const-



ant for series 5 experiments, but various aluminium additions were made and, between experiments 5 E1, and 5 E4, variations of the manganese additions were also made. (See Table 4.2). Tables 4.22 - 4.25 show that the manganese oxide content of deoxidation products increased as the manganese content of the alloy was increased. Increasing the aluminium content of alloys with constant manganese: silicon ratio can be seen from tables 4.22, 4.26 and 4.27 to have caused an increase in the alumina content of the products.

It is clear therefore, that initial product compositions depend upon the deoxidiser elements added and for series 5 melts, these additions have been calculated from deoxidation alloy compositions and total alloy additions made. These additions and their ratios with respect to aluminium are shown on table 5.4.

Table 5.4 Deoxidiser additions (Series 5)					
Exp No.	% Mn	% Si	% Al	% Mn/.Al	% Si/%Al
5E1	0.501	0.278	0.0067	74.8	41.5
5E2	0.755	0.276	0.0044	171.6	62.7
5E3	0.986	0.317	0.0030	328.7	105.7
5E4	0.244	0.286	0.0078	31.3	37.7
5E5	0.497	0.276	0.0172	28.9	16.1
5E6	0.503	0.286	0.0340	14.8	8.5

Relationships between (% Mn/%Al) and (% Si/%Al) and their respective oxide ratios in the initial products are

shown in figs. 5.23 and 5.24. Oxide ratios shown are those existing in the 1/2 min. samples except for experiment 5E6 in which the mean of 1/2 & 1 min. samples was taken to compensate for scatter due to heterogeneity. Aluminium and alumina are used as reference in the metal oxide ratios because aluminium was the strongest deoxidiser used and, at the residual oxygen contents intended, negligible residual aluminium concentrations were required for equilibrium. It may be assumed that all the added aluminium is converted to alumina when the initial oxygen content of the melt was in stoichiometric excess of the aluminium added.

Figures 5.23 and 5.24 may be considered to summarise the total addition of deoxidisers needed to meet the equilibrium and stoichiometric requirements for producing inclusions of a particular composition. They are not directly calculable from existing data however, because activity data are not available for the observed product composition range and low values of  $\gamma_{\text{MnO}}$  indicated by the present work, and also by fig. 2.10, suggest that solute manganese - oxygen equilibria occurs with a manganese oxide activity very much less than unity. (Equilibrium relationships between iron melts and MnO - SiO<sub>2</sub> - Al<sub>2</sub>O<sub>3</sub> deoxidation products are considered again in section 5.3.2.).

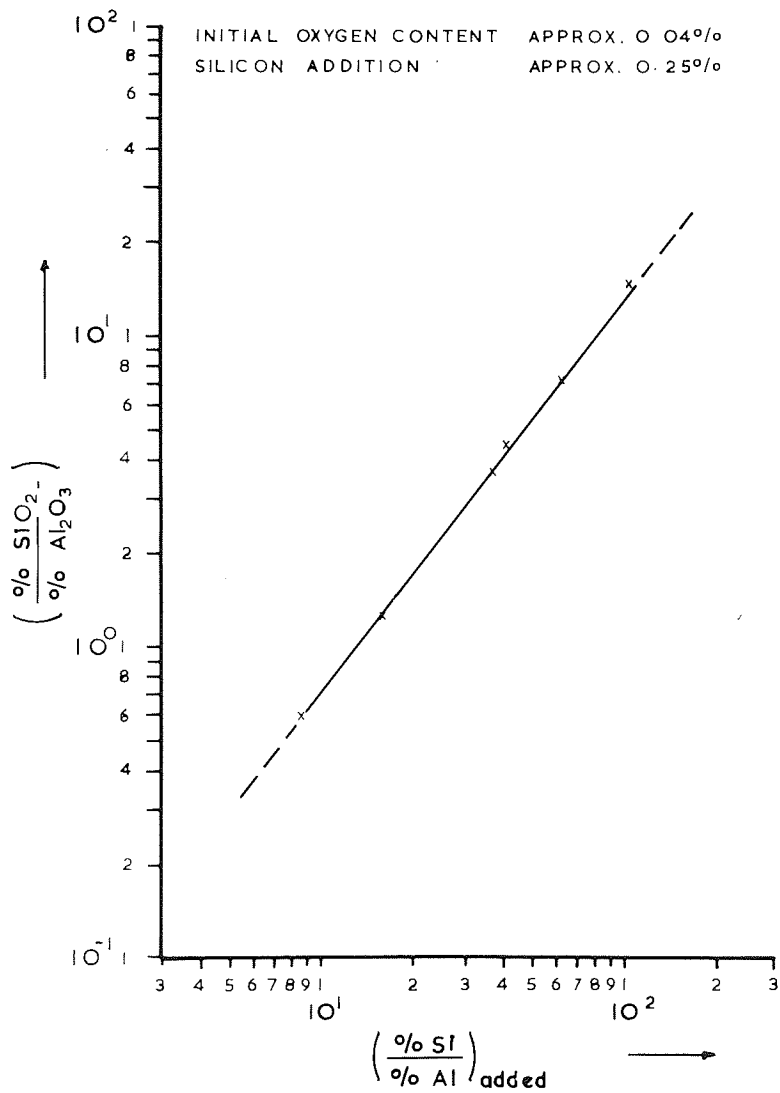


Fig. 5.23. Relationship between initial product composition and deoxidiser composition.

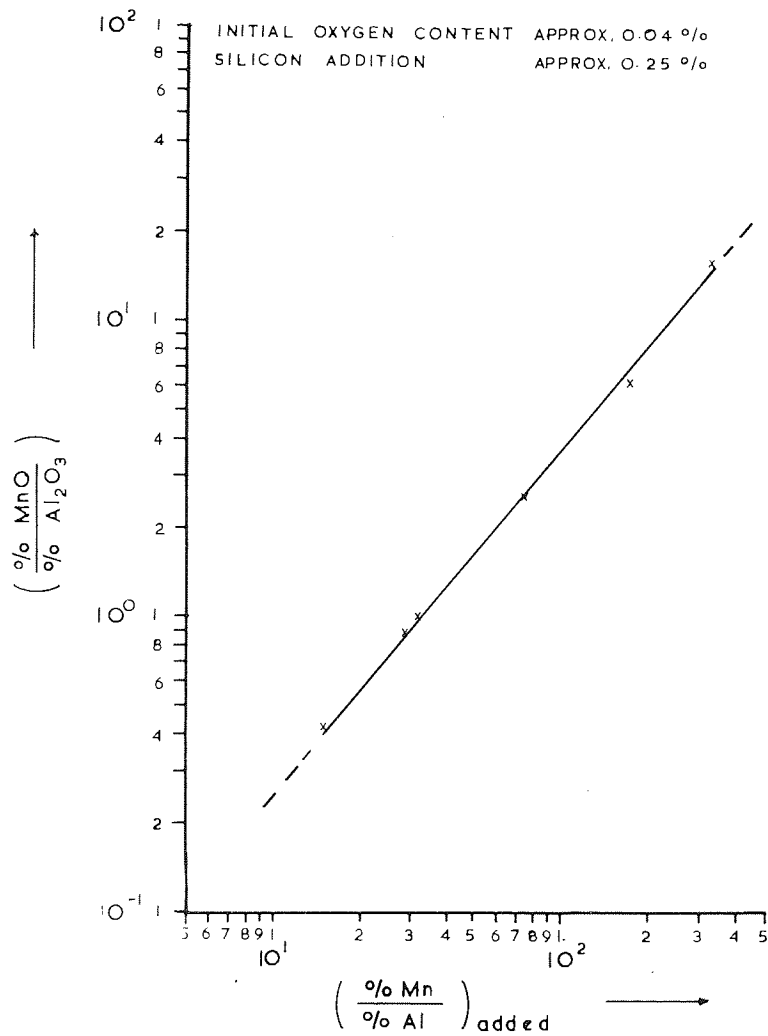


Fig. 5.24 Relationship between initial product composition and deoxidiser composition.

Ratios of  $(\text{MnO}/\text{SiO}_2)$  may easily be obtained as  $(\text{MnO}/\text{Al}_2\text{O}_3) \times (\text{Al}_2\text{O}_3/\text{SiO}_2)$  and similarly for ratios of  $\text{Mn}/\text{Si}$ . Graphical representation of these however, would give a series of lines corresponding to various alumina concentrations in the products. Decreasing the initial oxygen content of the melt would be expected to increase the proportion of alumina in the products according to the  $(\Delta\% \text{ O} / \% \text{ Al added})$  ratio discussed in section 5.2.2.1., and in consequence would lead to lower  $(\text{MnO}/\text{Al}_2\text{O}_3)$  and  $(\text{SiO}_2/\text{Al}_2\text{O}_3)$  ratios than indicated. Changing the silicon addition within a small range would be expected to have little effect on the figures. If the silicon addition were very low however, the residual oxygen content would be relatively high,  $\Delta\% \text{ O}$  due to silicon would be decreased and so the products would be richer in alumina. If the silicon addition were very high then a lower residual oxygen would be expected and this would result in  $\Delta\% \text{ O}$  being increased and some residual aluminium being involved in solute equilibria. Both of these effects would cause an increase of  $(\% \text{ SiO}_2 / \% \text{ Al}_2\text{O}_3)$ .

5.3.1.3. Effect of crucible material. Tables 4.22 - 4.25 show that alumina contents of the deoxidation products increased during the holding period of experiments

5E1 - 5E4, despite a high degree of consistency between product compositions found in individual samples. Products found in 5E5 showed a small increase in alumina content but the scatter of product compositions in experiment 5E6 was due to difficulties in obtaining the average analysis of heterogeneous particles by point analysis techniques. The X Ray data shown in figs 4.9 a - 4.9 f illustrate the segregation of alumina in products from experiment 5E6. Product composition changes are summarised in Fig. 5.25 which shows the trend towards alumina saturation at 1550°C and from figs. 5.26 and 5.27 it may be seen that this saturation is achieved 15 - 20 mins after deoxidation. This time corresponds to separation of most of the deoxidation products and is accounted for by the alumina crucibles participating in the melt/product reaction.

A mechanism for crucible/product reaction was suggested for some of the line containing products in section 5.2.1.3. but the mechanism is more clearly indicated by series 5 experiments. Initial products in 5E1 - 5E5 are seen from fig. 5.25 to have been liquid at 1,550°C and so they dissolved alumina from the crucible when they had separated from the melt. The maximum alumina content which could be achieved was determined by the alumina saturation boundary at 1550°C and this was the maximum alumina content

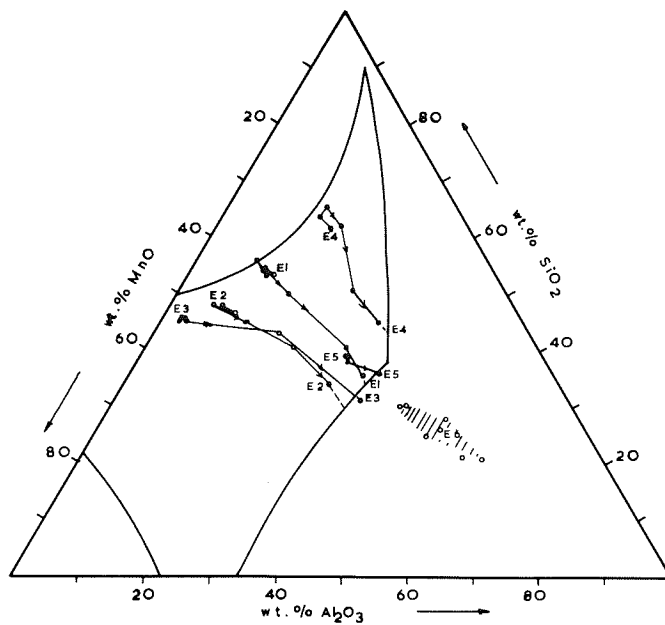


Fig. 5.25 Variation of deoxidation product composition during the holding period.

approached, except in the case of 5E6, which gave initial products already saturated with alumina. Alumina saturated slags at the melt surface/crucible interface resulted from this process and controlled solute equilibria in the melts. Product particles residual in the melt also changed their composition to maintain equilibrium between oxide and metal, and hence approached the same composition as the alumina saturated slag controlling that equilibrium.

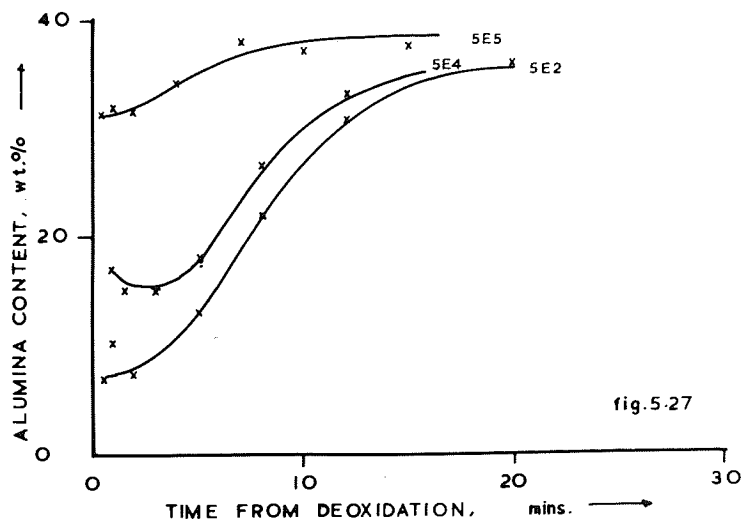
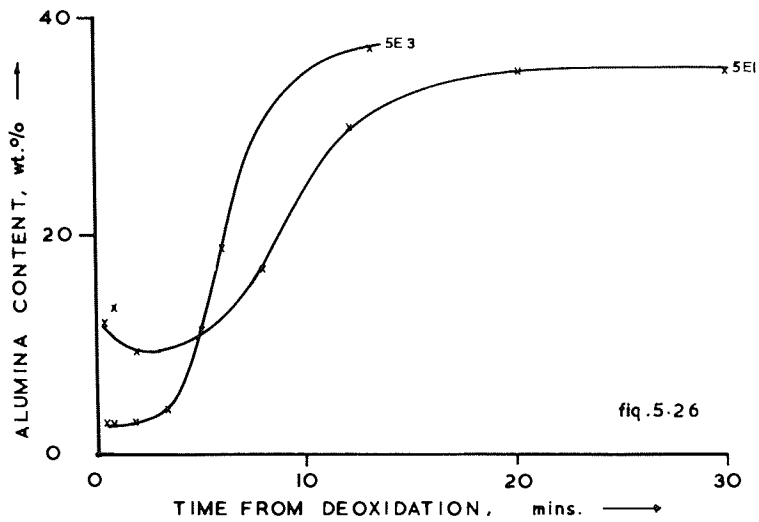
Changes of product composition shown in figs. 5.26 and 5.27 during the early stages of the holding period, and the rate of increase in alumina content of products will be considered further in connection with nucleation, growth and separation of products.

### 5.3.2. Equilibrium relationships.

#### 5.3.2.1. Equilibria with alumina saturated slags

It is assumed that equilibrium was approached in species 5 experiments because, from tables 4.22 - 4.28, only small reductions in oxygen content of the melt occurred between 60 and 90 min. samples. On this assumption, approximate values of silica and manganese oxide activities were calculated from the melt analyses using deoxidation constants of  $1.1 \times 10^{-5}$  and  $5.43 \times 10^{-2}$  for silicon and manganese respectively. These data are shown in table 5.5.





Variation of alumina content of deoxidation products during the holding period.

Table 5.5 Oxide activities in alumina saturated slags...

Exp No.	$f_O$	$f_{Si}$	$h_O$	$h_{Si}$	$h_{Mn}$	$a_{SiO_2}$	$a_{MnO}$
5E1	0.877	1.251	0.0039	0.294	0.460	0.406	0.033
5E2	0.874	1.27	0.0039	0.305	0.655	0.405	0.047
5E3	0.864	1.302	0.0026	0.322	0.833	0.197	0.040
5E4	0.877	1.282	0.0045	0.301	0.198	0.547	0.016
5E5	0.876	1.285	0.0027	0.302	0.415	0.262	0.021
5E6	0.671	1.297	0.0029	0.318	0.475	0.239	0.025

The activity coefficient of manganese,  $f_{Mn}$ , is unity, as is the activity of alumina in alumina saturated slags.

Alumina saturation of the observed products occurs at a ratio ( $n_{SiO_2}/n_{Al_2O_3}$ ) of 1.4 - 2. Manganese oxide activities in the pseudo binary system of manganese oxide with silica and alumina at a constant molar ratio of 1.8, have been taken from the data of Sharma and Richardson (76) shown in fig. 2.10 and presented in fig. 5.23 together with data from table 5.5. Sharma and Richardson's data were determined at 1650°C and manganese oxide saturation occurs at a concentration of 0.05  $n_{MnO}$  lower at 1,550°C. A slight increase in  $n_{MnO}$  at high manganese oxide concentrations would therefore be expected for 1550°C data.

The present data extend the manganese oxide activity curve to lower manganese oxide concentrations and show that  $n_{MnO}$  reaches a minimum value of 0.08 when

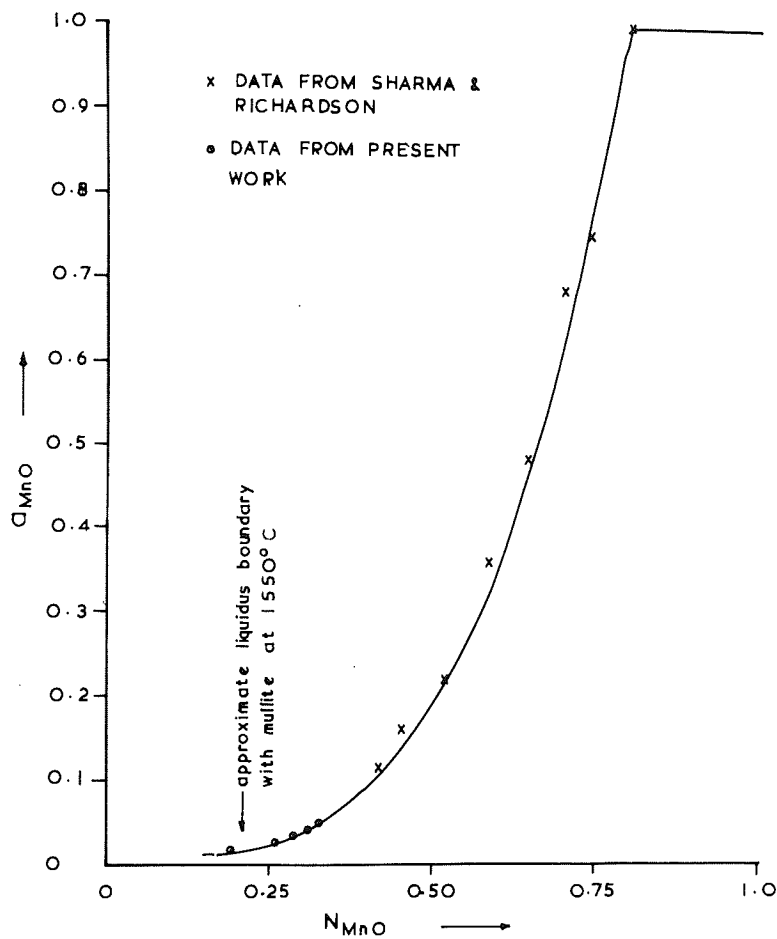


Fig. 5.28. Approximate manganese oxide activities in the pseudo binary system  
 $MnO - (NSiO_2/NA1_2O_3 = 1.8)$

N MnO is approximately 0.01. This concentration is at the 1,550°C liquidus boundary with solid mullite but the lowest point on fig. 5.28 was determined from the 12 min. sample of experiment 5H4. Product compositions for this sample were in the liquid phase field because  $\text{NSiO}_2/\text{NAL}_2\text{O}_3$  was 2 and at this ratio, the mullite boundary is at 0.18 N MnO.

#### 5.3.2.2. Equilibria with initial deoxidation products.

It has been shown that the final residual oxygen contents were obtained by approaching equilibrium with alumina saturated slags and it is likely that the equilibrium oxygen contents were lower than those equilibrating with the initial deoxidation products. Direct determination of the initial equilibrium oxygen was prevented by the presence of residual oxide particles, but according to Bell's (49) data, shown in fig. 2.8 for MnO - SiO<sub>2</sub> - FeO slags, the equilibria should have been with solid silica at unit activity when 0.2% silicon was present with less than 0.3% manganese. It may be seen from the phase diagram in fig. 2.21 that liquid MnO - SiO<sub>2</sub> - Al<sub>2</sub>O<sub>3</sub> mixtures exist at 1550°C with quite low manganese oxide contents when the alumina content is of the order of 10%. By promoting the formation of liquid products therefore, the presence of alumina enables manganese to participate in deoxidation at concentrations less than 0.3% or in the presence of more

than 0.2 % silicon.

Initial product compositions have been noted to vary within the first two minutes of the holding period and this cannot be due to crucible effects because; (a) most of the products are residual in the melt at this stage and are not in contact with alumina, and (b) the composition changes tend to reduce alumina content. The product compositions observed at 1/2 min. from the time of deoxidation are therefore considered to have been influenced by nucleation and growth effects and equilibrium between products and the melt was not approached until up to two minutes after deoxidation. At the two minute stage it may be seen that products of 5E1 and 5E4 are close to the compositions of silica saturation and so silica activities in these can be assumed as unity. Silica activities in the products of 5E2, 5E3 and 5E5, at the two minute stage, were estimated from the binary  $\text{Al}_2\text{O}_3\text{-SiO}_2$  data (Fig. 2.9) and alumina saturated data (Table 5.5) as 0.9, 0.75 and 0.6 respectively. Residual oxygen contents in equilibrium with the deoxidation products after two minutes assuming this approximate activity data, the activity coefficients shown in table 5.5, and silicon deoxidation constant of  $1.1 \times 10^{-5}$  are shown in Table 5.5

Table 5.6 Initial equilibrium oxygen content

Exp.	% SiO <sub>2</sub>	$\frac{h}{O}$	$\frac{p}{O}$
5E1	1.0	0.0061	0.0070
5E2	0.9	0.0057	0.0067
5E3	0.75	0.0051	0.0057
5E4	1.0	0.0060	0.0060
5E5	0.6	0.0047	0.0054
5E6	-	-	0.0033

Products of experiment 5E6 are assumed not to alter, the analytical scatter being attributed to heterogeneity, and so the equilibrium oxygen content is also assumed not to alter.

Equilibrium between the melt and manganese oxide and silica in the products is established by reaction 11, and fig. 5.29 relates to this equilibrium.



The equilibrium constant  $K$ , is given by  $(\frac{p}{Si-O} / k_{Si-O})^2 (\frac{h}{Mn-O} / k_{Mn-O})$  where  $k_{Mn-O}$  &  $k_{Si-O}$  are the deoxidation constants of manganese and silicon respectively, and the slopes of the curves in fig. 5.29 correspond to  $(\frac{\delta SiO_2}{\delta^2 MnO} \cdot K)$ .

The constant slope found for the initial products may be qualitatively accounted for by considering the activity

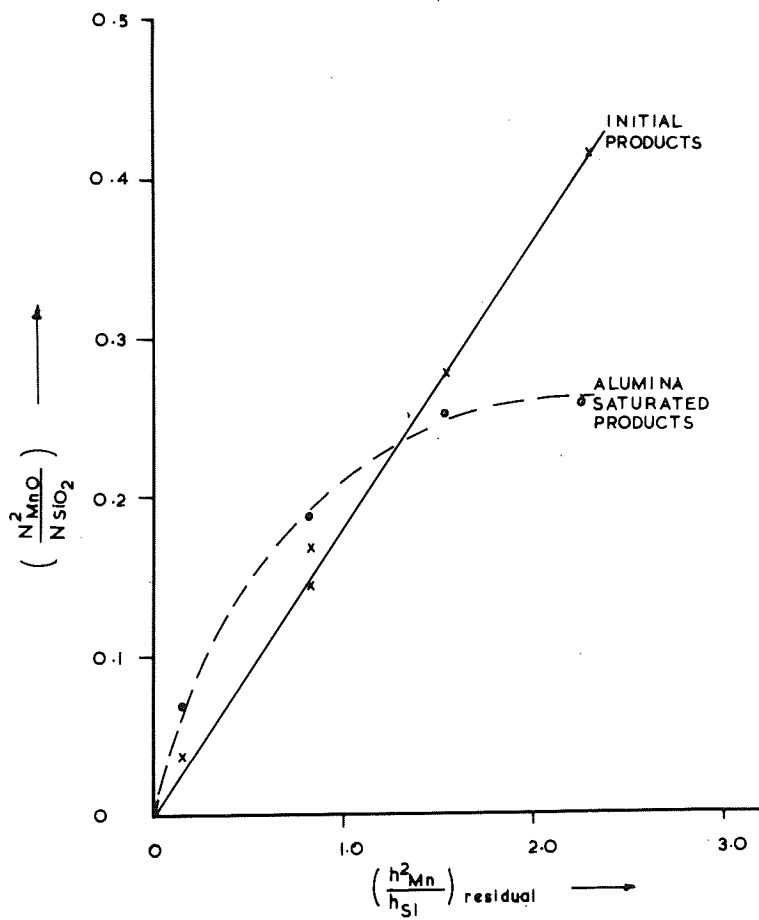


Fig. 5.29 Relationships between manganese oxide and silica in deoxidation products and the melt.

behaviour of the components. Manganese oxide shows an increase of its activity coefficient as its concentration increases, both in the binary MnO - SiO<sub>2</sub> system shown in fig. 2.11, and in alumina saturated slags as shown in fig. 5.28. Fig. 5.25 however, shows that initial product compositions lie close to the silica saturation boundary and that as alumina is increased the silica saturation composition becomes richer in silica. It may be seen therefore, that with decreasing alumina content from a maximum of 0.08N Al<sub>2</sub>O<sub>3</sub> and increasing manganese oxide, the activity coefficient of silica will rise to a maximum value of 1.3 (126) in the MnO-SiO<sub>2</sub> binary and will then decrease with further increases in manganese oxide content. In the range of observed compositions therefore,  $\gamma_{\text{SiO}_2}$  increases as the manganese oxide concentration increases and by chance this increase is sufficient to keep  $(\gamma_{\text{SiO}_2} / \gamma_{\text{MnO}}^2)$  approximately constant at 48.3, as  $\gamma_{\text{MnO}}$  also increases with increasing manganese oxide concentration. The activity coefficient of silica decreases from its maximum of 1.3 as the manganese oxide concentration exceeds 0.47 N MnO in the MnO - SiO<sub>2</sub> binary and so  $(\gamma_{\text{SiO}_2} / \gamma_{\text{MnO}}^2)$  would be expected to decrease as  $K^2 \text{MnO} / \text{NSiO}_2$  exceeds 0.41.

The curve shown in fig. 5.29 for alumina saturated products is of the form which may be expected for a constant



silica/alumina ratio with mullite or alumina at the low manganese oxide liquidus boundary.  $\chi$  MnO increases with increasing manganese oxide concentration as shown in fig. 5.28 and it is probable that  $\chi$  SiO<sub>2</sub> decreases to a minimum at manganese oxide saturation. No significant effects on  $\chi$  SiO<sub>2</sub> are likely to occur from changes in the mullite or alumina saturation compositions ( $\chi$  SiO<sub>2</sub>/ $\chi$  MnO) should therefore decrease with increasing manganese oxide concentration and this corresponds to the observed behaviour.

### 5.3.3. Formation and separation of products.

5.3.3.1. Nucleation and growth Degrees of supersaturation ( $\Delta G^{\text{hom}}$ ) obtained in series 5 experiments, assuming homogeneous distribution of solutes, have been calculated from the initial and equilibrium oxygen contents, and the added residual solute concentrations, using equation 2.21. These are shown in table 5.7 together with critical supersaturations ( $\Delta G_{\text{crit}}^{\text{hom}}$ ) for homogeneous nucleation of each oxide which were calculated from equation 2.20 using the data recommended by Turpin & Elliot (82) and a temperature of 1,550°C. Physical properties of manganese oxide are assumed to be similar to ferrous oxide.

Turkdogan's (84) treatment for homogeneous nucleation of MnSiO<sub>3</sub> indicates that a critical supersaturation of - 22.7 k.cals./mole is required and it is seen from table 5.7 that none of the melts have supersaturations exceeding

$\Delta G_{crit}^{hom.}$  for any of the oxide species. In the vicinity of the deoxidiser during its dissolution however, the supersaturations are likely to be very much higher and, as suggested by both Turpin & Elliot and Turkdogan homogeneous nucleation is possible at this stage.

Exp No.	$\Delta G_{crit}^{hom.}$ k. cal./mole		
	SiO <sub>2</sub>	Al <sub>2</sub> O <sub>3</sub>	MnO
$\Delta G_{crit}^{hom.}$	- 26.7	- 66.6	- 1.49
5E1	- 14.99	- 31.06	+ 3.29
5E2	- 12.89	- 25.23	+ 2.86
5E3	- 14.11	- 24.94	+ 1.27
5E4	- 14.85	- 31.50	+ 6.16
5E5	- 14.07	- 36.69	+ 3.73
5E6	- 14.86	- 42.46	+ 3.40

Considering further the formation of mixed oxide products in local regions of high deoxidiser concentration it would seem reasonable that they may have a lower oxygen potential than the equilibrium products obtaining when solute deoxidiser and oxygen are uniformly distributed in the melt. If this were so, then the initial product composition would have to change in order to approach equilibrium as uniformity of solute concentration was achieved. A mechanism such as this would account for the compositional changes observed in the initial products of 5E4 and 5E1, which by decreasing their alumina content in

the first 2 - 3 mins approach a higher silica activity and hence, equilibrium with a higher oxygen content.

Initial product compositions were shown in figs. 5.23 and 5.24 to depend on the deoxidiser additions, and it appears from figs. 5.26 and 5.27 that alumina contents exceeded those of the equilibrium products only in 5E1 and 5E1. Products of high average alumina content noted in the 1 minute samples of these experiments are due to the contributions of a few large inclusions having approximately 14% alumina instead of the 8.5% present in smaller inclusions. It can be seen from table 4.29 that particles exceeding 20  $\mu$ m diameter represent only a small part of the total oxide content and are considered therefore, to result in a high estimate of the average alumina content of the products. The presence of the few alumina rich particles cannot be readily explained, but it is possible that traces of alumina in the deoxidiser may be responsible, especially as not all the large inclusions were richer in alumina.

Growth of nuclei and the time taken to achieve oxygen desaturation of the melt by a solute diffusion controlled process can be examined in the light of the metallographic data given in tables 4.29 - 4.31 and the model described by Turkdogan (84). Table 5.6 gives the inclusion concentration as calculated from equation 5.2 which is due to Fullmans (127) analysis of particle size

$$N_v = 2 \cdot \bar{n} \cdot N_s / \pi \quad \dots \dots \dots \text{equation 5.2}$$

$N_v$  and  $N_s$  are the number of particles per unit volume and area respectively,  $\bar{n}$  is the reciprocal of the mean observed particle diameter ( $\bar{d}$ ) . Resolution of the 0.25 N.A. objective used with the Quantimet for metallographic analysis was 0.92  $\mu$ m.

Table 5.8 Inclusion concentration.

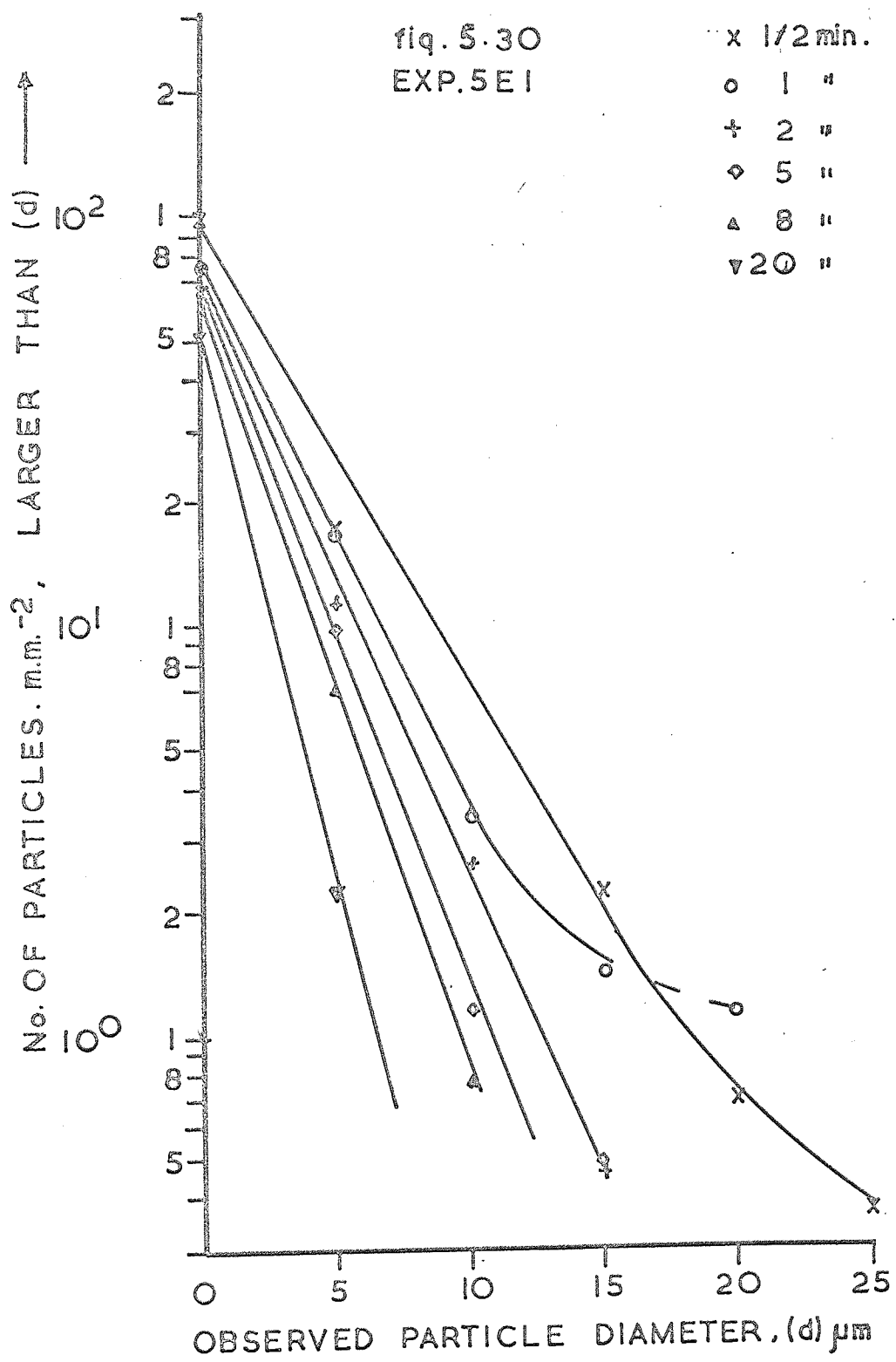
Exp No.	$N_s \cdot \text{mm}^{-2}$	$\bar{d} \mu\text{m}$	$N_v \cdot \text{cm}^{-3}$
5E1	98.8	3.23	$1.6 \times 10^7$
5E2	119.8	3.24	2.4 "
5E3	139.4	3.22	2.3 "
5E4	210.4	3.59	3.7 "
5E5	232.8	3.35	4.4 "
5E6	251.4	3.34	4.8 "

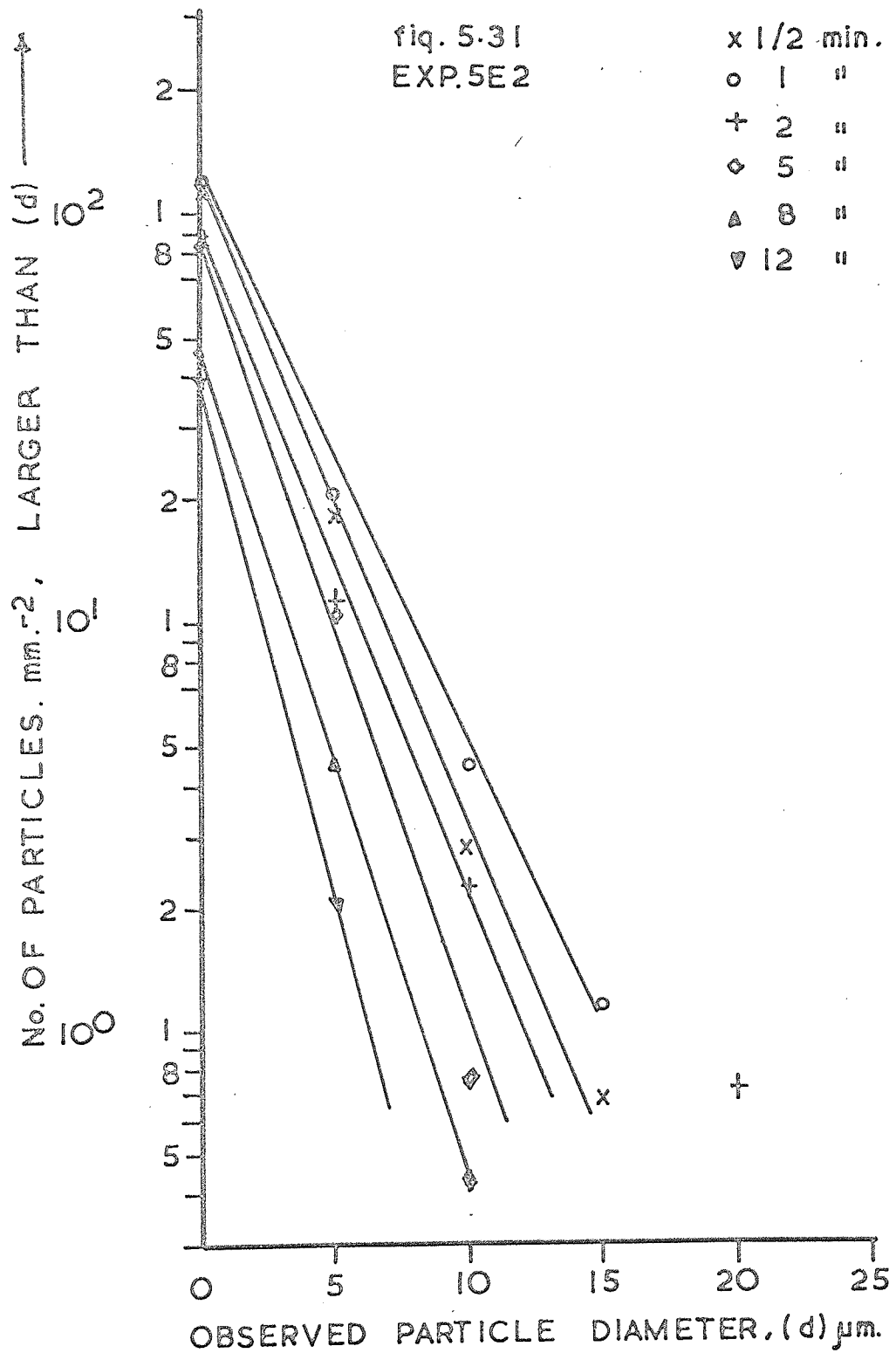
Assuming that  $N_v = 10^7 \text{ cm}^{-3}$  represents the approximate nuclei concentration and applying the diffusion model already mentioned, it is found that 99% oxygen desaturation is achieved in 1.4 secs. of fig. 2.16 (6) which indicates 5 secs for similar conditions but with  $10^6$  nuclei  $\text{cm}^{-3}$ . It is also found that when  $N_v = 10^7 \cdot \text{cm}^{-3}$ , the value of  $r_0$  in equation 2.22 is 2.88  $\mu$ m and substituting in equation 2.22 for complete oxygen desaturation, the maximum value of  $r_i$  is calculated as 3.27  $\mu$ m. This shows that solute diffusion does not seriously limit the particle growth rate and also

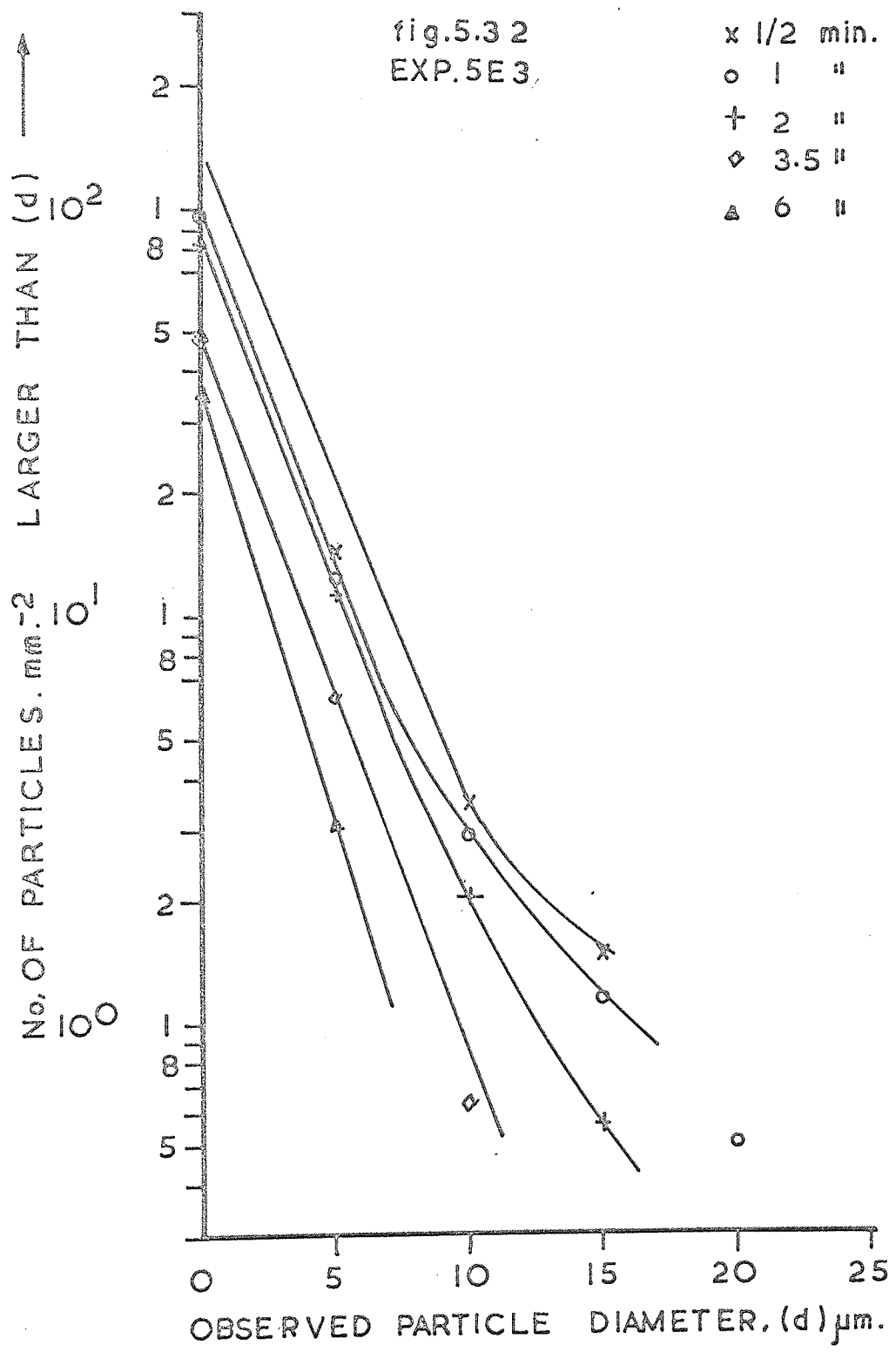
that very little growth occurs because of the large number of nuclei present. The predictions of Turpin & Elliot (82), concerning the formation of small particles in large numbers by local supersaturation are supported to this point by the present results.

Product particles exceeding  $3.3 \mu\text{m}$  however, are not accounted for by this nucleation and growth mechanism and it is necessary to assume coalescence or agglomeration of particles in order to explain them. Evidence supporting growth by coalescence can be found in figs. 5.30 - 5.35 which show particle size distribution in series 5 experiments. These figures were derived from tables 4.29 - 4.31 expressing the size distribution as the number of particles/ $\text{mm}^2$ , larger than a given diameter. They show curves which are similar in form to that expected from equation 2.26 and values of A derived from the curves are given in table 5.9, together with values of  $\mu$ .

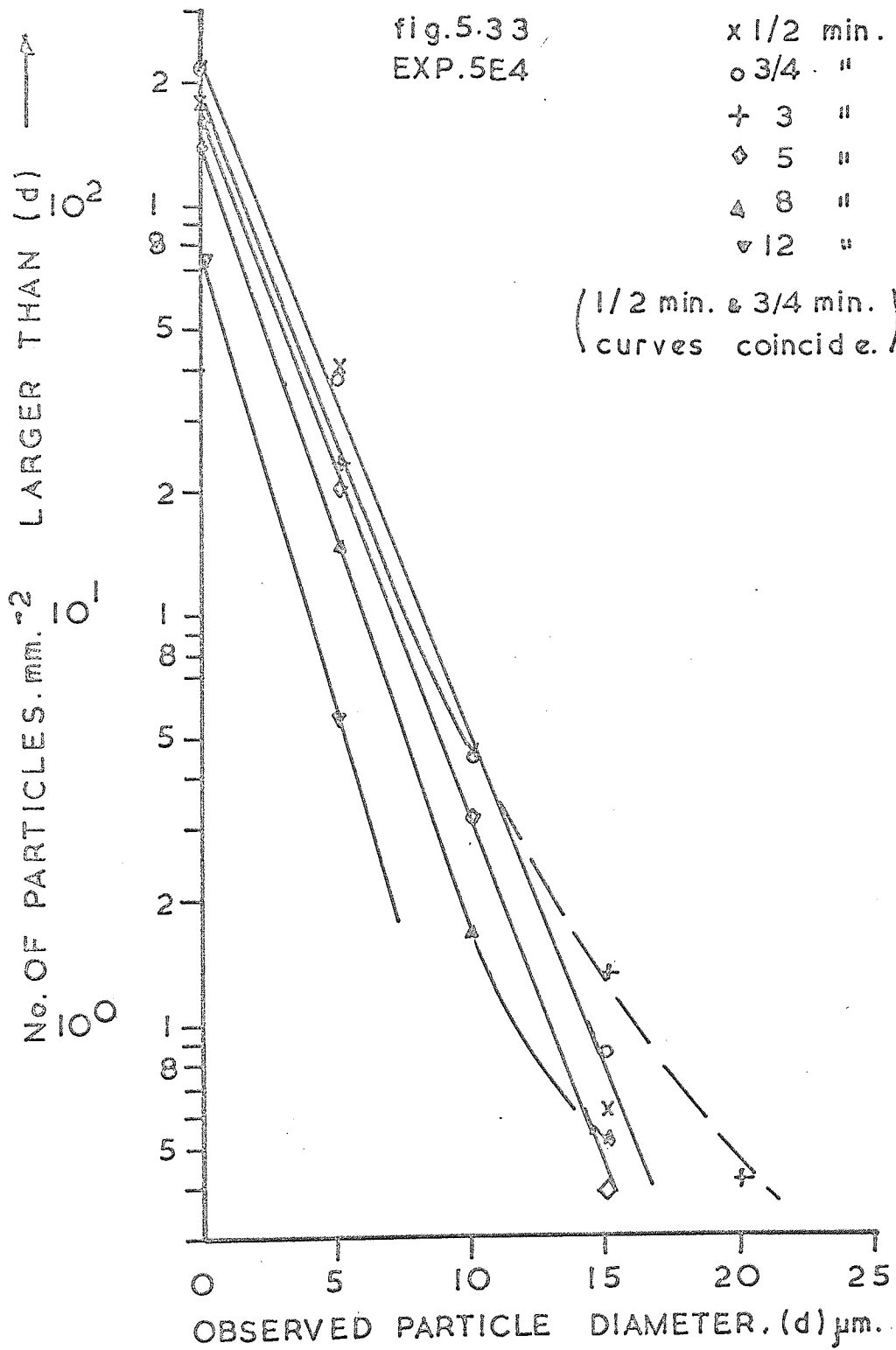
If there were no change in particle size by coalescence and product separation occurred by flotation according to Stoke's Law, then, the only change to be expected in particle size distribution in a plane at a given distance from the bottom would be termination of the curve at a diameter of  $2(h/kt)^{\frac{1}{2}}$ . (Using the notation

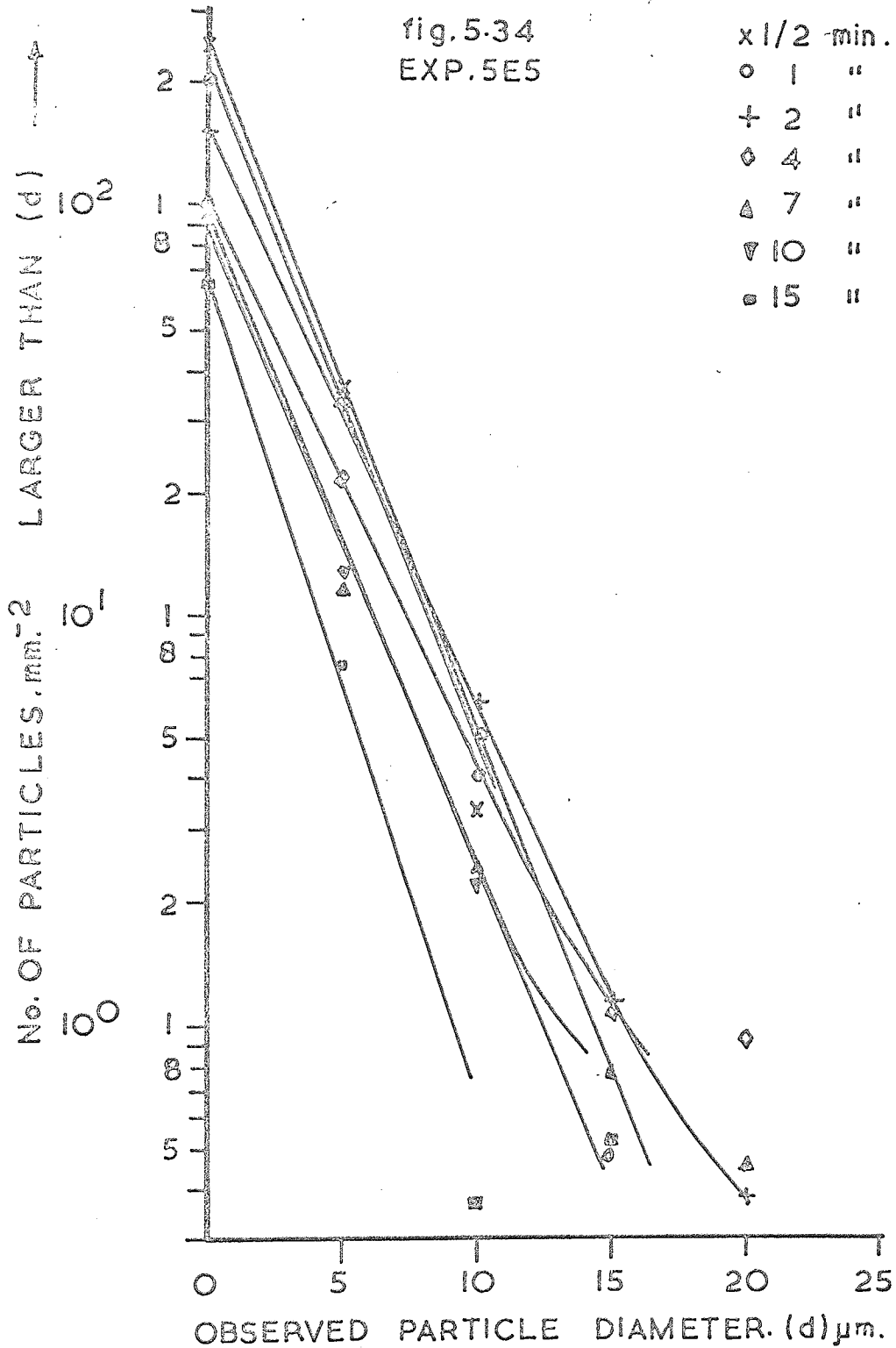


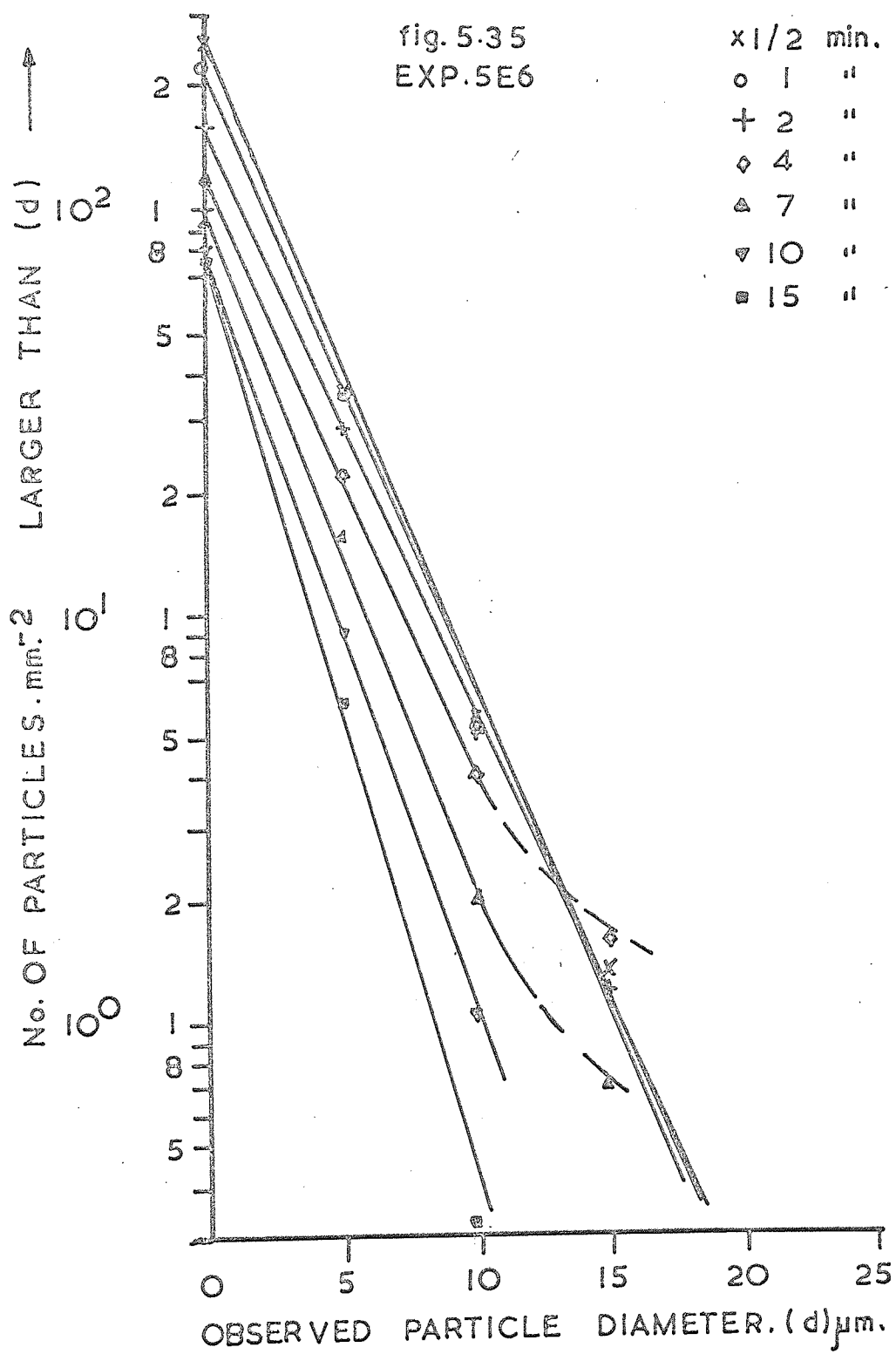












defined on p.49). Particles of a smaller diameter floating out of the plane would be replaced by particles floating into it from below and the values of  $n_0$  and  $A$  would remain constant as assumed by Kawawa et.al.(97)

TABLE 5.9 Particle size distribution

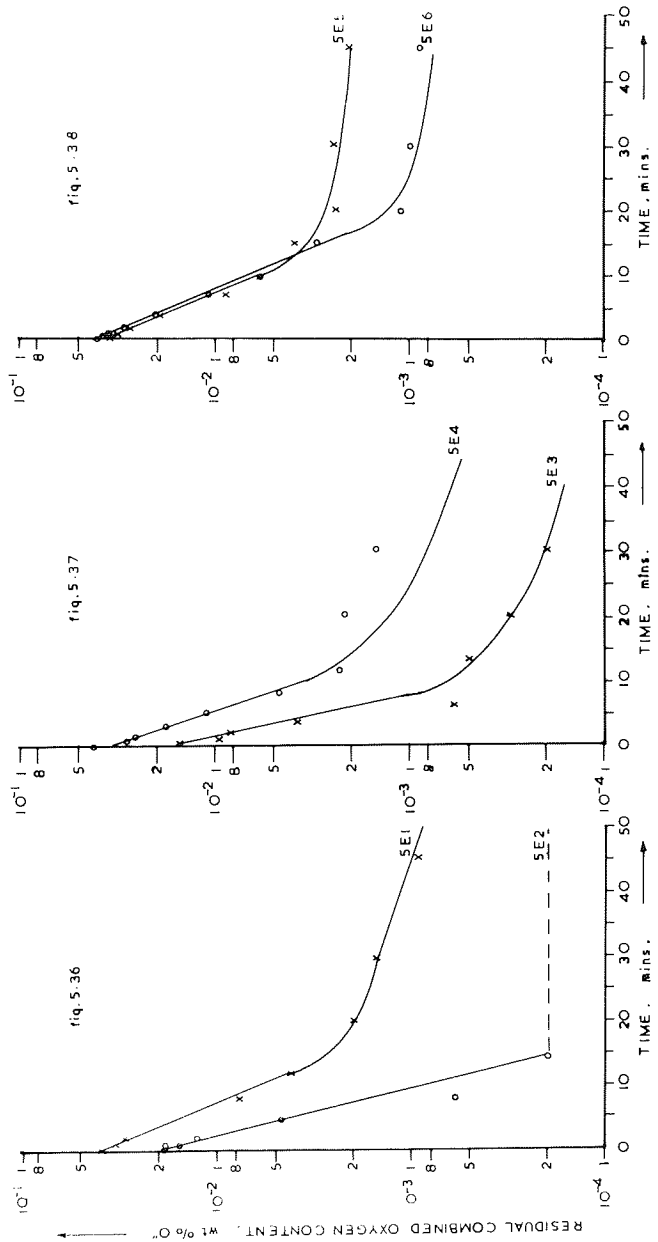
SAMPLE	no./mm <sup>-2</sup>	Slope cm <sup>-1</sup>	-A/cm. <sup>-1</sup>
5E1, 1/2	98.8	1.14 x 10 <sup>3</sup>	3.4 x 10 <sup>3</sup>
" 1	75.6	1.33 "	3.9 "
" 2	73.5	1.41 "	4.3 "
" 5	67.9	1.71 "	5.0 "
" 8	60.9	1.90 "	5.7 "
" 20	50.0	2.67 "	7.8 "
5E2, 1/2	119.8	1.57 "	4.6 "
" 1	126.2	1.40 "	4.1 "
" 2	84.8	1.63 "	4.8 "
" 5	84.2	1.90 "	5.6 "
" 8	44.8	2.00 "	5.9 "
" 12	38.4	2.50 "	7.3 "
5E3, 1/2	139.4	1.60 "	4.7 "
" 1	93.4	1.74 "	5.1 "
" 2	80.8	1.70 "	5.0 "
" 3 $\frac{1}{2}$	46.9	1.74 "	5.1 "
" 6	35.4	2.10 "	6.1 "

Table 5.9 Particle size distribution (Continued)

SAMPLE	no. mm <sup>-2</sup>	Slope. cm <sup>-1</sup>	-A. cm <sup>-1</sup>
5E4, 1/2	210.4	1.63 x 10 <sup>3</sup>	4.8 x 10 <sup>3</sup>
" 3/4	217.3	1.63 "	4.8 "
" 3	172.1	1.57 "	4.6 "
" 5	158.9	1.54 "	4.5 "
" 8	138.9	2.00 "	5.9 "
" 12	72.7	2.22 "	6.5 "
5E5, 1/2	232.8	1.67 "	4.9 "
" 1	196.7	1.60 "	4.7 "
" 2	149.0	1.40 "	4.1 "
" 4	99.7	1.37 "	4.0 "
" 7	92.4	1.53 "	4.5 "
" 10	87.6	1.50 "	4.4 "
" 15	62.7	1.90 "	5.6 "
5E6, 1/2	251.4	1.57 "	4.6 "
" 1	217.6	1.51 "	4.4 "
" 2	160.0	1.43 "	4.2 "
" 4	113.8	1.45 "	4.3 "
" 7	90.7	1.61 "	4.7 "
" 10	75.3	1.82 "	5.3 "
" 15	75.9	2.22 "	6.5 "

Growth by coalescence would be expected to result in a smaller total number of inclusions, which is in accordance with the observed decrease in  $n$  with increasing time, and would increase the proportion of larger inclusions. If the large inclusions were retained then  $A$  would decrease with increasing time as particle growth by coalescence occurred, but as large particles float out more rapidly the observed effect is a general increase of  $A$  with time. Indications of a decrease in  $A$  are reflected in some cases by a departure of the log function from linearity at large particle diameters. Values of  $A$  shown in table 5.9 for such curves represent the linear portion of the curve at smaller diameters.

5.3.3.2. Separation rate. The progress of product separation for series 5 experiments is represented by the changes in oxygen content with time, as previously described in section 5.2.2.3., but allowances have been made for changes occurring in equilibrium oxygen content of the melt as products became saturated with alumina. Figs. 5.36 - 5.38 show that in the early part of the holding period, during which most products separate,  $(d \log \% O'' / dt)$  can be considered constant and the parameters described previously can be used for comparing



Separation of deoxidation products. Series 5 experiments.

separation rates.

In addition to oxygen analyses however, direct determination of inclusion content has been made by measuring area fractions of inclusions in polished sections. Smith and Guttman (128) have shown that area fraction is equal to volume fraction and figs. 39a - f show the approximate linear relationship between % oxygen and % oxide inclusions by area. The slopes of these lines indicate product densities of 2 - 2.4 gm. cm<sup>-3</sup>, which are of the order expected, but in the case of 5E1 a product density of 6 gm. cm<sup>-3</sup> is indicated. This exceptional result can only be attributed to incomplete resolution and detection of inclusions in 5E1 when using an objective of 0.25 N.A. Product separation has been represented by the metallographic data in figs. 40 (a) and 40 (b) and derived separation rates from both metallographic and vacuum fusion data are given in table 5.10.

Quantitative agreement between the two sets of data is fair with the maximum deviation shown at the high separation rates. Fig. 5.26 indicates that products of 5E3 separated most rapidly because alumina saturation was most rapidly achieved in this experiment, and alumina saturation could only occur in experiments 5E1 - 5E4

when most of the products had segregated



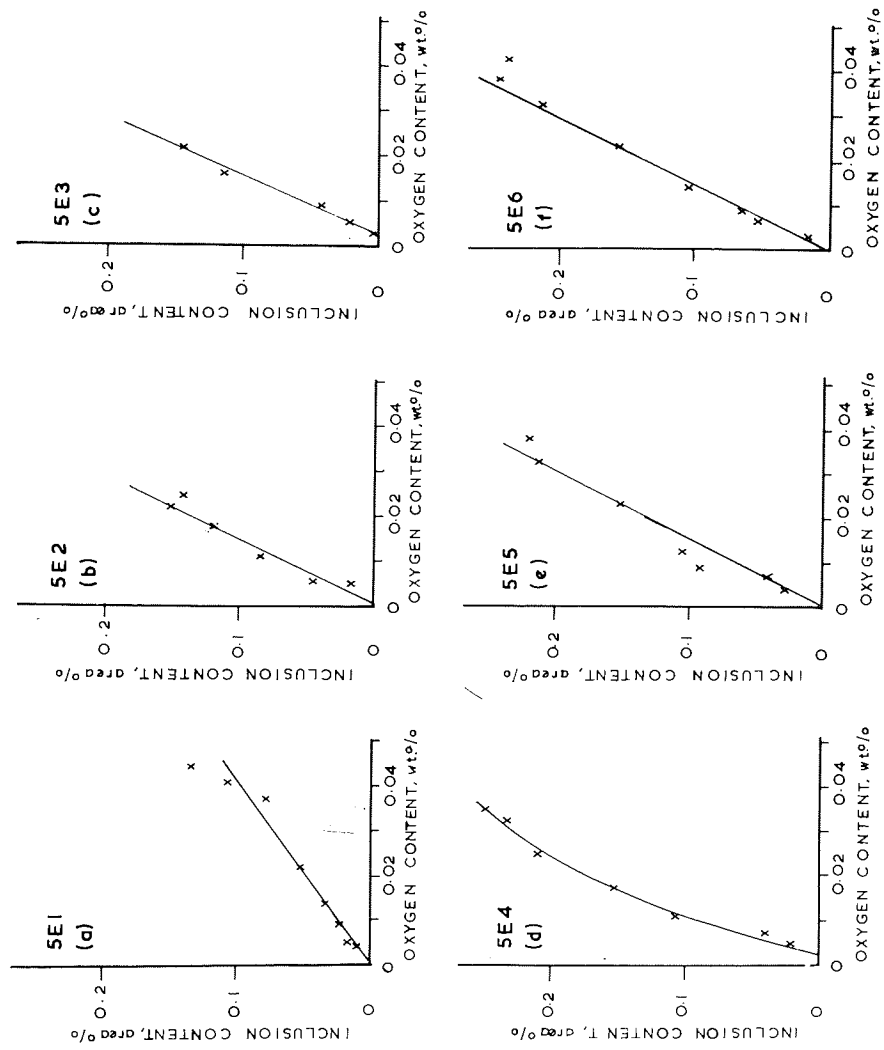


Fig. 39a - 39f. Correlation of inclusion area to oxygen content.

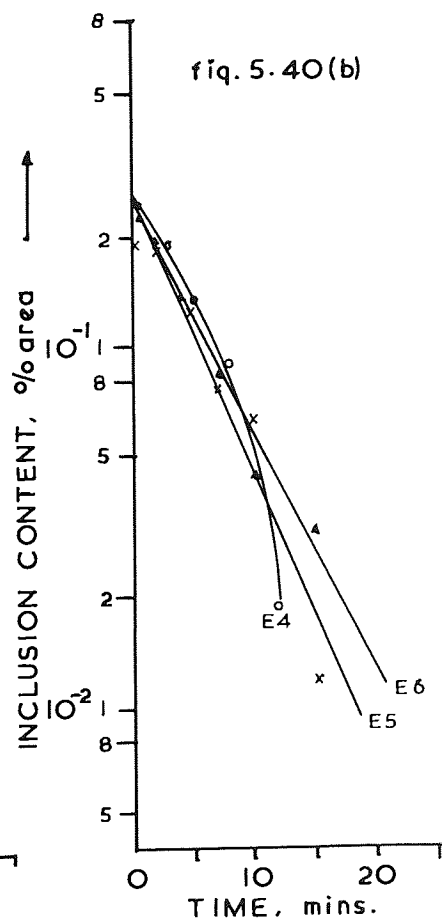
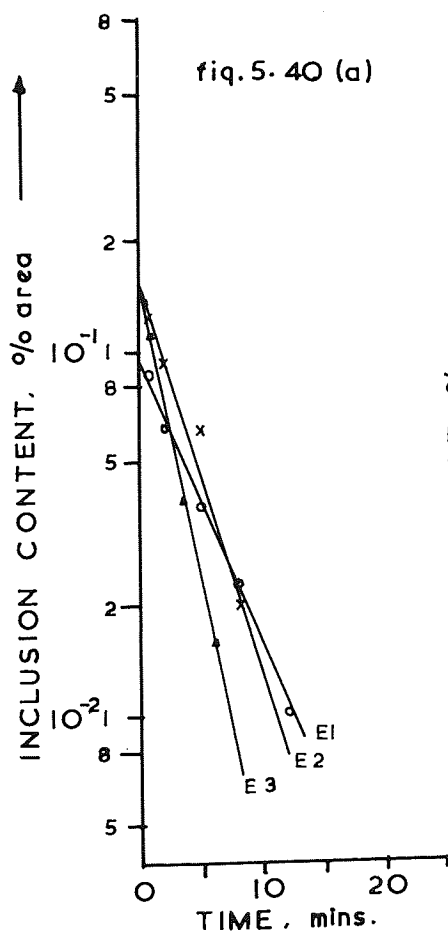


Fig. 40a

Fig. 40b

Separation of deoxidation products, Series 5 experiments.

TABLE 5.10 PRODUCT SEPARATION RATES				
Oxygen data			Metallographic Data	
Exp No.	time for 90% sep.	$\frac{d \log_{10} 0''}{dt}$	time for 90% sep	$\frac{d \log_{10} \mu}{dt}$
5E1	12.2 mins.	-0.082	13.0 mins.	-0.08
5E2	7.2 "	-0.139	9.0 "	-0.11
5E3	6.2 "	-0.162	5.6 "	-0.18
5E4	9.8 "	-0.102	11.5 "	-0.09
5E5	12.5 "	-0.080	12.8 "	-0.08
5E6	12.5 "	-0.080	15.5 "	-0.07

to the melt surface/crucible interface,

Approximate interfacial tensions between product particles and the melt have been calculated from equation 5.1 and data contained in figs. 5.22 and 5.41. These interfacial tensions are in the range 1,030 - 1,180 ergs. cm<sup>-2</sup>, which is lower than values found in section 5.2.2.3. for pure alumina or pure silica particles and less than that required to explain the differences in separation rate by interfacial tension effects. Some separation rates are quite rapid, especially the products of 5E3 and it appears that rates tend to increase as product liquidus temperatures decrease. Table 5.11 gives estimated values of interfacial tensions and liquidus temperatures.

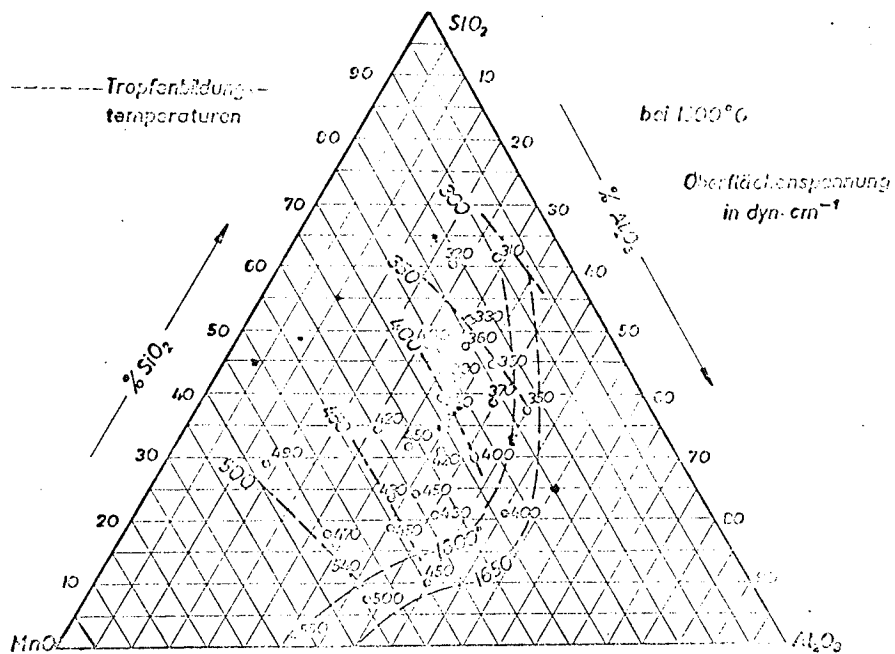


Abb. 33. Oberflächenspannungen von MnO--SiO<sub>2</sub>--Al<sub>2</sub>O<sub>3</sub>-Schlacken

Fig. 5.41 Surface tension of MnO - SiO<sub>2</sub> - Al<sub>2</sub>O<sub>3</sub> slags at 1600°C, according to Gohler(109)  
 Oberflächenspannung = Surface tension  
 Tropfenbildungs temperaturen = end of drop formation temperatures. (A temperature somewhat less than the liquidus).

EXP No.	$\sigma_{Ox - Fe}$	Liquidus Temp.
5E1	1,050 ergs.cm <sup>-2</sup>	1,600 6C
5E2	1,040 " "	1,380 "
5E3	1,030 " "	1,250 "
5E4	1,100 " "	1,520 "
5E5	1,100 " "	1,480 "
5E6	1, 180 " "	1,680 "

Decreasing product liquidus temperatures is likely to reduce product viscosity and it may be noted that a high fluidity is expected to enable coalescence to occur. It is suggested therefore, that although interfacial tensions are not sufficient to account for observed differences of separation rates in series 5, the propensity of particles to coalesce may be responsible for the observed variation. Solid silica or alumina particles can tend to agglomerate but cannot coalesce and so the interfacial tension effect predominates for these particles.

An attempt has been made to test the applicability of equation 2.27 to the present results by substituting  $(\rho_{Fe} - \rho_{Ox}) = 4.5 \text{ gm.cm}^{-3}$ ,  $\eta = 0.05$  poise and the values of  $A$  shown in table 5.9. C/Co data computed in this way

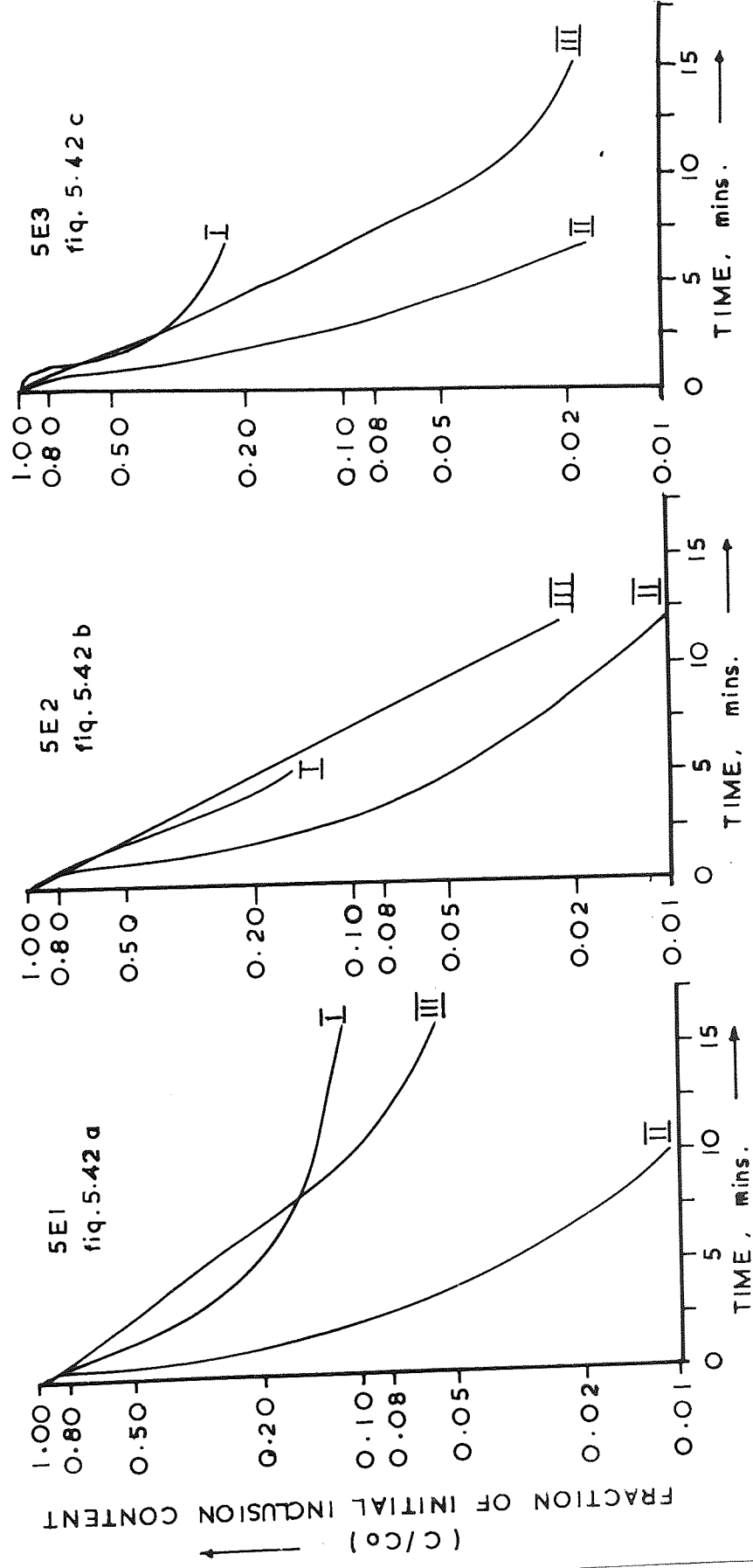
are shown in figs. 5.42 a - f by the curves labelled I, and these indicate the last 10 - 20% of deoxidation products are removed only very slowly which does not represent the observed behaviour very well. An expression for C/Co was therefore derived independently as shown in appendix D, using the model proposed by Kawawa et.al (97) and this resulted in equation 5.3, below.

$$\frac{C}{C_0} = \frac{n_p}{n_0} \left( \frac{A'}{\Lambda} \right)^4 \cdot \left[ \frac{1 - e^{-A'\delta}}{6} \left\{ (\Lambda\delta)^3 + 3(\Lambda\delta)^2 + 6(\Lambda\delta) + 6 \right\} \right]$$

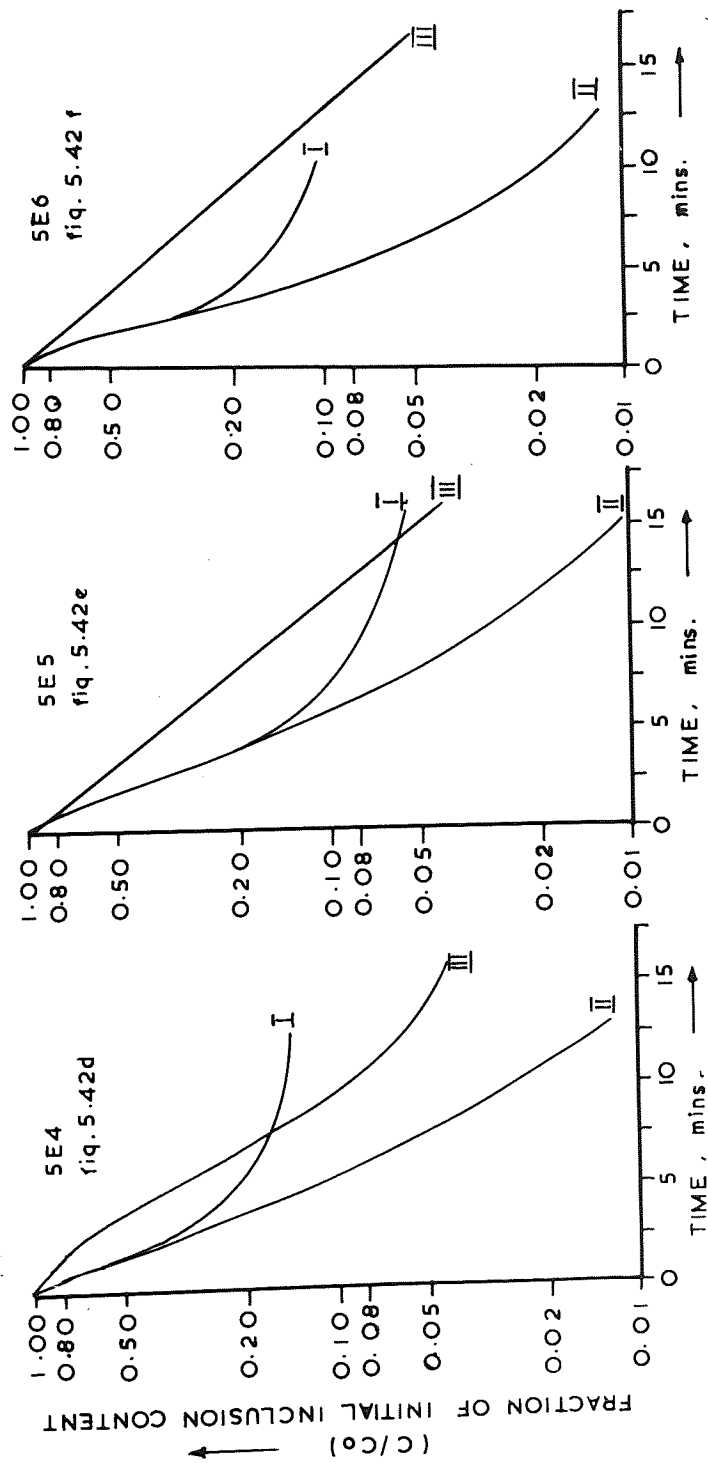
where  $\delta$  is the radius as defined on p.49,  $n_0'$  and  $A'$  are the constants in equation 2.26 which apply immediately after addition of the deoxidiser. If the particle size distribution is assumed to remain constant then equation 5.3 simplifies to the form shown in equation 2.27 but this assumption has been shown above to be invalid.

$n_0'$  and  $A'$  are not known, but if it is assumed that they are similar to the values obtaining at 1/2 min., approximate C/Co ratios may be computed from equation 5.3. Results of such computation are shown in figs. 5.42 a - f by the curves identified as II and these have a greater similarity to the observed results than those derived from equation 2.27.

Using the parameters described previously for comparison of separation rates, it was found that values of  $(d \log (C/Co) / dt)$  over 90% separation range



Figs. 5.42 a - c. Calculated progress of product separation.



Figs. 5.42 d - f. Calculated progress of product separation.



were 2 - 3 times greater than the observed separation rates included in fig. 5.42 as curve III, and so quantitative agreement was still not good. Factors contributing to the discrepancy are inaccuracy of measurement and definition of particle size distribution, deviation of experimental conditions from ideality and the inability to take interfacial tension effects into account. The interfacial tension effect is considered to be the greatest single factor preventing equation 5.3 accurately representing progress of product separation, because table 5.3 shows that  $(d \log \% O''/dt)$  varies by a factor of 4 - 5 between silica, and alumina products and this difference has already been attributed to interfacial tension effects.

#### 5.4 Practical Implications:

The main condition for preventing blowholes in steel ingots is to achieve a low oxygen activity such that carbon monoxide cannot be formed, and a low equilibrium oxygen content in the liquid is also the condition by which formation of secondary deoxidation products during solidification is minimized. The total inclusion content resulting from deoxidation is the sum of secondary products mentioned above and the primary products which remain in the melt.

Lowest residual oxygen contents and maximum separation rates can undoubtedly be obtained with aluminium deoxidation, due to the low aluminium deoxidation constant and the high interfacial tension between alumina and oxygen free steel. Residual alumina particles however, even in small quantities can be very harmful and so aluminium cannot be used as the principal deoxidiser when maximum steel properties are required. In such cases, the lowest residual oxygen contents may be obtained by using complex deoxidisers which result in products whose oxide activities are less than unity.

Calcium and magnesium are not effective in determining final oxygen contents because of their volatility but they do participate in the early stages of deoxidation and could probably combine a larger proportion of the total oxygen if they were added as more dilute alloys, and as several small additions plunged to the bottom of a deep bath. These measures would

enable a larger vapour / melt interface area to be active during the course of making a total addition.

Alumina contents of products can be related approximately to deoxidation practice by fig. 5.2. Primary MnO - SiO<sub>2</sub>-Al<sub>2</sub>O<sub>3</sub> product compositions may be related to the deoxidation alloys by means of figs. 5.23 and 5.24 but more oxide activity data are required for the system to enable reasonable estimates of equilibrium oxygen contents to be made. It is possible however, to select the deoxidiser required to give products of a chosen composition and this choice may be influenced by considerations regarding the attainment of;

- (a) Lowest equilibrium oxygen content of the melt.
- (b) Fastest product separation rates.
- (c) Plasticity of products during hot working.

Residual oxygen contents will be reduced, for a given silicon addition, by increasing amounts of manganese oxide and alumina in the products up to their liquidus boundary compositions.

Maximum separation rates are obtained, where large variations in interfacial tension are absent, by products which coalesce to the greatest extent, and these are the products with lowest liquidus temperatures in the MnO - SiO<sub>2</sub> - Al<sub>2</sub>O<sub>3</sub> system.

Products are likely to be plastic during hot working if their solidus temperatures are less than the hot working temperatures, but if their liquidus temperatures are also less than hot working temperatures, then they may cause defective steel because of hot shortness.

Effects of refractory materials on product composition and residual oxygen contents are likely to be less pronounced on large melts, when the surface area / volume ratio is relatively small. Equilibrium oxygen contents required in the ladle should therefore, be those in equilibrium with the primary deoxidation products. Lining refractories and slag covers will influence solute equilibria to some extent during the holding period between tapping and teeming, and will generally lead to higher residual oxygen contents.

Slag and refractory materials are likely to influence product separation during the periods of turbulence, for example during tapping, adding volatile deoxidisers and teeming, in accordance with the deoxidation model proposed by Okubo et al. for agitated melts.

#### 5.5 Suggestions for further work.

The practical value and theoretical significance of the present work would be increased by investigation of the following topics:-

- (a) Determination of oxide activity data  
in  $\text{FeO} - \text{SiO}_2 - \text{Al}_2\text{O}_3$  slags.
- (b) Effect of reducing supersaturation when  
deoxidizers are added, on the concentration  
of product nuclei and the size of particles  
resulting from their growth.
- (c) Quantitative correlation of interfacial  
tension with other factors involved in  
determining product separation rates.
- (d) Influence of inclusion composition,  
concentration, size and distribution on  
the hot workability of steel.

## SECTION 6 CONCLUSIONS

6.1.. Melt analyses 90 mins. after deoxidation represented approximate equilibrium solute concentrations and a silicon deoxidation constant was obtained which agreed well with that obtained from equilibrium studies of other workers. The observed aluminium deoxidation constant however, was lower than indicated by equilibrium studies because of trace amounts of residual oxide and analytical errors at low aluminium or oxygen concentrations.

6.2 . Calcium and magnesium were not residual in the melt in sufficient quantities to influence solute equilibria, although lime or magnesia present in deoxidation products reduced the activity of silica and thus contributed to achieving a low equilibrium oxygen content.

6.3 . Calcium and magnesium boiled off very rapidly when deoxidisers containing them were added to the melt but their oxides, probably formed by vapour / melt reaction, led to some high and inconsistent lime or magnesia content particles in the initial products. Deductions made by Koch concerning coalescence and rapid separation of those initial products with high lime contents and low liquidus temperatures, were supported by the present results.

6.4 . Addition of lime powder to the deoxidiser did not result in products of high lime content and did not appear to influence the rate or product removal.

6.5. Alumina contents of  $\text{SiO}_2 - \text{Al}_2\text{O}_3$ ,  $\text{CaO-SiO}_2-\text{Al}_2\text{O}_3$  and  $\text{MgO-SiO}_2-\text{Al}_2\text{O}_3$  products increased to approach pure alumina as  $(\Delta\% \text{O} / \% \text{Al added})$  decreased to less than the stoichiometric ratio.

6.6. Product separation rates increased as the interfacial tension between product particles and the melt increased, thus confirming Plockinger's results and supporting his theory concerning the influence of surface properties of particles on their separability.

6.7. Initial  $\text{MnO} - \text{SiO}_2 - \text{Al}_2\text{O}_3$  deoxidation products were nucleated in highly supersaturated zones surrounding the deoxidizers during their dissolution, by the homogeneous nucleation process suggested by Turpan & Elliot. The concentration of nuclei was of the order  $10^7 \text{ cm}^{-3}$  and oxygen desaturation of the melt was complete in 1.5 secs., resulting in a mean particle diameter of approximately  $3 \mu\text{m}$ .

6.8. Initial product compositions, resulting from deoxidation with manganese-silicon-aluminum alloys, were related to deoxidizer compositions by a logarithmic function between ratios of  $(\% \text{Mn} / \% \text{Al})$  added,  $(\% \text{Si} / \% \text{Al})$  added and the respective oxide ratios. As they were formed in a deoxidizer rich zone however, a small change of composition sometimes occurred to maintain equilibrium with the melt as uniformity of solute distribution was achieved.

6.9. 90% of the deoxidation products separated within 15 mins., and in most cases formed a liquid slag at the melt surface/crucible interface. These self generated slags dissolved crucible material to become saturated with alumina at 1550°C. Oxide activities in these alumina saturated slags then determined the solute equilibria and residual dissolved oxygen content.

6.10. Manganese oxide activities in the pseudo binary system of manganese oxide with silica and alumina at a molar ratio ( $N_{\text{SiO}_2}/N_{\text{Al}_2\text{O}_3}$ ) of 1.8, indicated an agreement with Sharma and Richardson's data and extended them to lower manganese oxide concentrations, where  $\gamma_{\text{MnO}}$  was a minimum of 0.08 at  $0.2N_{\text{MnO}}$ .

6.11. In the range of initial MnO - SiO<sub>2</sub> - Al<sub>2</sub>O<sub>3</sub> products observed, ( $\gamma_{\text{SiO}_2}/\gamma_{\text{MnO}}^2$ ) was approximately constant at 48.8 because  $\gamma_{\text{SiO}_2}$  increases along the 1550°C silica saturation boundary to a maximum in the SiO<sub>2</sub> - MnO binary and this compensated for the increase in  $\gamma_{\text{MnO}}^2$  which occurred as  $N_{\text{MnO}}$  increased. In alumina saturated products ( $\gamma_{\text{SiO}_2} / \gamma_{\text{MnO}}^2$ ) decreased as ( $N_{\text{MnO}}^2 / N_{\text{SiO}_2}$ ) increased because  $\gamma_{\text{SiO}_2}$  decreases and  $\gamma_{\text{MnO}}$  increases over the observed composition range.

6.12. Oxide contents represented by vacuum fusion analyses were correlated with direct measurement of oxide content by quantitative metallography.



Fair agreement was obtained between separation rates of MnO - SiO<sub>2</sub> - Al<sub>2</sub>O<sub>3</sub> products derived from both sets of data.

6.13. Product particle size distribution was reasonably represented by the exponential function used by Kawawa et.al., but the particle size distribution was found to vary with time because of particle coalescence.

6.14 Interfacial tensions between initial MnO-SiO<sub>2</sub> - Al<sub>2</sub>O<sub>3</sub> products and the melt were very similar but product separation rates increased as their liquidus temperatures decreased because coalescence was greater for very fluid particles.

6.15. Kawawa's model of decantation product separation from a quiescent bath according to Stokes' Law, resulted in qualitative agreement with observed separation rates when approximate corrections were made for the observed particle size distribution. The remaining discrepancy was attributed to the interfacial tension effects proposed by Plockinger.

A P P E N D I X 'A'.

EXAMPLE. CALCULATION OF DEOXIDISER COMPOSITION

The product composition intended was 14.7% alumina, 62% silica and 23.3% lime, which has a melting point of 1,170° C. A reduction in dissolved oxygen content of 0.04% was assumed with a residual oxygen content of 0.006%. Unit activity for each of the oxide components was assumed and also 100% utilization of deoxidiser elements was assumed.

Oxygen combined as Al <sub>2</sub> O <sub>3</sub>	per gm. of slag	=	0.0692 gm.
"	" SiO <sub>2</sub>	"	0.3306 gm.
"	" CaO	"	0.0666 gm.
<hr/>			
∴ Total oxygen per gm. of slag		=	0.4664 gm.

Fraction of total oxygen combined as Al <sub>2</sub> O <sub>3</sub>	=	0.1483
" " " " SiO <sub>2</sub>	=	0.7088
" " " " CaO	=	0.1429
		<hr/>
		1.0000

Available oxygen in the melt to be combined (O<sup>av</sup>) as

Al<sub>2</sub>O<sub>3</sub>, SiO<sub>2</sub>, and CaO follows as:-

O <sup>av</sup> as Al <sub>2</sub> O <sub>3</sub>	=	0.04 x 0.1483	=	0.00593%
O <sup>av</sup> as SiO <sub>2</sub>	=	0.04 x 0.7088	=	0.02835%
O <sup>av</sup> as CaO	=	0.04 x 0.1429	=	0.00572%

Stoichiometric decarburiser requirements are:

$$\text{Al} = 0.00595 \times 94/48 = 0.0067 \%$$

$$\text{Si} = 0.00335 \times 28/52 = 0.0018 \%$$

$$\text{Ca} = 0.00572 \times 40/56 = 0.0041 \%$$

For 0.0067% residual oxygen, the equilibrium aluminium and calcium contents are found from data in sections 2.1.2, 4. & 2.1.3. respectively, to be negligible. The equilibrium silicon content according to Matoba's (55) data is found to be 0.2437% and so total additions and alloy compositions follow as shown in the table.

Decarburiser	Addition	Composition
Aluminium	0.0067%	1.23%
Silicon	0.2435%	2.87%
Calcium	0.0143%	4.35%
TOTAL	0.2645%	100.00%

When lime is used instead of calcium, the same  $\text{O}^{2-}$  as  $\text{SiO}_2 / \text{O}^{2-}$  as  $\text{Al}_2\text{O}_3$  ratio is required, i.e.,  $0.5306/0.0692 = 4.778$

∴ Fraction of oxygen combined as $\text{Al}_2\text{O}_3$	= 0.1751
" " " " " $\text{SiO}_2$	= 0.8269
	<hr/>
	1.0000
	<hr/>

$$0'' \text{ as } Al_2O_3 = 0.04 \times 0.1731 = 0.0069\%$$

$$0'' \text{ as } SiO_2 = 0.04 \times 0.8269 = 0.331\%$$

$$\therefore \text{Stoichiometric Al} = 0.0069 \times 54/48 = 0.0078\%$$

$$\text{" Si} = 0.0331 \times 28/32 = 0.0290\%$$

Using the same equilibrium values as previously therefore, results in additions shown in the following table:-

Deoxidiser	Addition	Composition
Aluminium	0.0078	2.73
Silicon	0.2777	97.27
TOTAL	0.2855	100.00

Oxides produced by these deoxidiser additions are:

$$Al_2O_3 = 0.0069 \times 102/48 = 0.0147\%$$

$$SiO_2 = 0.0331 \times 60/32 = 0.0621\%$$

$$SiO_2 + Al_2O_3 = \underline{\underline{0.0768\%}}$$

This represents 76.7% of the oxide in the desired product and so the lime addition follows as:-

$$(0.0768 / 0.767) \times 0.0768 = 0.0233\%$$

and so the total deoxidiser addition is:

$$0.2855\% \text{ alloy} + 0.0233\% \text{ lime} = 0.3088\%$$

A P P E N D I X "B"

PRELIMINARY CALCIUM & MAGNESIUM

DEOXIDATION ALLOYS.

INTENDED COMPOSITION				ANALYSED COMPOSITION			
Ca	Mg	Si	Al	Ca	Mg	Si	Al
36.4	-	26.3	37.3	35.8	-	23.0	40.0
-	28.5	49.1	22.4	-	24.3	48.9	23.6
29.7	-	54.3	16.0	29.2	-	50.5	18.6
-	17.2	38.3	44.5	-	12.4	35.7	47.4
56.2	-	32.8	11.0	55.5	-	31.8	12.7
-	11.2	60.6	28.1	-	11.5	53.4	34.1
46.6	-	34.4	19.0	47.0	-	33.5	17.4
38.5	-	19.8	41.7	37.9	-	18.6	43.0

A P P E N D I X ' C '

ILLUMINON MOBE MICROANALYSIS CORRECTIONS.

Correction factors for oxide analyses were obtained by interpolation in tables relating true oxide compositions to apparent compositions obtained from the measured X ray intensity ratios. These tables, supplied by courtesy of English Steel Corporation, were computed by applying the Philibert corrections to a range of oxide compositions and deriving the corresponding apparent compositions.

An example of this is shown below, and table 1 gives all the relevant functions.

TABLE 1.	
$C^1_A = CA \left[ \frac{F(X)_A}{F(X)_B} \right] - (1 - CA)$	...( 1)
$F(X) = \frac{1}{\left(1 + \frac{X}{\sigma}\right) \left[1 + h \left(1 + \frac{X}{\sigma}\right)\right]}$	...( 2)
$X = (\mu / \rho) \operatorname{cosec} \theta$	...( 3)
$\sigma = 6.037 \text{ V(kv)}^{-1.699} \times 10^5$	...( 4)
$h = 1.2 \Lambda / Z^2$	...( 5)

S.

$C_A$  and  $C_i$  are the apparent and true concentration of element A expressed as wt. fraction,  $F(K)A$  and  $F(K)B$  are the correction factors for elements A & B respectively but in a system of more than two elements  $F(K)B$  will refer to the combined effects of B, C, D, etc.,  $A$  and  $Z$  are the atomic weight and atomic number relating to each element,  $V(kv)$ , is the energy of the electron beam in kilovolts,  $\theta$  is the take-off angle of the spectrometer, and  $(\mu/\sigma)$  is the mass absorption coefficient for  $K\alpha$  radiation.

Taking as an example the computation of apparent silica content corresponding to 55% silica in an oxide containing;

25% MnO, 20%  $Al_2O_3$ , 55%  $SiO_2$

and following the procedure of Ridal, Jones & Cummins (120), the data in table 2 were computed. At an electron probe potential of 20 kV.,  $\sigma$  is 3725 and the weighted value of  $h$ , ( $h'$ ), for aluminum, manganese and oxygen in the pseudo binary system Si - (Al, Mn, O) resulted from;

$$h' = \frac{1}{1 - C_{Si}} (h_{Al} \cdot C_{Al} + h_{Mn} \cdot C_{Mn} + h_O \cdot C_O)$$

Table 2.

Element x	wt % x	$h$	$h^1$	Si $\left(\frac{\rho}{\rho_x}\right)$	$\frac{x}{\sigma}$	$\left(\frac{x}{\sigma}\right)^1$	
Si	25.67	0.1714		0.1714	322	0.2528	0.2528
Al	10.59	0.1917	0.0273		3090	2.426	0.3455
Mn	19.37	0.1056	0.0275	0.2338	1951	1.532	0.3991
O	44.37	0.3000	0.1790		987	0.775	0.4625

$F(x) \text{ Si} = 0.6571$  &  $F(x) \text{ Mn, Al}_2\text{O}_3 = 0.2989$  are obtained by substituting in function 2 of table 1, and by further substitution in function 1 of table 1 a value of  $C'S$ ; of 0.143 was obtained which is equivalent to 30.6%  $\text{SiO}_2$ . The procedure is repeated to obtain apparent  $\text{MnO}$  and  $\text{Al}_2\text{O}_3$  contents.

Pure oxide standards were used in the analyses and so corrections were made for the apparent metal content of metal oxides. The procedure shown in table 2 for calculation of  $C'_{\text{Si}}$  was repeated for the binary systems to obtain  $C'\text{Si}$  in  $\text{SiO}_2$ ,  $C'\text{Mn}$  in  $\text{MnO}$ ,  $C'\text{Al}$  in  $\text{Al}_2\text{O}_3$ ,  $C'\text{Mg}$  in  $\text{MgO}$ ,  $C'\text{Fe}$  in  $\text{Fe}_3\text{O}_4$  and  $C'\text{Ca}$  in  $\text{CaF}_2$ . Using silicon again as an example, the apparent oxide content was obtained by the X ray intensities of  $K_{\alpha}$  radiation,  $I_{\text{Si}}$ , from sample and standard according to the following expression. ..



$$\text{apparent wt.\% SiO}_2 = \frac{\text{ISi (sample)} \times \text{C'Si (in SiO}_2\text{)}}{\text{ISi (pure silica)}} \times \frac{\text{mol.wt.SiO}_2}{\text{at.wt.Si.}}$$

## A P E N D I X 'D'

### PARTICLE SEPARATION FROM A QUIESCENT BATH.

RS.

Starting with the initial premise of Miyoshita (130), that the concentration of inclusions having a radius between  $\gamma$  and  $\gamma + d\gamma$  can be represented by  $f(\gamma) d\gamma$  and if the inclusion density is  $\rho$  and the number of inclusions of radius  $\gamma$  is  $n(\gamma)$  then  $f(\gamma) d\gamma$  is given by expression (1).

$$f(\gamma) d\gamma = (4/3) \pi \gamma^3 \rho n(\gamma) d\gamma \quad (1)$$

and the total concentration of inclusions having radii between 0 and  $\infty$  is given by  $C_0$  in expression (2)

$$C_0 = \int_0^{\infty} f(\gamma) d\gamma \quad (2)$$

substituting  $n_0 e^{-\Lambda' \gamma}$  for  $n(\gamma)$  according to equation 2.26, where  $n_0$  &  $\Lambda'$  are the constants before separation has occurred, gives  $C_0$  as:

$$C_0 = \frac{4 \cdot \pi \cdot n_0 \cdot \rho}{3} \int_0^{\infty} \gamma^3 e^{-\Lambda' \gamma} d\gamma = \frac{4 \cdot \pi \cdot n_0 \cdot \rho}{3} \cdot \frac{6}{(\Lambda')^4}$$

After a time  $t > 0$  from deoxidation, and at a depth  $h$  from the bottom,  $\delta$  will be limited to a maximum according to Stoke's Law as shown by expression 3.

$$\delta = (h / kt)^{\frac{1}{2}} \quad (3)$$

where  $k = (60 \times 2 / 9) \cdot g \cdot \Delta \rho / \eta$  and  $\Delta \rho$  is the density difference between the inclusions and liquid iron,  $g$  is the gravitational constant,  $\eta$  is the viscosity of the steel and  $t$  is expressed in minutes. Inclusion concentration  $C$  at  $t > 0$  is then given by setting the limits of 0 and  $\delta$  to the integral shown in expression (2).

$$C = \frac{4 \cdot \pi \cdot n_0 \cdot \rho}{3} \int_0^{\delta} \delta^3 e^{-\Delta \delta} d\delta$$

$$C = \frac{4 \cdot \pi \cdot n_0 \cdot \rho}{3} \left[ \frac{-e^{-\Delta \delta}}{\Delta^4} \cdot 6 \left\{ \frac{(\Delta \delta)^3}{6} + \frac{(\Delta \delta)^2}{2} + (\Delta \delta) + 1 \right\} \right]_0^{\delta}$$

$$C = \frac{4 \cdot \pi \cdot n_0 \cdot \rho}{3} \cdot \frac{1}{\Delta^4} \left[ 6 - e^{-\Delta \delta} \left\{ (\Delta \delta)^3 + 3(\Delta \delta)^2 + 6(\Delta \delta) + 6 \right\} \right]$$

The proportion of inclusions remaining in a quiescent melt after a given time can therefore, be represented by  $C / C_0$  with  $\delta$  being a function of time as shown in expression 3.

$$\therefore \frac{C}{C_0} = \frac{n}{n_0} \left( \frac{\Delta'}{\Delta} \right)^4 \left[ 1 - \frac{e^{-\Delta \delta}}{6} \left\{ (\Delta \delta)^3 + 3(\Delta \delta)^2 + 6(\Delta \delta) + 6 \right\} \right]$$

If no coalescence of particles occurred, and Stoke's Law

separation and flotation only terminated the particle size distribution, at a specific maximum radius, then  $\frac{n_0}{\bar{n}_0} \left( \frac{\Lambda}{\bar{\Lambda}} \right)^4$  would be equal to unity and the expression of  $C / C_c$  would reduce to that quoted by Kawawa et. al. (97)

ERS.

## ACKNOWLEDGEMENTS.

The author wishes to thank his supervisor, Dr. J.C. Billington, for all the encouragement and helpful advice given during the course of this work.

Thanks are also due to Dr. J.A. Belk of the metallurgy department and Messrs. H.A. Jones and R. Cummins of English Steel Corporation Ltd., for their valuable advice concerning microanalysis. Grateful acknowledgements are made to the following technical staff of the metallurgy department; Mr. G. Reeves who was responsible for most of the oxygen analyses, Mr. R. Lyden who was responsible for preparation of graphite susceptors and maintenance of the experimental equipment, and finally to Messrs. N. Shirley, and R. Cox for their assistance in photographic reproduction of many of the illustrations included in this thesis.

ERS.

REFERENCES.

1. J. Marsh, Elec. Furn. Proc. I.I.R.I., 1944 V.16 P.135
2. K. Petters & J. Chipman, Trans. I.I.R.I., 1940 V.140 P.170
3. R.H. Bellman-Con C.J.M. Charles, J.I.S.I. 1963 V.201. P.863
4. J. G. Witt & A. F. Pander, J.I.S.I. 1946 V.154 P.371.
5. D.C. Conroy & A.C. Ludolph, Elec. Furn Steel Proc.,  
A.I.R.I., 1953, V.11P.274
6. C.A. Post & G.J. Leurssen, Trans. A.I.R.I., 1949, V.185 P.15
7. H.P. Hedcock, Elect. Furn. Steel Proc. A.I.R.I., 1953,  
V.11. P.269.
8. C.W. Sams & J. Forger, Electric Furnace Steelmaking  
Vol.III 1963, P.38, Interscience, New York.
9. W.D. Klinevalka, & A.V. Korosov, Izvest, Akad Nauk.  
S.S.S.R. Obshch. Leht Nauk, 1957, No.9. P.402
10. A. Daltzen, Elect. Furn. Steel Proc. I.I.R.I. 1946,  
74. P.50
11. K. Naito, Tetsu to-Hagane Overseas, 1963, V.3 P.106.
12. H.H. Richardson, I.I.S.I. Spec. Rep. No.77, 1963, P.57.
13. M. Stefan, Hutnacké Listy 1962, V.17 P.479
14. E. Flockinger, J.I.S.I. 1963, V.201, P.576.
15. H.H. Conlin et.al. Trans. A.S.I. 1957 P.482.
- 15.a. W. Rees and G. Hopkins, J.I.S.I. 1952, V.172, P.403

SERS.

16. P.H. Brath, J.I.S.I. 1959, V.180 P.16.
17. J.D. Murray and R.B. Johnson, I.S.I. Spec. Rep. No.77.  
1963, P.110.
18. M. Atkinson, J.I.S.I. 1960 V.195, P.64.
19. W.H. Duckworth and E. Ineson, I.S.I. Spec. Rep. No.77.  
1963, P.87.
20. M.L. Libinowitz, Steel in English, 1963, V.3. P.185.
21. C.H. Hertz & L. Gaines, Mining & Met. Invest. Bul. No 34,  
1927.
22. A. Scherck & Introduction to the Physical Chemistry of  
Steelmaking P.183, translation by A.I.S.R.A. 1945, London
23. W. Rosenhan, P.O. Tritton, & D. Hansen, J.I.S.I., 1924  
V.110, P.90
24. F. Kessler and W. Colson, Mitt. Kaiser Wilhelm Inst. Eisen-  
forsch, 1928, V.11. P.181
25. J. Chipman & H.L. Fetter, Trans. A.I.S.I. 1941, V. 1. P.953.
26. C.R. Taylor & J. Chipman Trans. A.I.S.I. 1943, V.194. P.228
27. J. Chipman Basic Open Hearth Steelmaking, 3rd Edition, 1964  
P.650, A.I.M.M.P. New York
28. H.B. Bell, Iron & Steel, 1954, V.27 P.493, 531, & 559.
29. H.S. Sloman, J.I.S.I. 1941, V.143, P.311.
30. W.L. Fischer & H. vom Ende, Archiv, Eisenhutt, 1952, V.23,  
P.31.

31. H.A. Gokcen, Trans. A.I.I.S.I., 1956, V.208, P.1358
32. T.P. Floridis, & J. Chipman, Trans. A.I.I.S.I., 1958, V.185  
P.441.
33. J.F. Elliot, L. Gleiser, & V. Ramakrishna, Thermochemistry  
For Steelmaking Vol.II P.406, 1963, Addison-Wesley, Reading
34. T. Wever, W.A. Vascher & E. Ingelbrecht, Stahl u. Eisen,  
P.1954, V.74, P.1521.
35. A.U. Baysolt, Trans, A.I.I.S.I., 1959, V.215, P.298
36. A.U. Baysolt, Ibid., 1954, v.200. P.641.
37. J.M. Kitchener, J.M. Bockris, L. Gleiser, & J.W. Evans,  
Acta. Met. 1955, V.1. P.93.
38. E.B. Baktina, & H.A. Gokcen, Trans, A.S.I., 1961, V.53,  
P.843.
39. I.M. Hogworth R.P. Smith, & L.F. Burkloper, Trans. A.I.I.S.I.,  
1966, V.236, P.1278
40. J.F. Elliott, The Physical Chemistry of Steelmaking, 1958  
P.37, Wiley, New York
41. J. Chipman, Electric Furnace Steelmaking Vol II. 1966,  
P.114, Interscience, New York.
42. C. Bodsworth, Physical Chemistry of Iron & Steel,  
Manufacture, 1960, P.371. Longmans, London.
43. T. Pura, & J. Chipman, Trans, A.I.I.S.I., 1958, V.212, P.549.
44. L. Gust, & J. Chipman, The Physical Chemistry of Steel-  
making, 1958, P.5. Wiley, & Sons, New York.

45. B.F. Turkdogan, L.L. Leake, & C.R. Mason, Acta Met., 1956,  
V.4. P.596.
46. F.D. Richardson, & T.B. Dennis, Trans, Metall. Soc., 1953,  
V.43, P.171.
47. M.L. Loomis, & H.P. DeGarmo, Phase Diagrams for Cermetists  
Part I. P.55, Am. Ceram. Soc. Columbus, Ohio, 1956.
48. J. Chipman, J.B. Nero & R.D. Finkler, Trans. A.I.M.E. . 1950  
V.198 P.341.
49. H.P. Bell, J.I.S.I., 1963, V.201, P.116.
50. W.L. Fischer, & H.J. Fleischer, Archiv. Eisen, 1961, V32  
P.1.
51. D.D. Chrysal & R.G. Ward, J.I.S.I. 1967, V.205, P.28.
52. D.C. Hillby, & W. Cr Pta, Trans. A.I.M.E. 1950, V.188, p.341.
53. R.L. Gibson, & J. Chipman, Trans. A.I.M.E. 1953, V.194 P.131
54. R.A. Massé, S. Raichandran, & J.C. Fulton, Trans A.I.M.E.  
1963, V.227, P.1380.
55. S. Matsuda, K. Gunji, & T. Masuda, Tetra-to-Hogano, 1959,  
V.45, P. 29.
56. J. Chipman, & D.C. Hillby, Trans, A.I.M.E. 1961, V.221  
P.1277.
57. J. Chipman, Open Hearth Steelmaking, 2nd. Edition, 1951,  
P.641, J.I.M.E. . New York.
58. A. McLean, & H.J. Fiedl, J.I.S.I. 1966, V.204, P.8.
59. A. McLean, & H.P. Bell, J.I.S.I. 1965, V.203, P.123.



60. H. Wentrup & G. Hasler, *Archiv. Eisenhutt*, 1939, /40  
V.13, P.15.
61. W. Goebel, & K. Dicks, *ibid*, 1940, v.16, P.431.
62. D.C. Hillig, & W. Crafts, *Trans. A.I.M.E.*, 1950, V.188,  
P.495.
63. J. Chipman, *IME*, 1950, V.115, P.1342.
64. M.A. Gokcen, & J. Chipman, *ibid*, 1953, V.197, P.175.
65. J.C. D'Entremont, et.al., *ibid*, 1963, V.227, P.14.
66. C.L. Sims, *ibid*, 1959, V.115, P.367.
67. T.O. Pillsbury, et.al, *J. Amer. Ceram. Soc.* 1960, V.43,  
P.583.
68. J. Chipman, *Electric Furnace Steelmaking*, Vol II, 1963  
P.43, Interscience New York.
69. H.J. Richardson, & J.M.S. Joffe, *J.I.S.I.*, 1948, V.160  
P.261.
70. W.O. Philbrick, E.H. Collins, & M.M. Helzel, *Trans.  
A.I.M.E.*, 1950, V.188, P.561.
71. P.F. Trofan, & R.A. Minn, *Trans, A.S.M.* 1961, V.54,  
P.543.
72. D.L. Sponseller, & R.A. Minn, *Trans, A.I.M.E.*, 1964,  
V.190, P.576.
73. G.W. Healy, *ibid*, 1963, V.227, P.207.
74. R. Schurr, *Rev. Univ. Min*, 1963, V106, P.403.
75. E.L. Walsh, & S. Ramachandran, *Trans. A.I.M.E.* 1963, V.227  
P.560

76. R.A. Shanks & P.D. Richardson, *ibid*, 1965, V.233, P.1586
77. K.P. Abraham, H.W. Davies, & P.D. Richardson, *J.I.S.I.*  
1960, V.196, P.82.
78. J. Cameron, H.D. Gibbons, & J. Taylor, *J.I.S.I.* 1966.  
V.204, P.1223.
79. D. Henderson, & J. Taylor, *J.I.S.I.*, 1965, V.204, P.19.
80. L. von. Bogdanov, W. Meyer, & I.N. Stranski, *Archiv.*  
*Eisenhutt*, 1961, V.32, P.451.
81. L. von. Bogdanov, W. Meyer, & I.N. Stranski, *ibid*,  
P.1963, V.34, P.235
82. H.L. Turpin & J.W. Elliot *J.I.S.I.*, 1966, V.204, P.217.
83. W. J. Koehlbaer, & G.R.W. Rengsdorff, *Jorn. of Metals*,  
1967, V.19, P.50.
84. W.E. Garbagan, *J.I.S.I.* 1966, V.204, P.914.
85. H. Schenck, *Introduction to the Physical Chemistry of*  
*Steelmaking*, P.505, Translation by D.I.S.R.A.  
1945, London.
86. C.H. Herty & G.R. Fitterer, U.S. Bureau of Mines, R.I.  
No.5081(1931) and 3054 (1930)  
and C.H. Herty, C.F. Christopher, A.J. Lightner, and  
H. Frazer, *Man. & Met. Invest. Bull.* No.58, 1932
87. W.A. Fischer, *The Physical Chemistry of Steelmaking*, 1950  
P.117, Wiley, New York.
88. E. Plöchlinger, & R. Roesner, *Stahl, u. Eisen*, 1967, V.77.  
P.710, and P.798

89. G.C. Duderstadt, & R.D. Weller, Journal of Metals,  
1966, V.18, P.714.
90. E. Plockinger & M. Wahlster, Stahl U. Eisen, 1960, V.80  
P.659
91. W.A. Fischer & M. Wahlster, Archiv. Eisenhutt, 1957,  
V.28 P.609.
92. E.H. Levin, G.F. McMurdie & F.P. Hall, Phase, Diagrams  
for Ceramists, 1956, P.138, Amer. Ceram. Soc. Columbus Ohio
93. O. Repovsky, I. Oletas & P. Kozakevitch, Journal of  
Metals, 1967, V.19 P.45.
94. C. Grunwald, I.S.I. Spec. Rep. No.77 1963, P.66.
95. M. Ohkubo, T. Kawawa, Y. Sasajima & H. Tokunaga, Nippon  
Kokan Techn, Rep. 1966, V.37 P.161
96. M. Ohkubo, M. Masui, H. Tokunaga, Nippon Kokan Tech.  
Rep. Overseas, 1965, No.5 P.7.
97. T. Kawawa, M. Ohkubo, & Y. Sasajima, Tetsu-to-Hagane,  
1966, V.57, P.1457.
98. G.A. Lillqvist, Proc. Elect. Furn. Steel Conf. 1948.  
V.6. P.194.
99. C.F. Christopher, Elect, Furn, Steel Proc. A.I.M.E.,  
1953, V.2. P.101.
100. Y. van Eeghen, P. Altmann & A. de Sy, Giesserei, 1964,  
P.344.
101. J.H. Ludwig, Proc. Elec. Furn Steel Conf. 1948, V.6 P.208

102. E.J. Dunn, Modern Castings, 1962, V. P.57
103. M. Mandl & J. Skála, Freiburger Forschungshefte,  
1965, B.106 P.93.
104. T. Ototani, Y. Marooka & Y. Kataura, Science Rep.  
Res. Inst. Tohoku, Univ., 1965, V.17, P.326.
105. N.I. Tsekanski, Stal in English, 1962, V.6 P.688
106. W. Koch, Stahl, U. Eisen, 1961, V.81. P.1592
107. W.N. Rossborough, U.S. Patent, 3,150,966, (1964)
108. M. Wahlster, & W. Feldhaus, Stahl, U. Eisen, 1962  
V.82, P.193.
109. M. Göhler, Freiburger Forschungshefte, 1963, B.93 P.I
110. P.R. Clement & C. Wilson, Electrical Eng. Science  
P.161, 1960, McGraw Hill, New York,
111. G. Ramsey, O. Winkler, & T. Kraus, Trans. Vac. Met.  
Conf. (A.U.S.) 1964 P.421.
112. The United Steel Companies Ltd., Standard Methods  
of Analysis of Iron Steel and Ferro-alloys, 1951  
P.118. Lund. Humphries, London
113. The United Steel Companies Ltd., *ibid*, P.69.
114. U.F. Hill, Analytical Chem. 1959, V.31. P.429.
115. G. Picasso, Met. Ital. 1961, V.53, P.269 & 276.
116. The United Steel Companies Ltd., Standard Methods of  
Analysis of Iron, Steel & Ferro-alloys, 1951,  
P.40, Lund Humphries, London.

117. H.C. Pigott, *Ferrous Analysis*, 1953, P.120,  
Chapman Hall, London.
118. W. Westwood, & A. Mayer, *Chemical Analysis of Cast  
Iron & Foundry Materials*, 1951 P.440 Allen & Unwin,  
London.
119. W. Westwood & A Mayer, *ibid*, P.309.
120. K.A. Ridal, T.K. Jones, & R. Cummins, *J.I.S.I.*,  
1965, V.203, P.995.
121. C. Fisher, *Particle Size Analysis*, Conf. 1966, Coventry
122. H. Mårtensson, *Fagersta Forum*, 1965 No.4.
123. D.M.S. Peace, & L. Gowlett, *B.Sc. Project Reports*,  
1967, The University of Aston, in Birmingham.
124. The Non-metallic Inclusions Group of B.I.S.R.A.,  
*J.I.S.I.* 1966, V.204, P.142.
125. J. Forsten, & H.F. Miehk-oja, *J.I.M.* 1967, V.95 P.143
126. S.R. Mehta, & F.D. Richardson, *J.I.S.I.* 1965, V.203  
P.524.
127. R.L. Fullman, *Trans. A.I.M.E.* 1953, V.197 P.127 & 452
128. C.C. Smith & L. Guttman, *Trans. A.I.M.E.* 1953, V.197  
P.81.
129. J.F. Elliot, M. Gleiser & V. Ramakrishna, *Thermo-  
chemistry for Steelmaking Vol. II* P.633 Addison  
Wesley, Reading, 1963.
130. Y. Miyoshita, & K. Nishikawa, *Tetsu-to-Hagané*, 1966  
V.52, P.1454.